Universität Hamburg
DER FORSCHUNG | DER LEHRE | DER BILDUNG

Interleukin-15-mediated activation and dysregulation of CD8$^+$ T cells in the pathogenesis of primary sclerosing cholangitis

---

Dissertation

to obtain the degree

Doctor rerum naturalium (Dr. rer. nat.)

at the Faculty of Mathematics, Informatics and Natural Sciences
of the University of Hamburg

submitted by

Nico Will

Hamburg, February 2026

This study was performed in the period from July 2022 to February 2026 in the research laboratories of the I. Department of Medicine of the University Medical-Center Hamburg-Eppendorf. Supervision during this time was thankfully taken by Prof. Dr. Christoph Schramm and Dr. Dorothee Schwinge.

Date of thesis defense and approval for publication: 10.07.2026

REFEREES:

Prof. Dr. med. Christoph Schramm

I. Department of Medicine and Martin Zeitz Center for Rare Diseases

University Medical Center Hamburg-Eppendorf

Martinistrasse 52

20251 Hamburg

Prof. Dr. Tim Gilberger

Department of Cellular Parasitology

Bernhard Nocht Institute for Tropical Medicine

Bernhard Nocht Straße 74

20359 Hamburg

Affidavit

I hereby declare and affirm that this doctoral dissertation is my own work and that I have not used any aids and sources other than those indicated. If electronic resources based on generative artificial intelligence (gAI) were used in the course of writing this dissertation, I confirm that my own work was the main and value-adding contribution and that complete documentation of all resources used is available in accordance with good scientific practice. I am responsible for any erroneous or distorted content, incorrect references, violations of data protection and copyright law or plagiarism that may have been generated by the gAI.

Eidesstattliche Versicherung

Hiermit versichere ich an Eides statt, die vorliegende Dissertationsschrift selbst verfasst und keine anderen als die angegebenen Hilfsmittel und Quellen benutzt zu haben. Sofern im Zuge der Erstellung der vorliegenden Dissertationsschrift generative Künstliche Intelligenz (gKI) basierte elektronische Hilfsmittel verwendet wurden, versichere ich, dass meine eigene Leistung im Vordergrund stand und dass eine vollständige Dokumentation aller verwendeten Hilfsmittel gemäß der Guten wissenschaftlichen Praxis vorliegt. Ich trage die Verantwortung für eventuell durch die gKI generierte fehlerhafte oder verzerrte Inhalte, fehlerhafte Referenzen, Verstöße gegen das Datenschutz- und Urheberrecht oder Plagiate.

Hamburg, 18.02.2026 — Nico Will

Ort, den / City, date — Unterschrift / Signature

Table of Contents

1 Introduction 1

1.1 Primary sclerosing cholangitis: clinical, pathological and therapeutic overview 1

1.2 Pathogenic mechanisms in PSC: Molecular and immunological perspectives 4

1.3 $CD8^+$ T cells in liver immunology 6

1.4 IL-15 biology: its role in T cell activation and auto-aggression 8

1.5 Knowledge gap and rationale for this study 10

2 Aim of study 12

3 Results 13

3.1 Peripheral blood $CD8^+$ T cells from people with PSC present a distinct cytotoxic profile 13

3.2 Intrahepatic $CD8^+$ T cells in end-stage PSC display an effector memory phenotype with elevated cytotoxicity 15

3.3 PSC-derived $CD8^+$ T cells exhibit an IL-15-induced bystander-activated phenotype 18

3.4 Single-nucleus mRNA sequencing reveals *IL15* upregulation in cholangiocytes of people with PSC 20

3.5 Cholangiocytes express increased IL-15 and IL-15Rα upon IFNγ stimulation 23

3.6 Spatial transcriptomics reveals close proximity of $CD8^+$ T cells and biliary epithelial cells in inflamed bile ducts 26

3.7 Portal niches exhibit high *IL15* and *IL15RA* expression and are enriched for bystander-activated $CD8^+$ T cells 32

3.8 Mouse model of acute cholangitis showed increased frequencies of intrahepatic bystander-activated $CD8^+$ T cells 36

4 Discussion 40

5 Conclusion and outlook 46

6 Methods 47

6.1 Patient selection and acquisition of blood and tissue samples 47

6.2 Human cell isolations from liver tissue and peripheral blood 50
6.2.1 Isolation of mononuclear cells from peripheral blood for spectral flow cytometry 50
6.2.2 Magnetic-activated cell sorting of $CD8^+$ T cells 50
6.3 Culturing and stimulation of H69 biliary epithelial cells 51
6.4 Generation and stimulation of human intrahepatic cholangiocytes organoids 51
6.5 Flow cytometry of H69 BECs 52
6.6 pSTAT5 quantification after $CD8^+$ T cell and H69 BEC co-culture 52
6.7 Gene expression assays 52
6.8 Mice 53
6.8.1 Induction of acute cholangitis in mice 53
6.8.2 Isolation of lymphocytes from liver and spleen 53
6.9 Data analysis of single-cell CITE sequencing dataset 54
6.9.1 Data processing: 54
6.9.2 Dimension reduction, clustering and expression analysis: 55
6.9.3 Gene set expression scoring and pathway enrichment analysis 55
6.10 Data analysis of single-nuclei sequencing dataset 56
6.11 Spatial transcriptomics of human liver biopsies 56
6.12 Statistical analysis 57
7 Materials 58
8 References 67
9 Use of artificial intelligence tools 77
10 Danksagung 78

List of Figures

Figure 1: Pathological and clinical progression of primary sclerosing cholangitis (PSC). 2

Figure 2: IL-15/IL-15Rα expression, trans-presentation, and downstream signaling in CD8⁺ T cells. 9

Figure 3: Flow cytometry-based phenotypic characterization of peripheral blood CD8⁺ T cells in individuals with PSC. 14

Figure 4: Single-cell CITE-seq analysis of intrahepatic CD8⁺ T cells in end-stage PSC. 16

Figure 5: Granzyme expression profile and RNA velocity analysis of intrahepatic CD8⁺ T cells in PSC. 17

Figure 6: Bystander-activated phenotype in liver- and blood-derived CD8⁺ T cells from PSC. 19

Figure 7: Bystander-activated CD8⁺ T cell profiles and *IL15* expression in single-nucleus RNA sequencing (sNucSeq) data from PSC and control livers. 21

Figure 8: Interferon-γ expression in single-cell and single-nucleus sequencing datasets. 23

Figure 9: IL-15 and IL-15Rα expression in cholangiocyte organoids and H69 BEC *in vitro* cultures. 24

Figure 10: Schematic overview of liver zonation and sample composition for spatial transcriptomics 26

Figure 11: Representative liver biopsy sections across PSC disease stages and control. 27

Figure 12: Representative examples of CD8⁺ T cell interactions with cholangiocytes in late-stage PSC 28

Figure 13: Spatial gene expression in cholangiocytes and CD8⁺ T cells interacting in late stagePSC 29

Figure 14: Spatial proximity between CD8⁺ T cells and cholangiocytes in PSC liver tissue. 30

Figure 15: UMAP projection and cell type–specific *IL15* and *IL15RA* expression in the Xenium spatial transcriptomics dataset. 31

Figure 16: Spatial niche analysis of PSC and control liver samples. 33

Figure 17: Cholangiocyte-derived chemokine expression and spatial enrichment of $CD8^+$ T cells across liver niches 35

Figure 18: IL-15 and IL-15Rα expression in a mouse model of acute experimental cholangitis. 37

Figure 19: Time course of bystander-activated phenotypes in transferred and endogenous $CD8^+$ T cells. 38

Figure 20: Proposed model of IL-15-dependent crosstalk between cholangiocytes and $CD8^+$ T cells in PSC forming a potential positive feedback loop 43

List of Tables

Table 1: List of Consumables 58

Table 2: List of Comercial avaliable Solutions 59

Table 3: List of cell lines 59

Table 4: List of proteins and enzymes 59

Table 5: List of chemicals and solvents 60

Table 6: List of media, cell culture supplements and buffers 60

Table 7: List of anti-human antibodies 61

Table 8: List of anti-mouse Antibodies 61

Table 9: List of TaqMan Probes 62

Table 10: Geneset for spatial transcriptomics anaylsis. 62

Table 11: List of Devices. 64

Table 12: Composition of self-assambied Buffers and Media 64

Table 13: List of Softwares 65

Publications

(1) Lara Henze and Nico Will, Dakyung Lee, Victor Haas, Christian Casar, Jasper Meyer, Stephanie Stein, Franziska Mangler, Silja Steinmann, Tobias Poch, Jenny Krause, Johannes Fuss, Johanna Schröder, Alexandra E Kulle, Paul-Martin Holterhus, Stefan Bonn, Marcus Altfeld, Samuel Huber, Ansgar W Lohse, Dorothee Schwinge, Christoph Schramm (2025). Testosterone affects female $CD4^+$ T cells in healthy individuals and autoimmune liver diseases; JCI Insight; DOI: 10.1172/jci.insight.184544

(2) Mareike Kellerer, Sana Javed, Christian Casar, Nico Will, Laura K Berkhout, Dorothee Schwinge, Christian F Krebs, Christoph Schramm, Katrin Neumann, Gisa Tiegs (2024). Antagonistic effects of the cytotoxic molecules granzyme B and TRAIL in the immunopathogenesis of sclerosing cholangitis; Hepatology; DOI: 10.1097/HEP.0000000000000830

(3) Ittai B Muller, Marry Lin, Robert de Jonge, Nico Will, Baltasar López-Navarro, Conny van der Laken, Eduard A Struys, Cees B M Oudejans, Yehuda G Assaraf, Jacqueline Cloos, Amaya Puig-Kröger, Gerrit Jansen (2023). Methotrexate Provokes Disparate Folate Metabolism Gene Expression and Alternative Splicing in Ex Vivo Monocytes and GM-CSF- and M-CSF-Polarized Macrophages; International Journal of Molecular Sciences; DOI: 10.3390/ijms24119641

Conference Participations

(1) German association of the study of the liver (GASL), Annual meeting 2024, Essen, Germany, participation with conference paper: Testosterone as modulator of immune responses in female hepatic autoimmunity; DOI: 10.1055/s-0043-1777496

(2) European association for the study of the liver (EASL), The international liver congress 2024, Milan, Italy, participation with conference paper: Testosterone modulates T cells in healthy individuals and women with autoimmune liver disease; DOI: 10.1016/S0168-8278(24)01173-5

(3) Sex Difference in the Immune System Conference, 2024, Dublin, Ireland, participation with conference paper: Testosterone as modulator of T cells in health and autoimmune liver disease.

(4) German association of the study of the liver (GASL), Annual meeting 2026, Freiburg, Germany, participation with conference paper: IL-15-Driven Modulation of $CD8^+$ T Cells in Primary Sclerosing Cholangitis; DOI: 10.1055/s-0045-1814359

Abbreviations

Abbreviation	Full term
AASLD	American Association for the Study of Liver Diseases
ACK	ammonium-chloride-potassium
ADT	antibody-derived tag
AILD	autoimmune liver diseases
ALD	alcoholic liver disease
ALP	alkaline phosphatase
ALT	alanine aminotransferase
AMP	adenosine monophosphate
APCs	antigen-presenting cells
Bcl-2	B-cell lymphoma 2 apoptosis aegulator
BECs	biliary epithelial cells
CCA	cholangiocarcinoma
CCL	C-C motif chemokine ligand
CCR	C-C-chemokinrezeptor
CD	cluster of differentiation
CD122	interleukin-2/15 receptor subunit beta
CD132	common γ-chain receptor
CITE-sequencing	cellular indexing of transcriptomes and epitopes by sequencing
CM	central memory
DCs	dendritic cells
DEGs	differentially expressed genes
DMSO	dimethyl sulfoxide
EASL	European Association for the Study of the Liver
EBSS	Earle's balanced salt solution

ECs	endothelial cells
EDTA	ethylenediaminetetraacetic acid
EM	effector memory
EMRA	effector memory re-expressing CD45RA
Eomes	eomesodermin
FFPE	formalin-fixed, paraffin-embedded
GWAS	genome-wide association studies
GZM	granzyme
HD	healthy donors
HLA	human leukocyte antigen
HPRT	hypoxanthine-guanine phosphoribosyltransferase
HSCs	hepatic stellate cells
IBD	inflammatory bowel disease
IFN	interferon
IL	interleukin
IL-15Rα	interleukin 15 receptor subunit α
ILCs	innate lymphoid cells
JAK	janus kinase
KCs	kupffer cells
Lck	lymphocyte cell-specific protein-tyrosine kinase
LPS	lipopolysaccharide
LSECs	sinusoidal endothelial cells
MAC	membrane attack complex
MACS	magnetic-activated cell sorting
MAIT cells	mucosa-associated invariant T cells
MASLD	metabolic dysfunction-associated steatotic liver disease
Mcl-1	Myeloid Cell Leukemia 1 apoptosis regulator

MHC	major histocompatibility complex
mRNA	messenger RNA
MSigDB	molecular signatures database
N	naive
NFAT	Ca^{2+}/ nuclear factor of activated T cells
NF-κB	nuclear factor kappa-light-chain-enhancer of activated B cells
NK cells	natural killer cells
NKG2D	killer cell lectin like receptor K1
ORA	over-representation analysis
p-ANCA	anti-neutrophil cytoplasmic antibodies
PAR-1	protease-activated receptor-1
PBC	primary biliary cholangitis
PBG	peribiliary gland
PBMCs	peripheral blood mononuclear cell
PBS	phosphate-buffered saline
PD-1	programmed cell death 1
PD-L1	CD274 molecule/programmed cell death 1 ligand 1
PI3K-AKT-mTOR	phosphoinositide 3-kinase / protein kinase B / mechanistic target of rapamycin
PLCγ	phospholipase C gamma 1
PPAR	peroxisome proliferator-activated receptor
PSC	primary sclerosing cholangitis
Ras/MAPK	rat sarcoma / mitogen-activated protein kinase
RBCs	red blood cells
rRNA	ribosomal RNA
S100A8	S100 calcium binding protein A8
sNucSeq	single-nucleus RNA sequencing
STAT	signal transducer and activator of transcription

SYK	spleen tyrosine kinase
TCR	T cell receptor
Th17	T helper-17
TNF	tumor necrosis factor
UDCA	ursodeoxycholic acid
UMAP	uniform manifold approximation and projection
µm	micrometers

Gene nomenclature

Gene	Protein
ACTA2	actin alpha 2, smooth muscle
BACH2	BACH transcriptional regulator 2
CCL20	C-C motif chemokine ligand 20
CD28	CD28 molecule
CFTR	CF transmembrane conductance regulator
CTLA4	cytotoxic T-lymphocyte associated protein 4
CXCL10	C-X-C motif chemokine ligand 10
CXCL11	C-X-C motif chemokine ligand 11
CXCL16	C-X-C motif chemokine ligand 16
CXCL9	C-X-C motif chemokine ligand 19
CXCR3	C-X-C motif chemokine receptor 3
CXCR6	C-X-C motif chemokine receptor 6
CXCR6	C-X-C motif chemokine receptor 6
CYP2E1	cytochrome P450 family 2 subfamily E member 1
FOXP1	forkhead box P1
GLUL	glutamate-ammonia ligase
GPBAR1	G protein-coupled bile acid receptor 1
GZMK	granzyme K
HAL	histidine ammonia-lyase
HLA-DPA1	major histocompatibility complex, class II, DP alpha 1
HLA-DQB1	major histocompatibility complex, class II, DQ beta 1
HLA-DRB1	major histocompatibility complex, class II, DR beta 1
HNF4A	hepatocyte nuclear factor 4 alpha
IFNA1	interferon alpha 1

IFNB1	interferon beta 1
IFNG	interferon γ
IL12A	interleukin 12A
IL12B	interleukin 12B
Il15	mouse interleukin 15
IL15	interleukin 15
IL15RA	interleukin 15 receptor subunit alpha
Il15ra	mouse interleukin 15 receptor subunit alpha
IL1B	interleukin 1 beta
IL2	interleukin 2
IL21	interleukin 21
IL23A	interleukin 23 subunit alpha
IL2RA	interleukin 2 receptor subunit alpha
KLRB1	killer cell lectin like receptor B1
KLRK1	killer cell lectin like receptor K1
KRT19	keratin 19
KRT7	keratin 7
PDCD1	programmed cell death 1
RGS1	regulator of G protein signaling 1
SDS	serine dehydratase
SEMA4D	semaphorin 4D
SH2B3	SH2B adaptor protein 3
TGFB1	Transforming growth factor beta 1
TNF	tumor necrosis factor
TOX	thymocyte selection associated high mobility group box
TRDV2	T cell receptor delta variable 2

TRGV9	T cell receptor gamma variable 9

Abstract

Primary sclerosing cholangitis (PSC) is a chronic cholestatic liver disease characterized by progressive bile duct inflammation and fibrosis, frequently leading to cirrhosis and cholangiocarcinoma. Despite clear immune involvement, disease-modifying therapies are lacking, and the mechanisms driving biliary injury remain incompletely understood. $CD8^+$ T cells are enriched in inflamed portal tracts and localize in close proximity to cholangiocytes, yet their functional role in PSC has not been fully defined. Interleukin-15 (IL-15) is a pleiotropic cytokine capable of inducing antigen-independent bystander activation of $CD8^+$ T cells, but its relevance in PSC has not previously been addressed.

This thesis comprehensively characterizes $CD8^+$ T cell phenotypes in PSC and investigates the role of IL-15 within the biliary microenvironment. Spectral flow cytometry demonstrated that peripheral blood $CD8^+$ T cells from individuals with PSC, even at early disease stages, display increased expression of activation and exhaustion markers: HLA-DR and PD-1, together with altered granzyme profiles consistent with IL-15 exposure. Single-cell CITE-sequencing of intrahepatic $CD8^+$ T cells from end-stage PSC livers revealed a predominance of effector memory populations expressing MHC class II molecules, interferon-γ, NK cell-associated receptors, and cytotoxic effector molecules, with enrichment of IL-15-associated STAT5 signaling pathways.

Single-nucleus RNA sequencing across PSC stages identified expansion of bystander-activated effector memory $CD8^+$ T cell subsets with disease progression and revealed biliary epithelial cells as a relevant source of IL-15 and IL-15Rα. Increased *IL15* expression was detectable already in early PSC, whereas *IL15RA* expression increased with liver disease severity. These findings were validated in vitro using human cholangiocyte organoids and biliary epithelial cell lines, in which interferon-γ robustly induced IL-15 and IL-15Rα expression. Spatial transcriptomics demonstrated close proximity of activated $CD8^+$ T cells and IL-15–expressing cholangiocytes within inflamed portal areas. Finally, a murine model of acute cholangitis confirmed induction of IL-15 mediated bystander activation of endogenous $CD8^+$ T cells *in vivo*.

In conclusion, this work identifies an IL-15-associated bystander-activated $CD8^+$ T cell phenotype in PSC and provides evidence that biliary epithelial cells may contribute to shaping this immune response. These findings advance the understanding of immune-mediated biliary injury in PSC and highlight IL-15 signaling as a potential therapeutic target.

Zusammenfassung

Die primär sklerosierende Cholangitis (PSC) ist eine chronische cholestatische Lebererkrankung, die durch eine fortschreitende Entzündung der intra- und extrahepatischen Gallenwege gekennzeichnet ist und die Entstehung von Cholangiokarzinomen übergeht. Trotz klarer Hinweise auf eine immunvermittelte Pathogenese fehlen bislang krankheitsmodifizierende Therapien, und die Mechanismen der biliären Gewebeschädigung sind nur unvollständig verstanden. $CD8^+$ T-Zellen sind in entzündeten Portaltrakten angereichert und befinden sich in enger räumlicher Nähe zu Cholangiocyten. Ihre funktionelle Rolle in der PSC ist jedoch bislang nicht eindeutig geklärt. Interleukin-15 (IL-15) ist ein pleiotropes Zytokin, das eine antigenunabhängige, sogenannte bystander-Aktivierung von $CD8^+$ T-Zellen vermitteln kann, dessen Bedeutung für die PSC bisher nicht untersucht wurde.

Diese Arbeit charakterisiert umfassend die Phänotypen von $CD8^+$ T-Zellen bei PSC und untersucht die Rolle von IL-15 im biliären Mikromilieu. Mittels spektraler Durchflusszytometrie wurde gezeigt, dass $CD8^+$ T-Zellen aus dem peripheren Blut von Personen mit PSC bereits in frühen Krankheitsstadien eine erhöhte Expression der Aktivierungs- und Erschöpfungsmarker HLA-DR und PD-1 sowie veränderte Granzym-Profile aufweisen, die mit einer IL-15-Exposition vereinbar sind. Einzelzellsequenzierung intrahepatischer $CD8^+$ T-Zellen aus PSC-Lebern mit fortgeschrittener Fibrose zeigte eine Dominanz von Effektor-Gedächtnis-Populationen mit Expression von MHC-Klasse-II-Molekülen, Interferon-γ, NK-Zell-assoziierten Rezeptoren und zytotoxischen Effektormolekülen sowie eine Anreicherung IL-15-assoziierter STAT5-Signalwege.

Die Einzelkern-RNA-Sequenzierung über verschiedene Krankheitsstadien hinweg identifizierte eine Zunahme bystander-aktivierter Effektor-Gedächtnis-$CD8^+$ T-Zell-Subpopulationen im Krankheitsverlauf und wies biliäre Epithelzellen als eine wesentliche Quelle von IL-15 und IL-15Rα nach. Während eine erhöhte *IL15*-Expression bereits in frühen Stadien der PSC nachweisbar war, nahm die *IL15RA*-Expression mit der Schwere der Lebererkrankung zu. Diese Befunde wurden *in vitro* in humanen Cholangiocyten-Organoidkulturen und biliären Epithelzelllinien validiert, in denen Interferon-γ eine starke Induktion von IL-15 und IL-15Rα bewirkte. Räumliche Transkriptomanalysen zeigten eine enge räumliche Beziehung zwischen aktivierten $CD8^+$ T-Zellen und IL-15-exprimierenden Cholangiocyten in entzündeten Portalfeldern. Schließlich bestätigte ein murines Modell der akuten Cholangitis die Induktion von IL-15-vermittelter bystander-Aktivierung von endogenen $CD8^+$ T-Zellen *in vivo*.

Zusammenfassend identifiziert diese Arbeit einen IL-15-assoziierten, bystander-aktivierten $CD8^+$ T-Zell-Phänotyp bei PSC und liefert Hinweise darauf, dass biliäre Epithelzellen zur lokalen Prägung dieser Immunantwort beitragen könnten. Diese Ergebnisse erweitern das Verständnis der immunvermittelten biliären Schädigung bei PSC und identifizieren die IL-15-Signalübertragung als potenzielles therapeutisches Ziel.

1 Introduction

1.1 Primary sclerosing cholangitis: clinical, pathological and therapeutic overview

Primary sclerosing cholangitis (PSC) is a cholestatic autoimmune liver disease affecting the medium- to large-sized bile ducts[1]. It is considered a rare condition, with an incidence of approximately 0.6 per 100,000 individuals per year. The mean age at diagnosis is 15 years in pediatric cases and around 35 years in adults, with a slight male predominance[2]. In addition, 50-70 % of individuals with PSC also have inflammatory bowel disease (IBD), most often ulcerative colitis, which accounts for 76 % of these cases[3].

A hallmark histological feature of PSC is the periductal "onion-skin" fibrosis, which contributes to biliary strictures and impaired bile flow. As the disease progresses, fibrosis often advances to decompensated liver cirrhosis. Beyond its primary burden, PSC is associated with a higher incidence of additional autoimmune disorders, such as celiac disease, and significantly elevates the risk of malignancy[4]. Notably, the risk of developing cholangiocarcinoma (CCA) is increased over 400-fold in individuals with PSC[5,6]. CCA is responsible for 32 % of deaths among patients with PSC, compared with 15 % due to liver failure and 9 % related to complications following liver transplantation[7]. Key features of PSC-progression over different stages of the disease are summarized in Figure 1.

At present, liver transplantation is the only curative option, although the disease recurs in 10-27 % of patients after transplantation[8]. However, recurrent bacterial cholangitis is also common and can significantly reduce the probability of successful liver transplantation[9].

The strong association between PSC and IBD has directed attention toward the gut and biliary microbiome. 16S ribosomal RNA sequencing has revealed reduced microbial diversity and altered microbial abundance in the gut of people with PSC[10]. Additionally, bile duct colonization with species like *Enterococcus faecalis* has been linked to poor survival, and gut dysbiosis exacerbates symptoms in PSC mouse models[11-13].

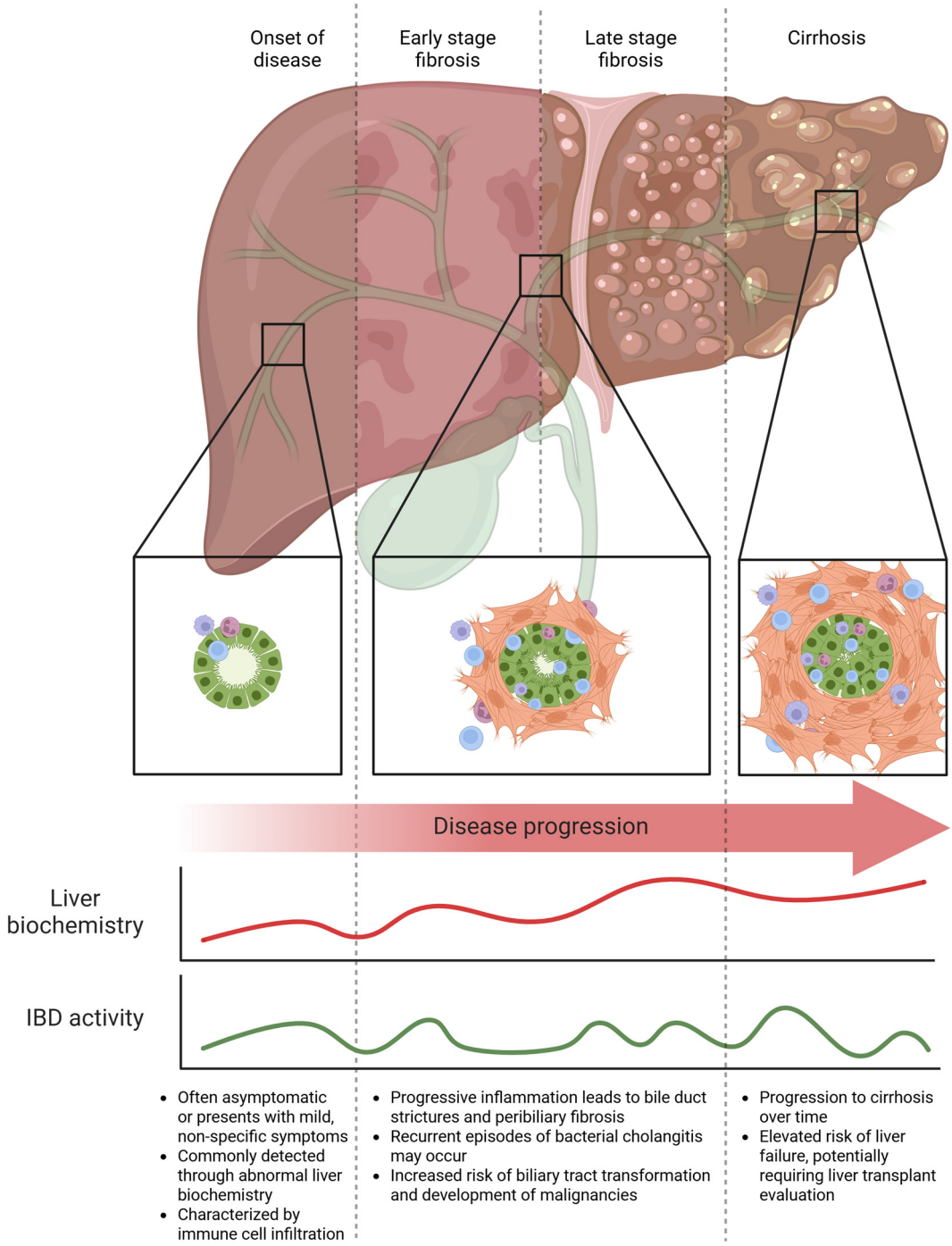

Figure 1: **Pathological and clinical progression of primary sclerosing cholangitis (PSC).**

Graphical representation of the pathological and clinical evolution of PSC from early to end stages. The illustration highlights four key disease stages: disease onset, early stage fibrosis, late stage fibrosis, and cirrhosis. In the early phase, PSC is often asymptomatic or associated with mild, non-specific symptoms and is typically detected through abnormal liver biochemistry. With disease progression, chronic inflammation promotes fibrotic remodeling, bile duct strictures, and an increased risk of recurrent bacterial cholangitis and malignant transformation. In advanced stages, extensive peribiliary fibrosis culminates in biliary cirrhosis and progressive liver dysfunction, frequently necessitating evaluation for liver transplantation. Throughout the disease course, liver biochemistry may fluctuate but shows an overall increasing trend, whereas inflammatory bowel disease (IBD) activity remains highly variable across all stages of PSC. Created with Biorender.com.

Research also focuses on the target cells of PSC, biliary epithelial cells (BECs), which line the bile ducts and regulate bile acid homeostasis. In PSC, BECs exhibit an activated phenotype characterized by cholangiocyte proliferation and peribiliary gland (PBG) expansion[14,15]. PBGs, located in large intra- and extrahepatic bile ducts, house progenitor cells vital for bile duct regeneration[16]. Furthermore, activated BECs have been described to interact with hepatic stellate cells (HSCs) and myofibroblasts, contributing to fibrogenesis[17]. Moreover, chronic exposure to toxic bile and inflammatory cytokines like interleukin (IL)-6 from BECs may drive malignancy development in PSC[18,19].

Genetic factors also play a significant role, which defines PSC as a disease with auto-immune background. Genes such as *GPBAR1* (encoding TGR5) and *CFTR* are crucial in maintaining the protective bicarbonate "umbrella" around cholangiocytes, which shields them from bile acid toxicity. Disruption of this layer is a hallmark of bile acid-induced damage in PSC[20,21]. Familial clustering studies report an 11-fold increased PSC risk among siblings[22], and genome-wide association studies (GWAS) have identified over 20 risk loci[23]. Interestingly, fewer than 10 of the 150 IBD-associated genes overlap with PSC, suggesting PSC-associated IBD is a distinct phenotype[24]. Most PSC-linked genes are involved in immune regulation, reinforcing the autoimmune background[25].

Despite the severity of PSC, effective treatment options remain limited[26]. Ursodeoxycholic acid (UDCA), a naturally occurring bile acid, is the most widely used pharmacologic treatment for cholestatic liver diseases. However, its precise mechanism of action remains unclear[27]. While UDCA has demonstrated efficacy in primary biliary cholangitis (PBC), such benefits have not been confirmed for PSC[28]. The largest double-blind randomized controlled trial involving 218 people with PSC treated with 17-23 mg/kg/day of UDCA versus placebo over five years showed non-significant reductions in alkaline phosphatase (ALP) and alanine aminotransferase (ALT) levels, with no impact on symptoms, quality of life, or clinical outcomes[29]. A five-year follow-up study involving 198 people similarly found no improvement in transplant-free survival[30]. Higher doses of UDCA (28-30 mg/kg/day) were associated with increased risk of mortality, liver transplantation, and severe adverse effects[31].

Current clinical guidelines reflect this limited benefit. The American Association for the Study of Liver Diseases (AASLD) and the European Association for the Study of the Liver (EASL) recommend treatment with UDCA at 13-23 mg/kg/day and 15-20 mg/kg/day, respectively[26,32]. Apart from UDCA, the EASL guidelines also advise endoscopic treatment of clinically significant biliary strictures, surveillance for complications, regular colonoscopy in cases with IBD, and supportive measures such as

vitamin supplementation[32]. These moderately effective interventions underscore the pressing need for new therapeutic strategies.

One promising candidate is norursodeoxycholic acid, a side chain–shortened homologue of UDCA. In animal models of PSC, norursodeoxycholic has demonstrated anti-cholestatic, anti-inflammatory, and anti-fibrotic effects[33]. A phase II clinical trial evaluating norursodeoxycholic (500-1500 mg/day for 12 weeks) reported significant reductions in ALP levels compared to placebo[34]. A phase III trial (NCT03872921) has recently reported efficacy in slowing disease progression[35].

Other novel therapeutic approaches include peroxisome proliferator-activated receptor (PPAR) agonists. PPARs are ligand-activated nuclear receptors involved in regulating hepatic transport and bile acid homeostasis[36]. Additionally, there is growing interest in targeting the gut-liver axis. People with PSC frequently suffer from recurrent bacterial cholangitis. Small studies have shown that antibiotics such as metronidazole and vancomycin may lower ALP levels in people with PSC[37,38].

Given the autoimmune nature of PSC, classical immunosuppressive agents like methotrexate and azathioprine have been tested but failed to demonstrate measurable benefit[39,40]. With the rise of biologic therapies in autoimmune diseases, several trials have investigated their efficacy in PSC, including vedolizumab (anti-α4β7 integrin) and infliximab (anti-tumor necrosis factor [TNF])[41,42]. However, none have shown meaningful improvements in disease progression[43].

Although several experimental therapies are under investigation, a deeper understanding of the immunological mechanisms driving PSC remains urgently needed. In particular, the role of liver-resident and infiltrating immune cells in mediating bile duct inflammation and fibrosis is not fully understood.

1.2 Pathogenic mechanisms in PSC: Molecular and immunological perspectives

The liver is a unique immunological organ that serves as a hub for immune surveillance, tolerance, and detoxification[44]. Its anatomical location and partial blood supply via the portal vein expose it to constant influxes of microbial products, food antigens, and environmental toxins, necessitating a tightly regulated balance between immune activation and tolerance[45]. Over the past decades, extensive research has identified both non-immune and immune-related contributors to PSC pathogenesis. Therefore, this

chapter outlines the complex molecular and immunological networks to drive the pathogenesis of PSC.

Early observations of elevated IgG levels and perinuclear anti-neutrophil cytoplasmic antibodies (p-ANCA) in 10-15 % of people with PSC hinted at autoimmune involvement. However, these markers are not diagnostic, and immunosuppressive therapies have largely failed in PSC[40,46]. The liver's immune environment is enriched with innate immune cells, including Kupffer cells (KCs), natural killer cells (NK cells), and unconventional T cells like mucosa-associated invariant T cells (MAIT cells)[47].

Several PSC-associated GWAS genes, such as *NFKB1* and *REL*, implicate altered innate immunity. Neutrophil infiltration in portal areas and bile ducts, along with elevated IL-8, C-C motif chemokine ligand (CCL)-24, and S100A8 in bile, suggests neutrophil-mediated inflammation[48,49]. Neutrophils are critical in acute infection responses, and their recruitment is supported by chemokines like IL-8 and CCL24[50-52].

Monocytes from people with PSC show a pro-inflammatory response to *Enterococcus faecalis* and *Candida albicans*, producing high levels of IL-1β and IL-6. These monocytes can differentiate into KCs, which accumulate around inflamed bile ducts[53-57]. Dendritic cells (DCs) are also found in higher numbers in portal areas, though their role remains less defined[58,59]. Recent findings linked the HLA-DPA102:01~B101:01 haplotype with NK cell activation via cholangiocyte interaction, reinforcing the role of HLA class II in immune cell activation[60].

Unconventional T cells such as MAIT and γδ T cells, which combine innate and adaptive immune features, are enriched in the liver. MAIT cells, activated by bacterial riboflavin metabolites via MR1, produce TNF and interferon (IFN)-γ upon stimulation. In PSC, MAIT cell frequencies in peripheral blood are reduced, and they show impaired cytokine production despite high activation[61,62]. Sulfated bile acids may act as ligands for MAIT cells, though their role in PSC is unclear[63]. γδ T cells in PSC produce elevated IL-17 and are major IL-17 sources in PSC mouse models[64,65].

Genetic studies have further linked T cell dysregulation to PSC. A family with autosomal dominant PSC carried a *SEMA4D* mutation affecting cluster of differentiation (CD)100, enhancing T helper-17 (Th17) differentiation[66,67]. Th17-skewed responses are common in people with PSC and disease models[68]. $CD4^+$ tissue-resident memory T cells in PSC bile ducts produce IL-17, and PSC-associated *miR4464-BACH2* variants promote Th17 polarization[49,69,70]. This is in line with the findings that most PSC GWAS loci are related

to T cell function, including *IL2, IL21*, *IL2RA*, *SH2B3*, *CTLA4*, *CD28*, *CCL20*, *FOXP1*, and *BACH2*[23].

T cells are the most abundant immune cells in PSC-inflamed portal areas, suggesting active interaction with BECs[71]. Cholangiocytes have been shown to recruit Th17 cells via C-C-chemokinrezeptor (CCR)-6[72]. Advances in single-cell and spatial transcriptomics have enabled detailed mapping of cell-cell interactions. For example, a PSC-enriched *KRT7*$^+$ *HNF4A*$^+$ cholangiocyte-like hepatocyte population shows increased TNF and IFN-γ signaling[73]. CD8$^+$ T cells are often found in close proximity to cholangiocytes in early PSC. Interactions occur via PD-1/PD-L1 signaling, which is enhanced by IL-17-induced PD-L1 upregulation on cholangiocytes[74]. However, the phenotype and drivers of CD8$^+$ T cell proximity to cholangiocytes, as well as their role in hepato-biliary inflammation, remain unresolved.

CD8$^+$ T cells remain understudied despite being the dominant T cell population in inflamed bile ducts and portal areas[49,75,76]. Their phenotype and role in PSC pathogenesis remain unclear.

1.3 CD8$^+$ T cells in liver immunology

CD8$^+$ T cells, alongside CD4$^+$ T cells, are a subset of conventional T lymphocytes that express the T cell receptor (TCR) chains α and β. CD8$^+$ T cells are antigen specific activated via major histocompatibility complex (MHC) class I (HLA-A, HLA-B, and HLA-C)-restricted peptide presentation. MHC class I molecules are expressed by nearly all cells in the human body and present intracellular antigens from pathogens such as viruses or tumor cells to CD8$^+$ T cells[77]. T cells develop from progenitor cells in the bone marrow and undergo maturation in the thymus. From there, naive T cells are released into circulation[78]. Their differentiation into effector T cells requires strong TCR signaling alongside co-stimulation through CD28[79]. Co-stimulatory ligands for CD28, such as CD80 or CD86, are expressed only by professional antigen-presenting cells (APCs) including monocytes, DCs, and B cells. Upon receiving these activating signals from APCs, CD8$^+$ T cells initiate downstream signaling via phosphorylation of CD3ζ by the Lymphocyte Cell-Specific Protein-Tyrosine Kinase (Lck), activating pathways including Phospholipase C Gamma 1 (PLCγ), Ca^{2+}/ nuclear factor of activated T cells (NFAT), Rat Sarcoma / Mitogen-Activated Protein Kinase (Ras/MAPK), and Nuclear Factor kappa-light-chain-enhancer of activated B cells (NF-κB) signaling cascades[80]. CD28 co-signaling is essential for maintaining Phosphoinositide 3-Kinase - Protein Kinase B -

Mechanistic Target of Rapamycin (PI3K-AKT-mTOR) signaling cascade signaling, promoting all together survival, proliferation, and effector function[81]. Upon activation, $CD8^+$ T cells produce cytokines such as IFN-γ, TNF, and IL-17. They also exert cytotoxic functions through the release of proteases (granzymes) and the pore-forming protein perforin, inducing target cell death[82]. Once the pathogen has been eliminated, a fraction of effector T cells transitions into memory T cells, which can mount a rapid response upon reinfection. Memory $CD8^+$ T cells have a lower activation threshold and can be triggered by non-professional APCs without CD28 co-stimulation[83].

Understanding liver T cell-mediated immunity requires consideration of its unique anatomical features. The liver is supplied with oxygenated blood via the hepatic artery and with nutrient- and microbe-rich blood through the portal vein[84]. These blood sources mix within the liver sinusoids, which drain into the central vein[85]. Sinusoids are lined by liver sinusoidal endothelial cells (LSECs), which lack tight junctions and a continuous basement membrane[86]. LSECs contain fenestrae that allow molecular exchange between blood and hepatocytes. Hepatocytes are arranged in double rows between sinusoids and secrete bile into canaliculi. Bile flows in the opposite direction of blood flow, ultimately reaching the bile ducts, which are composed of cholangiocytes and drain into the gallbladder or gut[84].

These anatomical and functional characteristics create a unique microenvironment for T cell activation. T cells play a central role in maintaining liver homeostasis and mediating inflammation. Within the hepatic environment, they can complete their full differentiation cycle, including: antigen recognition, effector differentiation, and memory formation[87]. A skewed $CD4^+$/$CD8^+$ T cell ratio favoring $CD8^+$ T cells has been observed in the liver, suggesting tissue-specific modulation of T cell responses[88]. Typically, naive $CD8^+$ T cells circulate between blood and lymphoid tissues. However, Bertolino et al. (2001) proposed the liver as a site for naive $CD8^+$ T cell priming[89]. LSEC-mediated activation can induce $CD8^+$ T cell effector functions without cytotoxic capabilities[90], and liver-resident DCs are less efficient at $CD8^+$ T cell priming compared to DCs from other tissues[91].

Regardless of the activating cell, effector $CD8^+$ T cells enter the liver within the sinusoids by binding $CD44^+$ platelets, which themselves adhere to LSECs[92]. Following pathogen clearance, up to 5 % of effector $CD8^+$ T cells transition into memory T cells[93]. Memory T cells exist either in circulation or as tissue-resident subsets that remain in non-lymphoid organs to provide rapid immune responses upon reinfection[94]. In the human liver, approximately 60 % of $CD8^+$ T cells express tissue-residency markers CD103 and

CD69[95]. Additionally, toll like receptor 9-induced liver inflammation has been shown to promote antigen-independent $CD8^+$ T cell priming and memory formation[96].

Cytokines in the hepatic microenvironment, particularly IL-15, are crucial for memory $CD8^+$ T cell development. However, IL-15-driven damage of the liver parenchyma has been shown in various chronic liver diseases[97-100].

1.4 IL-15 biology: its role in T cell activation and auto-aggression

The cytokine IL-15 is composed of four α-helices and belongs to a group of cytokines signaling through the common γ-chain receptor (CD132)[101,102]. Other members of this family include IL-2, IL-4, IL-7, IL-9, and IL-21, all of which signal via CD132 in combination with distinct co-receptors. For IL-15 and IL-2, the co-receptor is CD122 (Interleukin-2/15 Receptor Subunit Beta)[103]. Upon IL-15 binding, multiple downstream signaling cascades are activated. The major signaling pathway is signal transducer and activator of transcription (STAT)5-mediated and summarized in Figure 2. The Janus kinase (JAK)-STAT5 pathway leads to phosphorylation and dimerization of STAT5, which in turn activates anti-apoptotic proteins Bcl-2 and Mcl-1[104]. IL-15 also activates the PI3K-AKT-mTOR pathway, promoting cell proliferation and survival. These pathways collectively induce expression of Eomesodermin (Eomes), which upregulates CD122, establishing a positive feedback loop[105]. Additionally, phosphorylated AKT induces the transcription factor T-bet, enhancing expression of inflammatory and cytotoxic molecules such as IFN-γ and Granzyme B[106].

The sources of IL-15 are as diverse as its signaling pathways. Major producers include monocytes, DCs, and epithelial cells[107]. Unlike most cytokines, IL-15 is rarely secreted by the producing cell. Instead, it typically signals through trans-presentation, wherein IL-15 is presented on the cell surface in complex with interleukin 15 receptor subunit α (IL-15Rα). These IL-15/IL-15Rα complexes are assembled in the endoplasmic reticulum and Golgi apparatus before being transported to the cell surface[108]. In rare cases, cis-signaling is possible, where the IL-15-producing cell expresses all three necessary receptors (IL-15Rα, CD122, and CD132), allowing for self-activation, though this is tightly regulated[107]. A third mode involves the release of IL-15 or IL-15/IL-15Rα complexes into the extracellular space[109,110].

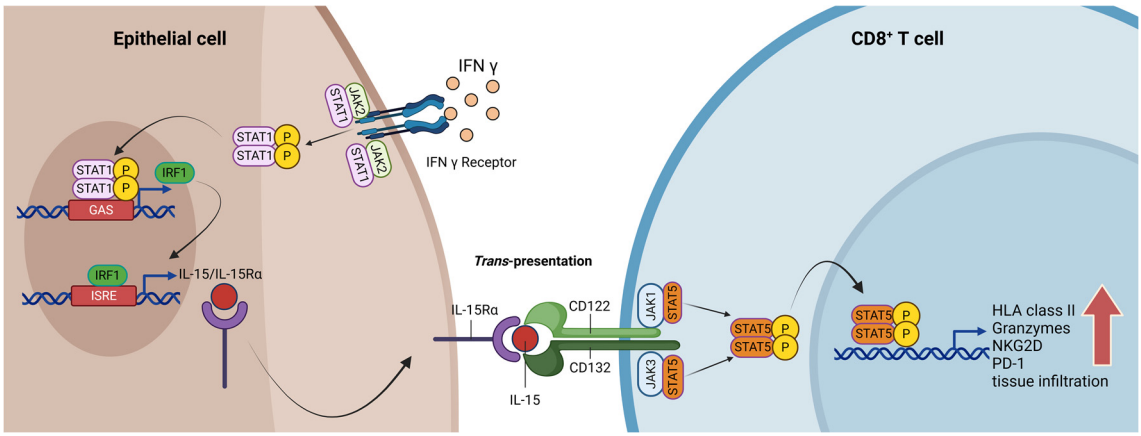

Figure 2: **IL-15/IL-15Rα expression, trans-presentation, and downstream signaling in CD8⁺ T cells.**

Schematic overview of IFNγ-induced IL-15 expression and signaling. Binding of IFNγ to the IFNγ receptor triggers phosphorylation of Signal Transducer and Activator of Transcription 1 (STAT1) by Janus kinase 2 (JAK2). Phosphorylated STAT1 forms dimers that translocate to the nucleus and bind gamma-activated sequence (GAS) elements, inducing expression of Interferon Regulatory Factor 1 (IRF1). IRF1 subsequently binds to interferon-stimulated response elements (ISRE) within the promoter regions of *IL15* and *IL15RA*. Following translation, the IL-15/IL-15Rα complex is transported to the cell surface and trans-presented to CD8⁺ T cells. IL-15 binding occurs via the CD122/CD132 heterodimer, leading to phosphorylation of STAT5 by JAK1 and JAK3, followed by STAT5 dimerization and nuclear translocation. Enhanced IL-15 signaling promotes expression of HLA class II molecules, granzymes, the NK cell receptor NKG2D, and the inhibitory receptor PD-1 in CD8⁺ T cells, and supports increased tissue infiltration and effector differentiation. Created with Biorender.com.

IL-15 production increases in response to infection, inflammation, and prolonged cellular stress[111]. Various stimuli have been shown to upregulate *IL15* expression *in vitro* in DCs, monocytes, macrophages, and epithelial cells. Potent inducers include bacterial components like lipopolysaccharide (LPS) and polyinosinic:polycytidylic acid, as well as type I and II interferons (IFN-α, IFN-β, and IFN-γ)[112-115]. Notably, IFN-γ has been identified as the most potent inducer of IL-15 production[116]. Interestingly, IL-15 signaling can also be enhanced through recycling of pre-formed IL-15/IL-15Rα complexes to the cell surface, independent of new gene transcription or translation[117].

Because CD122 and CD132 are expressed on various immune cells, including NK cells, monocytes, T cells, and DCs, IL-15 can induce responses across multiple cell types. Early studies found the most significant effects in NK cells and memory CD8⁺ T cells in IL-15-deficient mice[118]. IL-15 also lowers the TCR signaling threshold required for CD8⁺ T cell activation and enhances their IFN-γ production and proliferation[119,120].

Exposure of memory CD8⁺ T cells to IL-15 often induces an NK cell-like phenotype, characterized by the expression of NK cell receptors and increased cytotoxicity[107,121]. Meresse et al. (2004) first described TCRαβ⁺ CD8⁺ T cells with increased killer cell lectin like receptor K1 (NKG2D) expression in response to IL-15 dysregulation. These cells contributed to intestinal tissue damage in celiac disease via NK-like, TCR-independent

cytotoxicity[122]. Dudek et al. (2021) later identified a CXCR6$^+$ PD-1^{high} CD8$^+$ T cell population in a mouse model of Metabolic Dysfunction-Associated Steatotic Liver Disease (MASLD), driven by IL-15. These cells responded to metabolic stimuli like acetate and ATP and exhibited MHC class I-independent cytotoxicity[99]. Preliminary, unpublished data suggest that this phenotype may differ slightly between mice and humans. Further studies in chronic liver disease identified IL-15-induced HLA-DR$^+$ CD38$^+$ CD8$^+$ T cells in human hepatitis A and B-infected livers. These cells also exhibited antigen-independent killing[97,100].

1.5 Knowledge gap and rationale for this study

PSC remains a chronic, progressive liver disease for which no effective medical treatment is currently available. Liver transplantation is the only curative option, but disease recurrence and complications significantly limit long-term success[7,8]. Despite decades of research, the precise molecular and immunological mechanisms driving PSC pathogenesis remain poorly understood[123]. This limited understanding hampers the development of targeted therapies.

Although PSC is widely considered an immune-mediated disease, most studies have focused on innate immune mechanisms or CD4$^+$ T cell-driven inflammation[47,68,69]. In contrast, the role of CD8$^+$ T cells, despite their predominance in inflamed bile ducts and portal tracts, has received minimal attention[49,74]. Their phenotype, function, and potential contribution to tissue damage in PSC are largely unexplored.

IL-15 is a cytokine known to promote survival, proliferation, and cytotoxicity of CD8$^+$ T cells[104-106]. In several chronic liver diseases, including viral hepatitis and MASLD, IL-15 has been shown to drive auto-aggressive CD8$^+$ T cell populations that contribute to tissue damage in an antigen-independent manner[97,99,100]. Due to their antigen-independent activation via IL-15, these cells are also called “bystander-activated CD8$^+$ T cells”, which will be used in the following sections to describe this cell type.

Despite being the predominant T cell population in inflamed portal areas and bile ducts, the role of CD8$^+$ T cells in PSC remains poorly understood. Their activation state, effector function, and potential contribution to biliary injury have not been systematically investigated. IL-15, a cytokine known to drive cytotoxicity and auto-aggressive killing of target cells in CD8$^+$ T cells, may play a critical role in this context. However, IL-15 has not been studied in PSC to date, its expression levels, cellular sources, and influence on

$CD8^+$ T cell behavior are entirely unknown. This represents a significant gap in our understanding of PSC pathogenesis and limits the identification of novel therapeutic targets.

This study aims to address this gap by characterizing IL-15-driven $CD8^+$ T cell responses in PSC and evaluating their potential role in mediating biliary injury.

2 Aim of study

The aim of this study was to investigate the IL-15-mediated interaction between $CD8^+$ T cells and cholangiocytes in the context of PSC. We hypothesized that cholangiocytes act as a local source of IL-15 within the inflamed biliary microenvironment and thereby promote an antigen-independent, bystander-activated phenotype in $CD8^+$ T cells, contributing to chronic biliary inflammation and tissue injury in PSC. Furthermore, we hypothesized that this interaction establishes a self-sustaining inflammatory circuit driven by reciprocal signaling between cholangiocytes and $CD8^+$ T cells.

Accordingly, the specific aims of this study were:

(i) to define the phenotype and activation state of circulating and intrahepatic $CD8^+$ T cells in PSC, with a particular focus on features associated with cytokine-driven, bystander activation;

(ii) to identify the cellular sources and spatial distribution of IL-15 and IL-15Rα within the PSC liver microenvironment;

(iii) to determine the spatial relationship and potential interaction between IL-15–expressing cholangiocytes and $CD8^+$ T cells in inflamed bile ducts; and

(iv) to functionally assess the capacity of cholangiocytes to induce IL-15–dependent $CD8^+$ T cell activation *in vitro* and *in vivo*.

To this end, the phenotype of intrahepatic and circulating $CD8^+$ T cells in PSC was defined using spectral flow cytometry and single-cell RNA sequencing. IL-15 expression patterns within the PSC liver microenvironment were characterized using single-nucleus RNA sequencing, and spatial transcriptomics was applied to assess the proximity and interaction between $CD8^+$ T cells and cholangiocytes. To explore potential mechanisms underlying IL-15 induction in cholangiocytes, *in vitro* stimulation experiments were conducted using patient-derived organoid cultures and co-culture systems with $CD8^+$ T cells. Finally, the IL-15-induced phenotype of $CD8^+$ T cells was functionally characterized in a murine model of acute cholangitis. Together, these combined approaches aimed to provide novel insights into IL-15-driven immune dysregulation in PSC and its potential contribution to biliary injury.

3 Results

The following section presents the experimental findings of this study, which aimed to elucidate the role of IL-15 in modulating $CD8^+$ T cell responses and their interaction with cholangiocytes in the pathogenesis of PSC. $CD8^+$ T cells represent one major lymphocyte population within inflamed portal tracts and bile ducts in PSC livers[49,75], yet their functional contribution to disease progression remains poorly defined. A deeper understanding of $CD8^+$ T cell phenotypes and effector functions is therefore essential to uncover key immunopathogenic mechanisms in PSC. To address this, a combination of high-dimensional techniques was employed to define intrahepatic and circulating $CD8^+$ T cell subsets, including spectral flow cytometry, single-cell and single-nucleus mRNA sequencing, and spatial transcriptomics. Human derived cholangiocyte cell culture models were used to investigate IL-15 *in vitro*, and a translational murine model of acute cholangitis was applied to assess the impact of IL-15 on $CD8^+$ T cell activation and tissue injury *in vivo*. Together, these experiments provide mechanistic insights into IL-15-driven immune dysregulation of $CD8^+$ T cells in PSC and its potential role in mediating biliary damage.

3.1 Peripheral blood $CD8^+$ T cells from people with PSC present a distinct cytotoxic profile

To characterize systemic $CD8^+$ T cell phenotypes in PSC, spectral flow cytometry has been used for peripheral blood mononuclear cell (PBMCs) from 21 individuals with PSC. For comparison, age- and sex-matched cohorts of healthy donors (HD, n = 18) and people with primary biliary cholangitis (PBC, n = 13) were included as control groups. This approach enabled the identification of disease-specific immune alterations in $CD8^+$ T cells and their discrimination from both healthy and autoimmune cholestatic controls.

Flow cytometry-based immunophenotyping of peripheral blood $CD8^+$ T cells revealed no significant changes in overall frequency or differentiation state, including naive (N), central memory (CM), effector memory (EM), and effector memory re-expressing CD45RA (EMRA) subsets, in people with PSC (Figure 3 A-E).

However, $CD8^+$ T cells from individuals with PSC showed increased expression of the inhibitory receptor PD-1 and the activation marker HLA-DR (Figure 3 F,G). Both

molecules are associated with increased T cell activation[124,125]. Additionally, PD-1 has been linked to T cell exhaustion in the context of chronic inflammation and cancer[126].

In line with increased activation marker expression, granzyme expression was assessed. Granzymes are a family of serine proteases that primarily cleave caspases to induce target cell death[127]. Among the most prominent are granzyme (GZM)B and granzyme K.

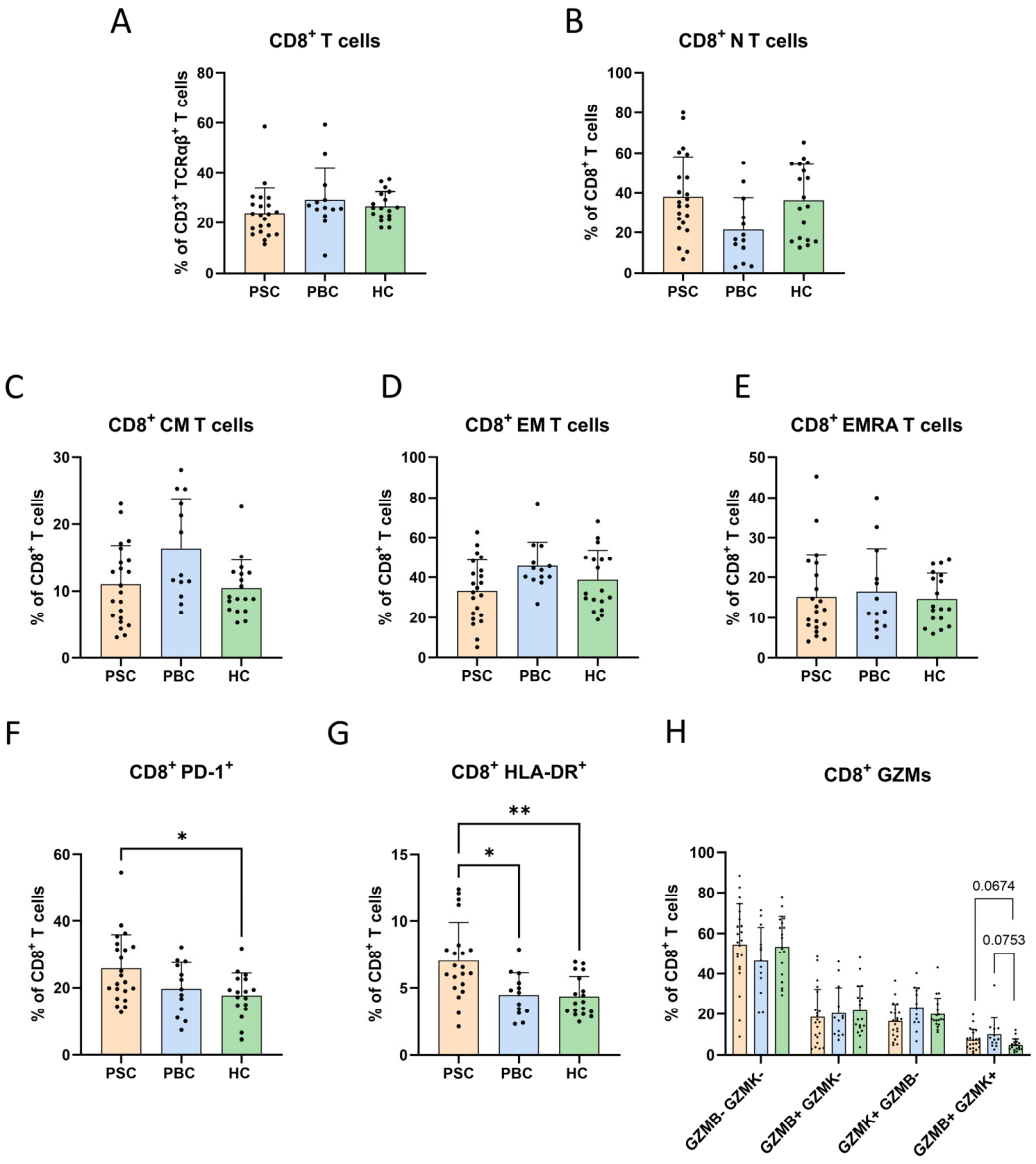

Figure 3: **Flow cytometry-based phenotypic characterization of peripheral blood CD8⁺ T cells in individuals with PSC.**

(A) Frequency of CD8⁺ T cells among total lymphocytes. **(B-E)** Distribution of CD8⁺ T cell subsets according to differentiation status, including naive (N), central memory (CM), effector memory (EM), and effector memory re-expressing CD45RA (EMRA) populations. **(F-G)** Frequencies of CD8⁺ T cells expressing the inhibitory receptor PD-1 and the activation marker HLA-DR. **(H)** Frequencies of CD8⁺ T cells expressing the cytotoxic effector molecules granzyme B (GZMB) and granzyme K (GZMK). Statistical analysis was performed using the Kruskal-Wallis test following assessment of data normality (* $p \leq 0.05$, ** $p \leq 0.01$).

Their expression levels vary depending on the activation state of $CD8^+$ T cells: GZMK is typically elevated in memory $CD8^+$ T cells and downregulated upon TCR stimulation, at which point GZMB becomes more prominent. Despite both being part of the same protease family, GZMB exhibits stronger cytotoxicity, while GZMK is more proinflammatory[128,129].

Interestingly, the frequencies of $CD8^+$ T cells expressing either GZMB or GZMK alone were not significantly altered in PSC. However, the proportion of $CD8^+$ T cells co-expressing both granzymes showed a trend towards higher expression in both cholestatic disease groups, although the difference narrowly missed statistical significance (Figure 3H). Such $GZMB^+GZMK^+$ double-positive cells are typically uncommon but have previously been observed in the synovial fluid of individuals with rheumatoid arthritis. Functional analyses of these cells identified them as a major cytokine source within inflamed joints and driver of multiple inflammatory diseases in different tissues[129].

Overall, $CD8^+$ T cells from peripheral blood of persons with PSC show increased activated phenotype, paired with altered cytotoxic profile and increased exhaustion marker expression.

3.2 Intrahepatic $CD8^+$ T cells in end-stage PSC display an effector memory phenotype with elevated cytotoxicity

To phenotype intrahepatic $CD8^+$ T cells in PSC, a publicly available single-cell Cellular Indexing of Transcriptomes and Epitopes by Sequencing (CITE)-sequencing dataset from end-stage PSC livers, published by our group (Poch et al., 2021)[69], was analyzed. In the original dataset, $CD3^+$ T cells were sequenced. For the purpose of this study, $CD8^+$ T cells were sub-grouped based on combined positive selection for CD8 mRNA and antibody-derived tag (ADT) expression, along with negative selection for CD4 expression, resulting in a purified $CD8^+$ T cell population.

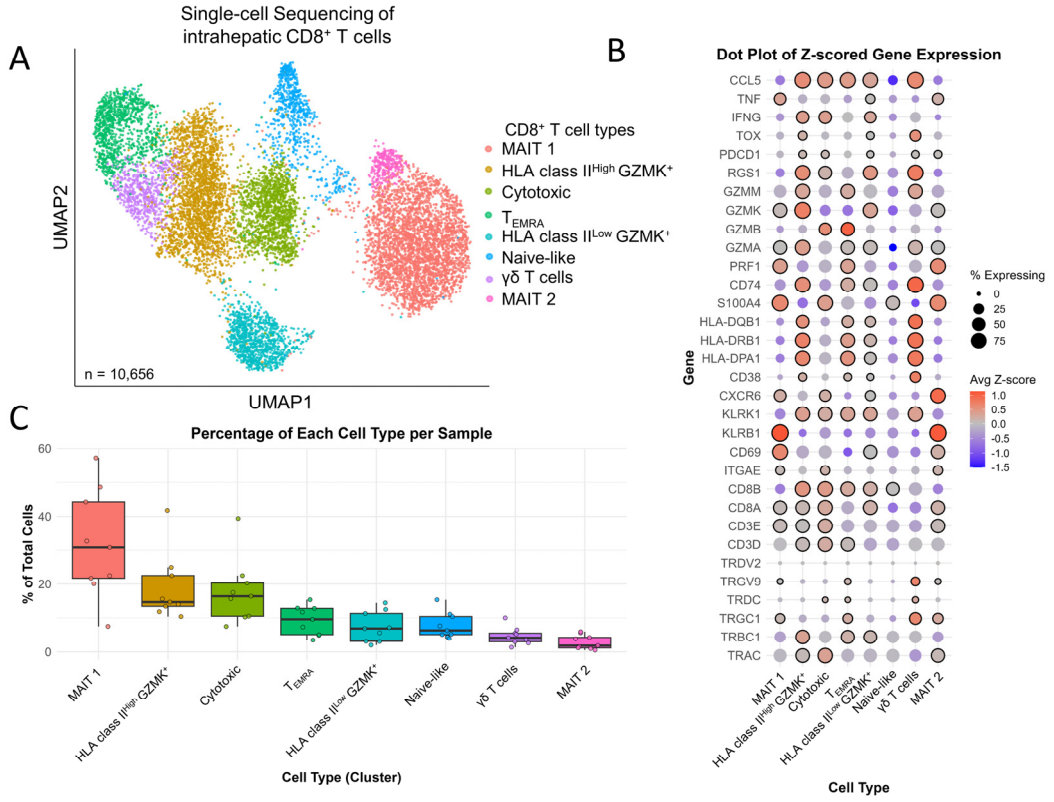

Figure 4: **Single-cell CITE-seq analysis of intrahepatic CD8⁺ T cells in end-stage PSC.**

(A) UMAP projection of intrahepatic CD8⁺ T cells isolated from end-stage PSC liver samples (n = 9), comprising mucosa-associated invariant T cells (MAIT1 and MAIT2), HLA class II^{high} GZMK⁺, cytotoxic, effector memory re-expressing CD45RA (T_{EMRA}), HLA class II^{low} GZMK⁺, naive-like, and γδ T cell clusters. **(B)** Dot plot displaying representative cluster-defining marker genes. Dot size indicates the proportion of cells expressing each gene within a cluster, while color intensity represents the z-score of scaled gene expression. **(C)** Sample-wise distribution of CD8⁺ T cell clusters across all donors.

This approach yielded a dataset comprising 10,656 CD8⁺ T cells from nine PSC liver samples. Unsupervised clustering using the Seurat pipeline identified eight distinct CD8⁺ T cell clusters (Figure 4A). Three of these clusters represented invariant T cell populations, including two MAIT cell clusters and one γδ T cell cluster. These were defined by high expression of canonical markers such as *KLRB1* (for MAIT cells) and *TRGV9*/*TRDV2* (for γδ T cells) (Figure 4B).

Among the conventional CD8⁺ T cells, the majority displayed EM phenotype, paired with high expression of *GZMK* and are grouped into two distinct clusters, characterized by either high or low HLA class II expression. The largest cluster (HLA class II^{high} GZMK⁺) showed elevated expression of multiple granzymes, natural killer cell receptor *KLRK1* (encoding for NKG2D), and *IFNG* (encoding for IFNγ) (Figure 4B). The second cluster (HLA class II^{low} GZMK⁺) exhibited a similar expression profile, albeit with reduced levels of *HLA-DQB1, HLA-DRB1*, and *HLA-DPA1*. Both clusters expressed exhaustion- and

activation-associated markers, including *RGS1, PDCD1* (encoding PD-1), and *TOX* (Figure 4B).

To better understand the cytotoxic and functional properties of intrahepatic CD8⁺ T cells, the expression of all granzyme family members was analyzed across clusters (Figure 5A). *GZMA* and *GZMK* emerged as the most highly expressed granzymes, followed by *GZMH* and *GZMM*. In contrast, GZMB, the most studied and classically cytotoxic granzyme, showed the lowest expression levels. While *GZMA* and *GZMB* are associated with classical cytotoxicity, *GZMK* is thought to exert primarily pro-inflammatory effects with limited cytotoxic potential[127]. Notably, the highest cumulative granzyme expression was found in the HLA class II^{high} GZMK⁺ cluster, with prominent expression of both *GZMA* and *GZMK* (Figure 5A). This suggests a mixed cytotoxic and pro-inflammatory phenotype, potentially shaped by chronic activation in the inflamed liver tissue.

To investigate the developmental relationships among CD8⁺ T cell clusters, we performed RNA velocity analysis. This computational approach predicts the future transcriptional state of individual cells by analyzing the content of unspliced and spliced

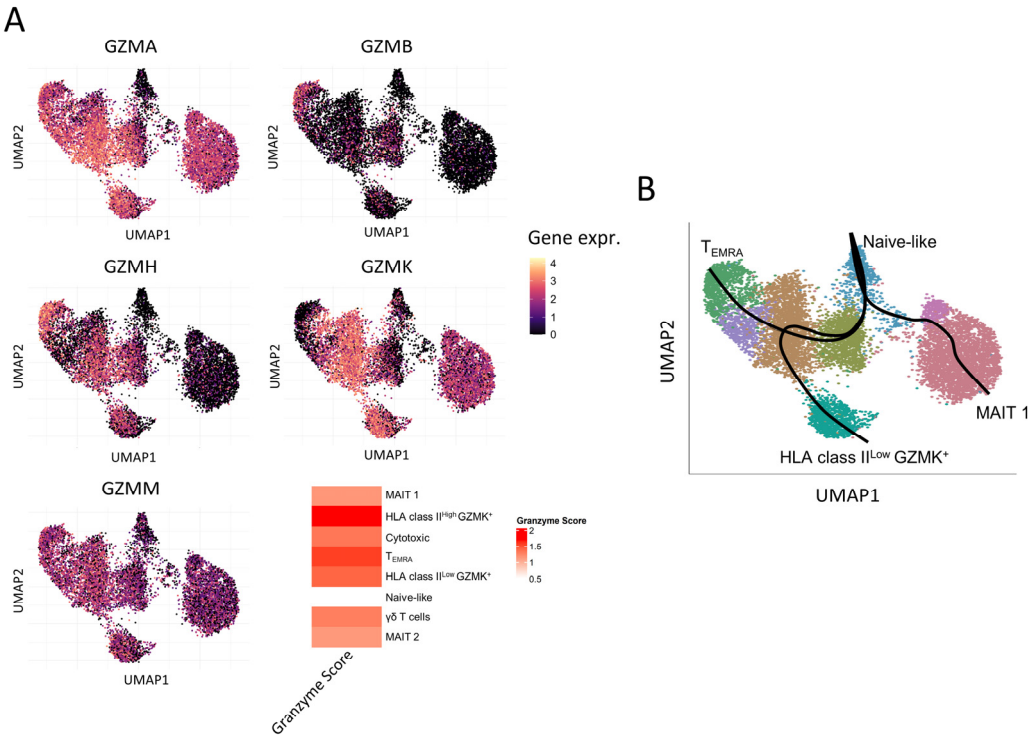

Figure 5: **Granzyme expression profile and RNA velocity analysis of intrahepatic CD8⁺ T cells in PSC.**

(A) UMAP projection showing expression of granzyme family members granzyme A, B, H, K, and M (*GZMA, GZMB, GZMH, GZMK*, and *GZMM*) in intrahepatic CD8⁺ T cells from end-stage PSC livers. The granzyme score represents the accumulated mean expression of all analyzed granzymes per cluster. **(B)** RNA velocity analysis overlaid on the UMAP projection, using naive CD8⁺ T cells as the inferred starting population. Black streamlines indicate predicted differentiation trajectories toward three terminal cell states.

mRNA. The analysis revealed three major differentiation endpoints, located within the MAIT1, T_{EMRA}, and HLA class II^{low} $GZMK^+$ clusters. Interestingly, the HLA class II^{high} $GZMK^+$ cluster appeared as a transitional population connecting the T_{EMRA} and HLA class II^{low} $GZMK^+$ states. This positioning suggests that these cells may represent a key intermediate stage, potentially linking terminal effector differentiation with chronic activation and exhaustion.

Taken together, these data suggest that intrahepatic $CD8^+$ T cells in PSC exhibit signs of chronic activation, deviating from a classical TCR-driven effector phenotype. Their expression of granzymes and exhaustion markers points toward alternative activation mechanisms, potentially shaped by the persistent inflammatory liver microenvironment.

3.3 PSC-derived $CD8^+$ T cells exhibit an IL-15-induced bystander-activated phenotype

A striking feature of the largest conventional $CD8^+$ T cell population (HLA class II^{high} $GZMK^+$) identified in PSC livers was the elevated expression of *HLA-DRB1, KLRK1, CXCR6*, and *PD-1*. This upregulation was confirmed not only at the transcriptomic level but also by corresponding antibody-derived tags (ADTs) for HLA-DR, NKG2D and PD-1 (Figure 6A). This suggests a chronically activated and cytotoxic role for this $CD8^+$ T cell subset in PSC[130].

The overall transcriptional signature of the $GZMK^+$ clusters, marked by high expression of granzymes, MHC class II molecules, NK cell receptors, chemokines, and *CD38*, points to an activated and immune-relevant state that diverges from classical TCR-mediated activation. Notably, this closely resembles a phenotype already described in multiple inflammatory conditions and tissue environments in response to the cytokine IL-15)[100,131].

IL-15 is a member of the common gamma-chain cytokine family (includes also e.g. IL-2) which signals primarily through the STAT5 pathway (see Figure 2). Consistent with this, over-representation analysis (ORA) of hallmark gene sets from the Molecular Signatures Database (MSigDB)[132] identified STAT5 signaling as the second most significantly enriched pathway in the HLA class II^{high} $GZMK^+$ cluster (Figure 6B).

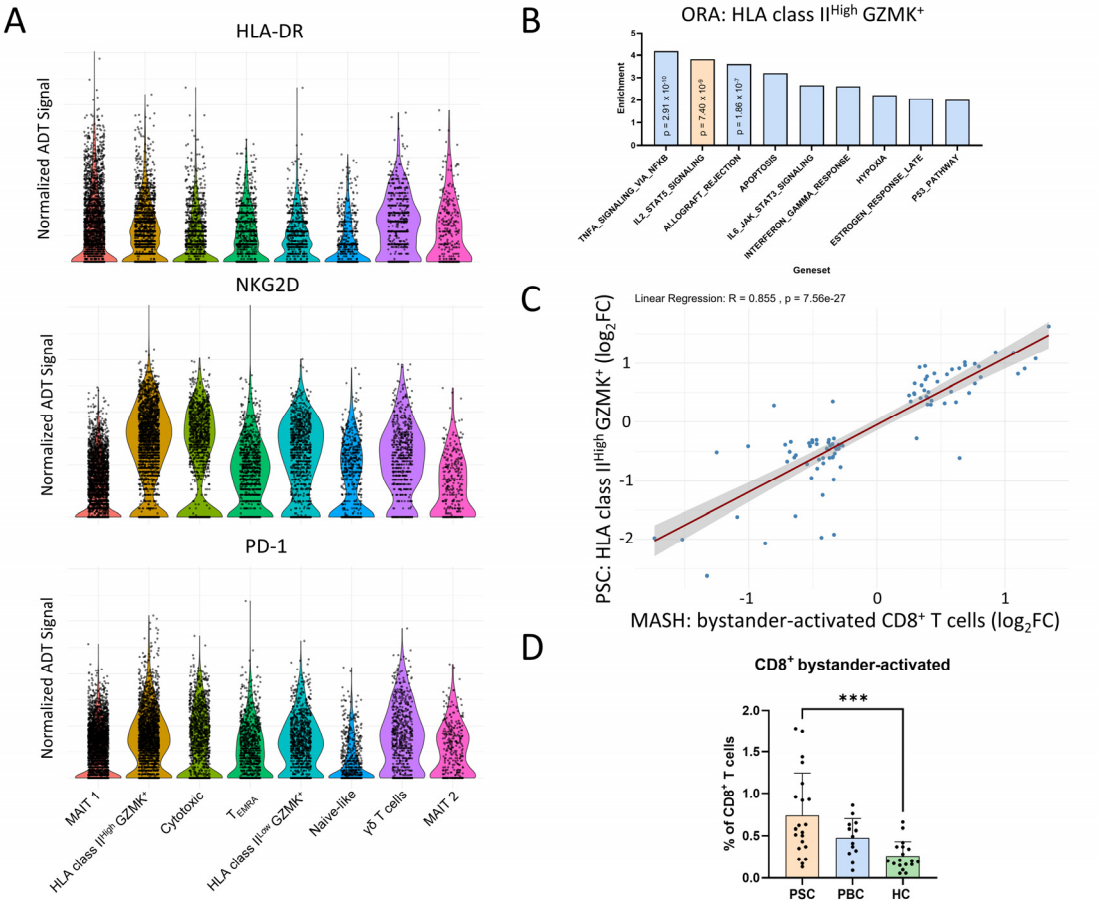

Figure 6: **Bystander-activated phenotype in liver- and blood-derived CD8⁺ T cells from PSC.**

(A) Violin plots showing antibody-derived tag (ADT) signal intensities from single-cell CITE-seq analysis of intrahepatic CD8⁺ T cells isolated from end-stage PSC livers. **(B)** Pathway enrichment analysis of the HLA class II^{high} GZMK⁺ CD8⁺ T cell cluster, highlighting increased activity of IL-15–associated signaling pathways. **(C)** Correlation analysis of differential gene expression (log_2 fold change) between the PSC-derived HLA class II^{high} GZMK⁺ CD8⁺ T cell cluster and bystander-activated CD8⁺ T cells identified in metabolic dysfunction–associated steatohepatitis (MASH), as reported by Dudek et al. (2021). **(D)** Frequency of bystander-activated CD8⁺ T cells in peripheral blood from individuals with non-cirrhotic PSC, primary biliary cholangitis (PBC), and age- and sex-matched healthy controls. Statistical analysis was performed using the Kruskal-Wallis test following assessment of data normality (*** $p \leq 0.001$).

A defining feature of IL-15-stimulated CD8⁺ T cells is their ability to kill target cells via innate-like or auto-aggressive mechanisms, independent of classical TCR engagement. Unlike conventional cytotoxic CD8⁺ T cells, which require TCR licensing to mediate cell killing, IL-15-induced CD8⁺ T cells can eliminate target cells via NK cell receptors or in response to metabolic cues. This mechanism has been observed in chronic liver diseases such as viral hepatitis and metabolic dysfunction-associated steatohepatitis (MASH)[99].

Dudek et al. (2021) previously identified a bystander-activated CD8⁺ T cell population in MASH, driven by IL-15. Correlation analysis between the differentially expressed genes

(DEGs) in the MASH-specific bystander-activated cluster and the HLA class II^{high} GZMK^{+} cluster from PSC revealed a strong transcriptional similarity (R = 0.855, p = 7.56 x 10^{-27}) (Figure 6C).

To further investigate this phenotype, we applied a combination of published bystander-activated CD8^{+} T cell marker (defined as TCRα/β^{+}, CD3^{+}, CD8^{+}, CD4^{-}, CD103^{+}, CCR7^{-}, HLA-DR^{+}, GZMA^{+}, GZMB^{+}, GZMK^{+}) to our flow cytometry data from peripheral blood. This analysis demonstrated a significant increase in bystander-activated CD8^{+} T cells in individuals with PSC, compared to both people with PBC and healthy controls (Figure 6D).

In summary, these findings demonstrate that PSC-derived CD8^{+} T cells, both in peripheral blood and the liver, exhibit transcriptional and phenotypic features consistent with IL-15-driven bystander-activation. This cell population may represent a critical effector subset contributing to immune-mediated biliary injury and disease progression in PSC.

3.4 Single-nucleus mRNA sequencing reveals *IL15* upregulation in cholangiocytes of people with PSC

As the development of bystander-activated CD8^{+} T cells has been described in chronic liver diseases and is closely linked to IL-15 exposure[99,100], single-nucleus RNA sequencing (sNucSeq) was employed to identify potential cellular sources of IL-15 in PSC livers.

A total of 52 liver samples from 44 individuals were analyzed. To identify PSC-specific alterations, the cohort included 12 obese controls with minimal liver pathology (low steatosis and no fibrosis), as well as PSC derived samples across different disease stages. This included 10 Tru-Cut biopsies from 7 individuals, grouped into PSC early and PSC late based on fibrosis stage, and 15 explant samples from 10 individuals. These were compared to liver samples derived from cirrhotic controls: alcoholic liver disease (ALD, n = 10) and MASLD (n = 5).

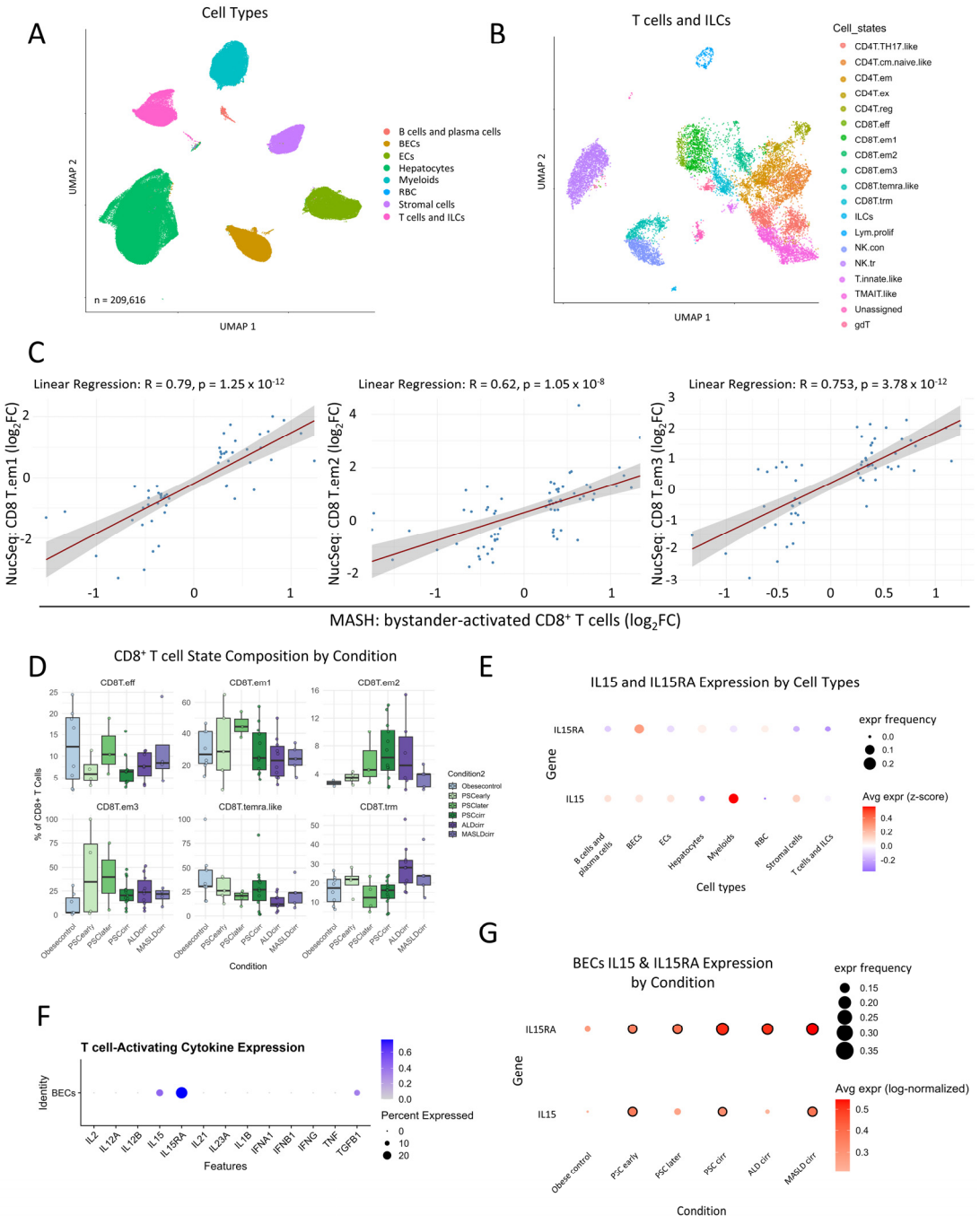

Figure 7: **Bystander-activated CD8⁺ T cell profiles and *IL15* expression in single-nucleus RNA sequencing (sNucSeq) data from PSC and control livers.**

(A) UMAP of sNucSeq data derived from early stage, later-stage, and cirrhotic PSC livers, as well as disease control samples. **(B)** Subclustering of T cells and innate lymphoid cells (ILCs) within the sNuc-seq dataset. **(C)** Correlation analysis between effector memory CD8⁺ T cell clusters identified in sNucSeq data and bystander-activated CD8⁺ T cells described in metabolic dysfunction–associated steatohepatitis (MASH). **(D)** Relative abundance of CD8⁺ T cell states expressed as a proportion of total CD8⁺ T cells in the sNucSeq dataset, stratified by disease and disease stage. **(E)** Dot plot depicting *IL15* and *IL15RA* expression across intrahepatic cell types in the sNucSeq dataset. Dot size indicates the proportion of expressing cells, and color represents z-scored expression levels. **(F)** Expression of T cell–activating cytokines by biliary epithelial cells (BECs). **(G)** Expression levels of *IL15* and *IL15RA* in BECs across disease entities and stages. Statistical significance was assessed using pairwise Wilcoxon tests versus obese control samples, with p-values adjusted using the Benjamini-Hochberg (BH) method. Filled circles indicate significantly increased expression ($p \leq 0.05$).

Uniform manifold approximation and projection (UMAP) of all 209,616 nuclei revealed eight main liver cell types: B cells and plasma cells, BECs, endothelial cells (ECs), hepatocytes, myeloid cells, red blood cells (RBCs), stromal cells, and T/innate lymphoid cells (ILCs) (Figure 7A).

Subclustering of T and ILC populations identified 19 transcriptionally distinct states, including multiple subsets of $CD4^+$ T cells, $CD8^+$ T cells, NK cells, MAIT cells, and γδ T cells (Figure 7B). Notably, all three $CD8^+$ EM (CD8T.em1, CD8T.em2 and CD8.em3) show significant correlations with the bystander-activated gene signature, published from people with MASH by Dudek et al. (2021) (Figure 7C)[99]. Among these, the CD8T.em1 population was the most abundant $CD8^+$ T cell subset and CD8T.em2 population displayed an increasing trend in abundance across PSC stages and was highly associated with bystander-activation. CD8T.em2 also showed the highest dysfunctional phenotype, by enriched *TOX*, *PDCD1* and *IFNG* expression. Overall, CD8T.em1 are similar to HLA class II^{high} $GZMK^+$ and CD8T.em2 to the HLA class II^{low} $GZMK^+$ cluster from single-cell sequencing (Figure 7D).

To further define the cellular sources of IL-15, expression of *IL15* and its receptor subunit *IL15RA* was examined. Importantly, *IL15RA* is essential for trans-presentation of IL-15 (as shown in Figure 2), a mechanism that enhances its bioactivity toward neighboring immune cells. Across all cell types, myeloid cells were identified as the main producers of *IL15*, followed by BECs, B cells, ECs, and stromal cells. Of note, BECs showed the highest expression of *IL15RA* (Figure 7E).

To contextualize these findings, the expression of a broader panel of T cell-stimulating cytokines by BECs was analyzed, including *IL2, IL12A, IL12B, IL15, IL15RA, IL21, IL23A, IL1B, IFNA1, IFNB1, IFNG, TNF* and *TGFB1*. Among these, IL15 and IL15RA were the most strongly expressed in BECs, and *TGFB1* was also detected (Figure 7F).

To assess disease specificity, *IL15* and *IL15RA* expression in BECs was compared across PSC stages and controls (Figure 7G). *IL15RA* expression increased progressively from early to late stage PSC and showed the highest expression in cirrhotic PSC livers. *IL15RA* was also significantly upregulated in both ALD and MASLD cirrhosis compared to obese controls. In contrast, *IL15* expression was selectively elevated in PSC stages (significantly in early and cirrhotic PSC) and in MASLD cirrhosis, but not in ALD cirrhosis, suggesting a disease-specific rather than fibrosis-associated upregulation of *IL15*.

In summary, sNucSeq analysis confirmed the presence of bystander-activated CD8⁺ T cell phenotype, particularly the expansion of the CD8T.em2 subset, which shows high transcriptional correlation with bystander-activated CD8⁺ T cells in MASH. Moreover, BECs were identified as the major source of *IL15RA*, and expressed both *IL15* and *IL15RA* at increasing levels throughout PSC disease progression. These findings further implicate cholangiocytes as potential drivers of IL-15-mediated CD8⁺ T cell bystander-activation in PSC.

3.5 Cholangiocytes express increased IL-15 and IL-15Rα upon IFNγ stimulation

As sNucSeq analysis showed increased *IL15* gene expression in biliary epithelial cells (BECs) in PSC, we further investigated potential upstream stimuli responsible for IL-15 induction. According to the literature, several signals can induce IL-15 expression, including microbial components such as LPS and, most prominently, interferons, particularly IFNγ[114,116].

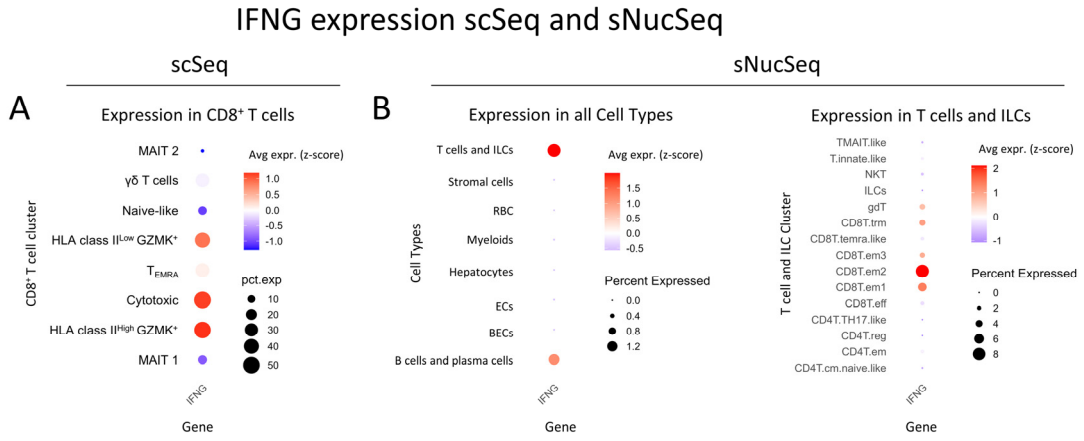

Figure 8: **Interferon-γ expression in single-cell and single-nucleus sequencing datasets.**

(A) *IFNG* (encoding interferon-γ) gene expression in intrahepatic CD8⁺ T cells from single-cell CITE-sequencing of end stage PSC livers. **(B)** *IFNG* expression in the single-nucleus RNA sequencing (sNucSeq) dataset, shown across major cell types (left) and within T cell and innate lymphoid cell (ILC) subsets (right).

Single-cell RNA sequencing of CD8⁺ T cells showed the highest *IFNG* expression in GZMK⁺ clusters and cytotoxic CD8⁺ T cells (Figure 8A). In the sNucSeq dataset, CD8⁺ effector memory T cells were identified as the main *IFNG*-expressing population (Figure 8B). Given that IL-15 signaling can also prime cells towards IFNγ expression[133], this raises the possibility of a positive feedback loop between IL-15-expressing cholangiocytes and IFNγ-producing CD8⁺ T cells in the PSC liver microenvironment.

To experimentally validate whether cholangiocytes are capable of IL-15 expression and IL-15-mediated signaling, we used two *in vitro* models: primary human cholangiocyte organoids and the H69 BEC cell line. Cholangiocyte organoids were derived from human liver explant tissue (visualized in Figure 9A) and stimulated for 24 hours with: 100 ng/mL IFNγ, 50 ng/mL IL17A, 1 ng/mL IL-1β. Furthermore, a combination of IFNγ and IL-17A or IL-1β was used to test for synergistic effects of the cytokines. We found that only IFNγ stimulation was able to significantly upregulated *IL15* and *IL15RA* expression in cholangiocytes (~10-fold increase). No synergistic effects were observed upon stimulation with the additional tested cytokines (Figure 9B).

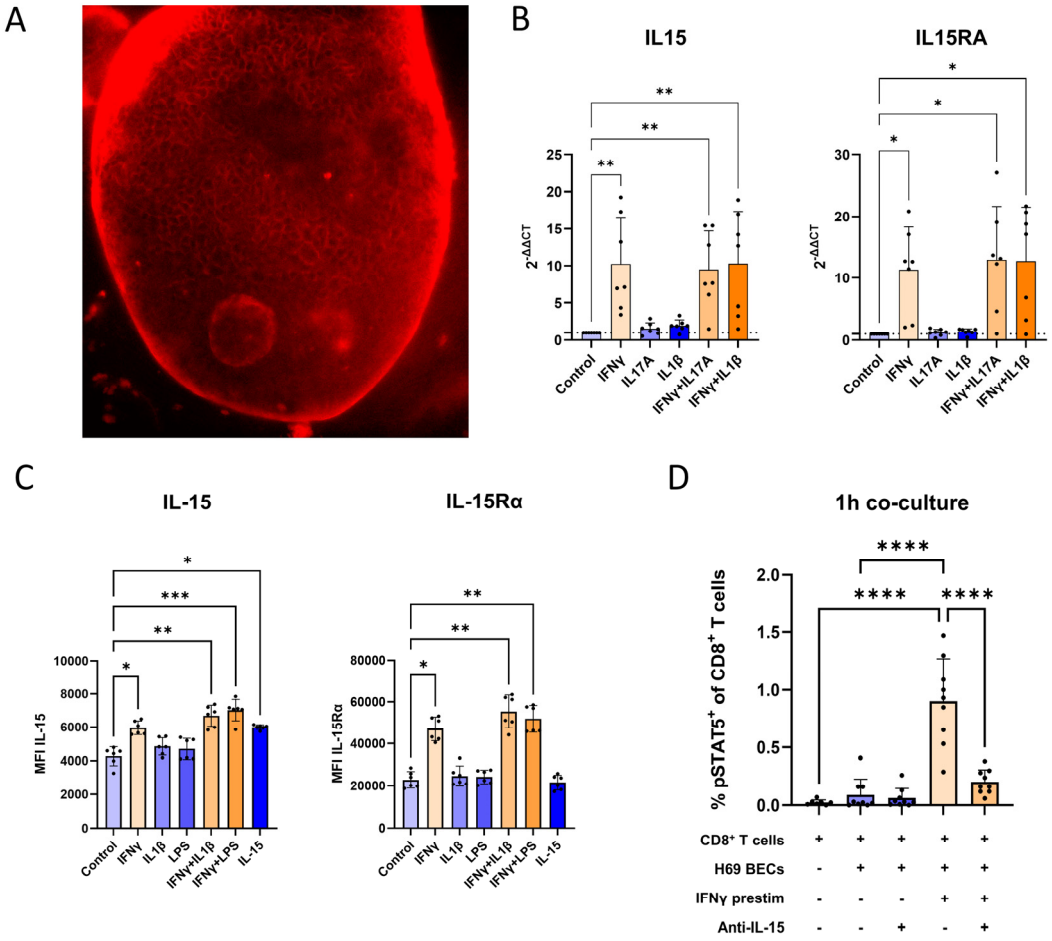

Figure 9: **IL-15 and IL-15Rα expression in cholangiocyte organoids and H69 BEC *in vitro* cultures.**

(A) Representative cell surface immunofluorescence staining of cholangiocyte organoids in culture. **(B)** Fold-change of *IL15* and *IL15RA* mRNA expression in cholangiocyte organoids following 24 h cytokine stimulation, as assessed by qRT-PCR. **(C)** Mean fluorescence intensity (MFI) of surface IL-15 and IL-15Rα measured by flow cytometry in the H69 BEC cell line after 24 h cytokine stimulation. **(D)** Frequency of pSTAT5$^+$ CD8$^+$ T cells after 1 h co-culture with H69 BECs with or without IFNγ pre-stimulation and in the presence or absence of an anti–IL-15 blocking antibody. Statistical analysis was performed using the Kruskal-Wallis test following assessment of data distribution (*$p \leq 0.05$, **$p \leq 0.01$, ***$p \leq 0.001$, ****$p \leq 0.0001$).

Because IL-15 and IL-15Rα expression is tightly controlled at the protein level, particularly regarding cell surface presentation, we performed flow cytometric analysis on H69 BECs. After 24 h of stimulation with IFNγ, surface expression of both IL-15 and IL-15Rα was significantly increased. Interestingly, even without stimulation, BECs exhibited baseline cross-presentation of exogenous IL-15 on the cell surface (Figure 9C).

To functionally assess IL-15 signaling, we measured STAT5 phosphorylation (pSTAT5) in $CD8^+$ T cells after co-culture with H69 BECs. $CD8^+$ T cells were previously cytokine-starved for 24 h followed by a co-cultured for 1 h with IFNγ-prestimulated H69 BECs. A significant increase in pSTAT5 was detected in co-cultured $CD8^+$ T cells, confirming IL-15 signaling via trans-presentation. This effect was reversed upon IL-15 neutralization with a blocking antibody (Figure 9D).

In summary, IL-15 and IL-15Rα mRNA and surface protein expression were confirmed *in vitro* in cholangiocytes. Both were upregulated by IFNγ, consistent with previous observations in other cell types. Unlike endothelial cells, cholangiocytes appear to present IL-15 independently of NF-κB signaling. Moreover, our data demonstrate effective IL-15 trans-presentation by cholangiocytes, resulting in $CD8^+$ T cell activation via STAT5 phosphorylation[131].

The ability to stimulate $CD8^+$ T cells through IL-15 trans-presentation introduce a novel mechanistic immunological function of cholangiocytes, which could be relevant in the context of PSC.

3.6 Spatial transcriptomics reveals close proximity of CD8⁺ T cells and biliary epithelial cells in inflamed bile ducts

Within this study, CD8⁺ T cells with an IL-15-induced bystander-activated phenotype have been described, and BECs were identified as a potential cellular source of IL-15 in PSC livers. However, a key limitation of single-cell and single-nucleus RNA sequencing approaches is the lack of spatial information, which is essential to understand cell-cell interactions within the tissue microenvironment.

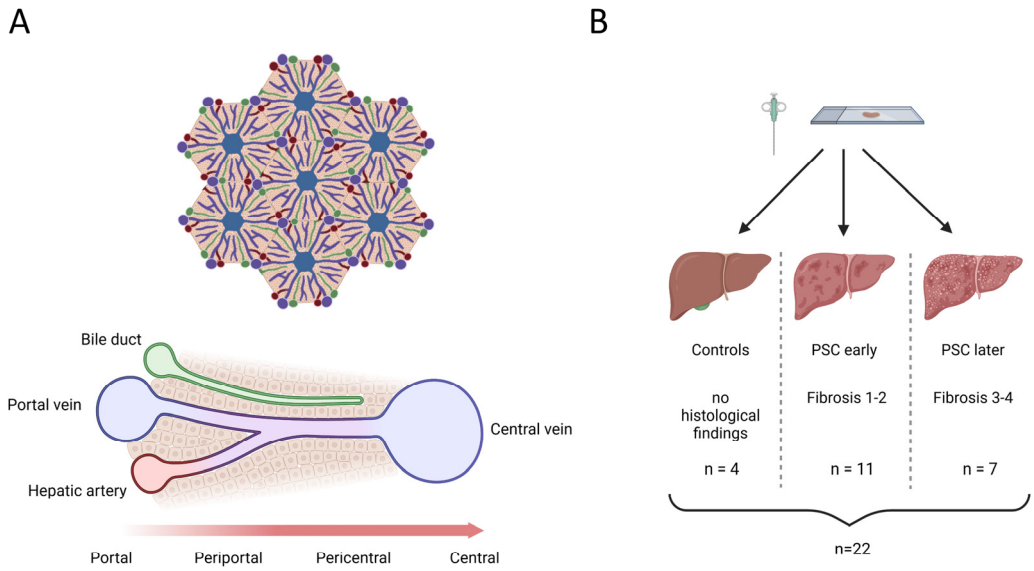

Figure 10: **Schematic overview of liver zonation and sample composition for spatial transcriptomics.**

(A) Schematic representation of hepatic lobule organization and zonation, extending from the portal fields, containing the portal triad of bile duct, portal vein, and hepatic artery, through periportal and pericentral zones to the central region marked by the central vein. Blood flows through the sinusoids from the portal toward the central region. **(B)** Overview of liver biopsy samples included in the spatial transcriptomic analysis, comprising histologically normal controls, early stage PSC (fibrosis stage 1–2), and late stage PSC (fibrosis stage 3–4).

The liver is a highly organized organ whose structure is closely linked to its metabolic and immunological functions. Its fundamental structural unit, the hepatic lobule, is organized around a central vein and surrounded by portal triads, each composed of a branch of the portal vein, a hepatic artery, and a bile duct. Blood flows from the portal triads through the sinusoids toward the central vein, generating spatial gradients of oxygen, nutrients, and metabolites. Along this axis, hepatocytes are organized into distinct zones. The portal region is exposed to high oxygen and nutrient levels and supports oxidative metabolism and bile acid handling, whereas oxygen tension decreases toward the central zone, favoring glycolysis, lipid metabolism, and xenobiotic

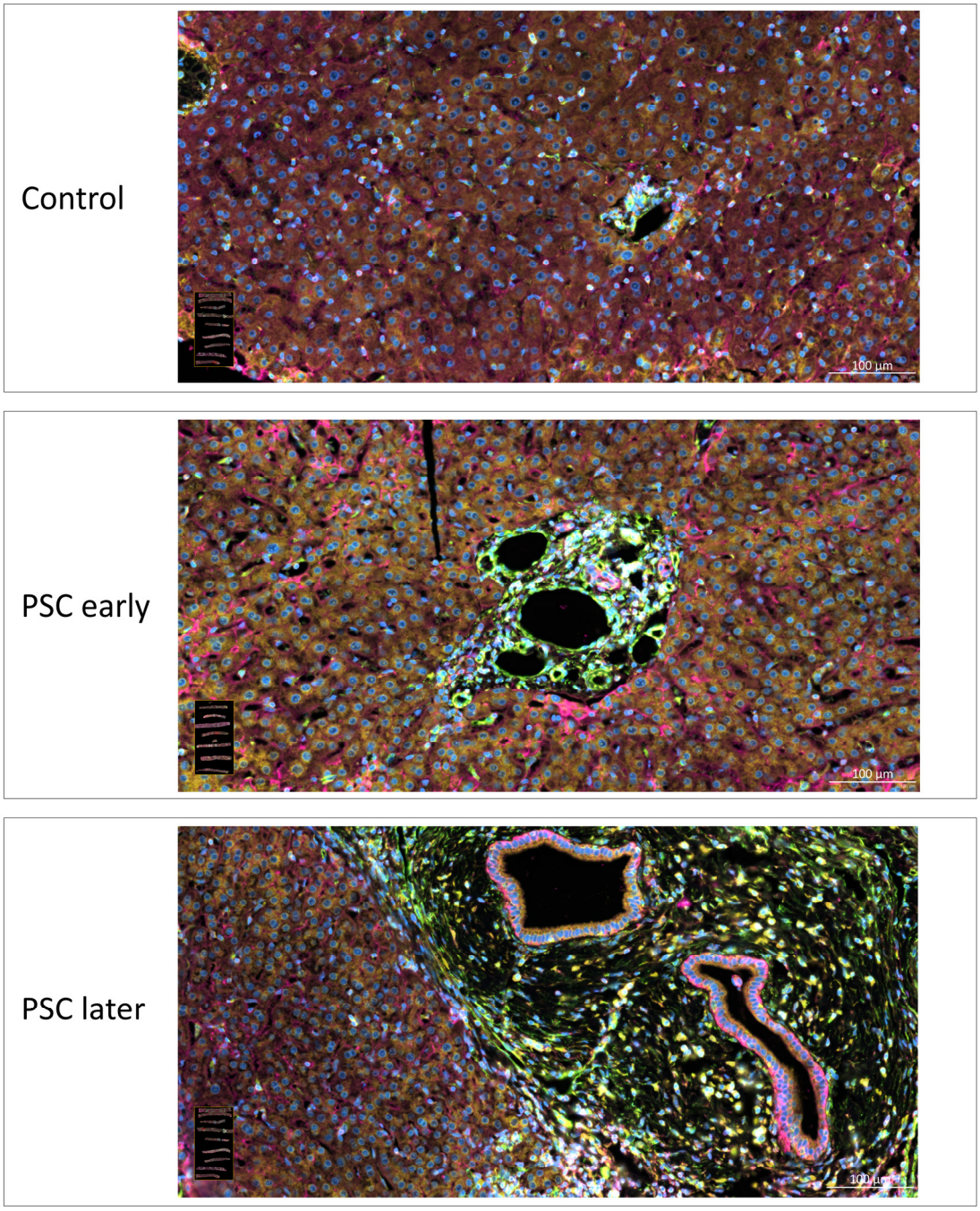

Figure 11: **Representative liver biopsy sections across PSC disease stages and control.**

Representative images of portal fields from histologically normal control, early stage PSC, and late-stage PSC liver biopsies. Cell segmentation staining includes: magenta, cell surface markers (ATPase Na^+/K^+ Transporting Subunit Alpha 1, E-cadherin, and CD45); yellow, 18S ribosomal RNA; green, intracellular proteins (α-smooth muscle actin and vimentin).

detoxification. The midzonal area represents a functional transition between these regions[134] (Figure 10A).

In PSC, a histological hallmark is periductal concentric (“onion-skin”) fibrosis, which leads to progressive bile duct narrowing and obliteration. Inflammatory infiltrates,

predominantly composed of lymphocytes, are present in portal tracts and around affected bile ducts. Over time, chronic biliary injury results in expansion of portal fibrosis and progression to biliary cirrhosis[135]. Due to this chronic inflammation surrounding BECs, portal and periportal regions represent the principal sites of immune cell accumulation in PSC. Until recently, a detailed characterization of immune cell composition within these regions was not feasible.

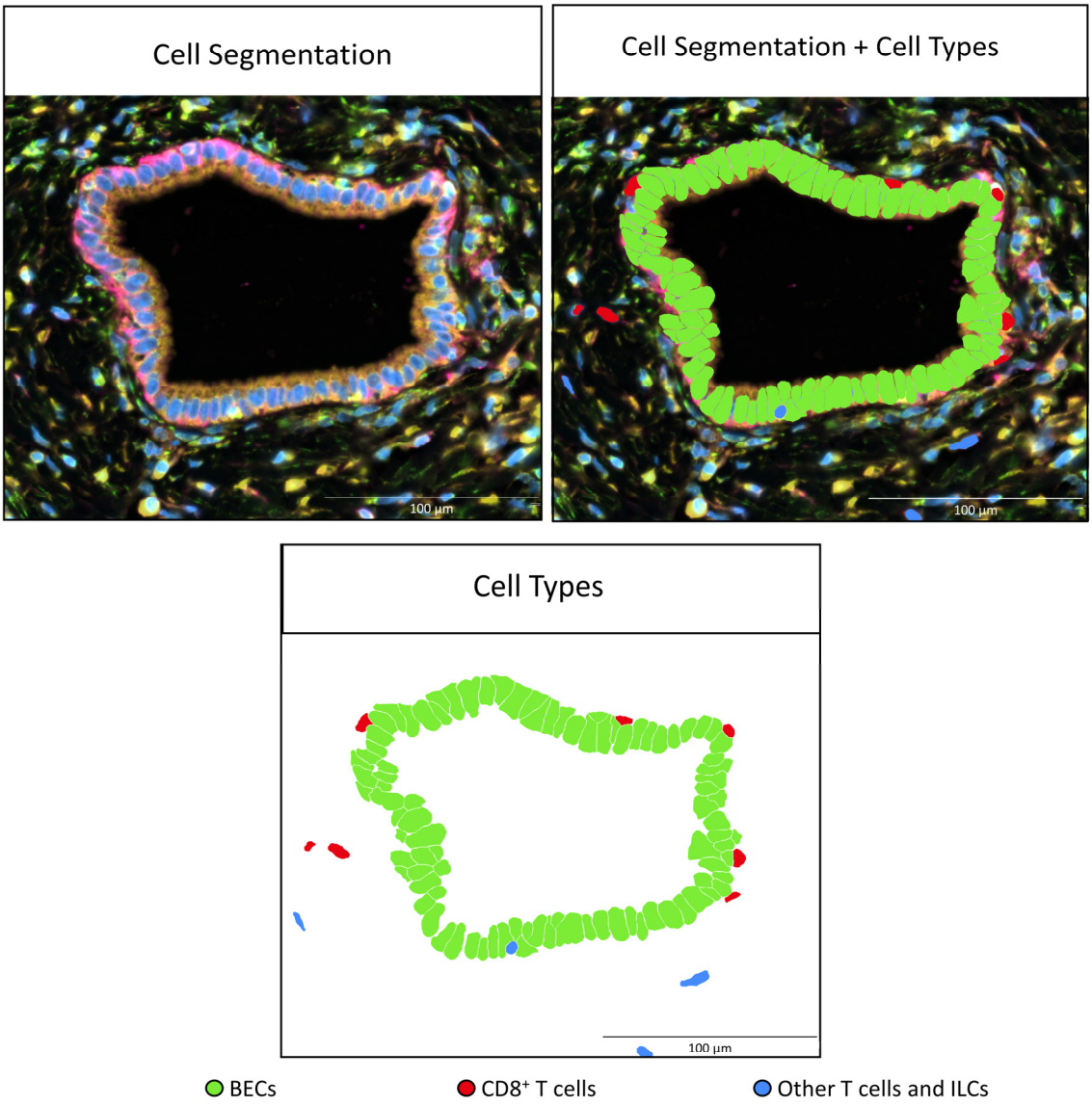

Figure 12: **Representative examples of CD8⁺ T cell interactions with cholangiocytes in late-stage PSC.**

High-magnification view of an inflamed bile duct from a late-stage PSC liver biopsy. Images display cell segmentation staining (upper left), cell type annotation (bottom), and an overlay of both (upper right). Selected cell populations are highlighted as follows: cholangiocytes (BECs, green), CD8⁺ T cells (red), and other T cells and innate lymphoid cells (ILCs, blue).

To address this, spatial transcriptomic analysis was performed on 22 liver biopsies, including 4 controls without histological abnormalities, 11 early stage PSC samples (fibrosis stage 1–2), and 7 late-stage PSC samples (fibrosis stage 3–4) (Figure 10B), using the Xenium in situ platform (10x Genomics). This approach enabled spatially resolved detection of 480 genes (Table 10) at subcellular resolution across entire tissue

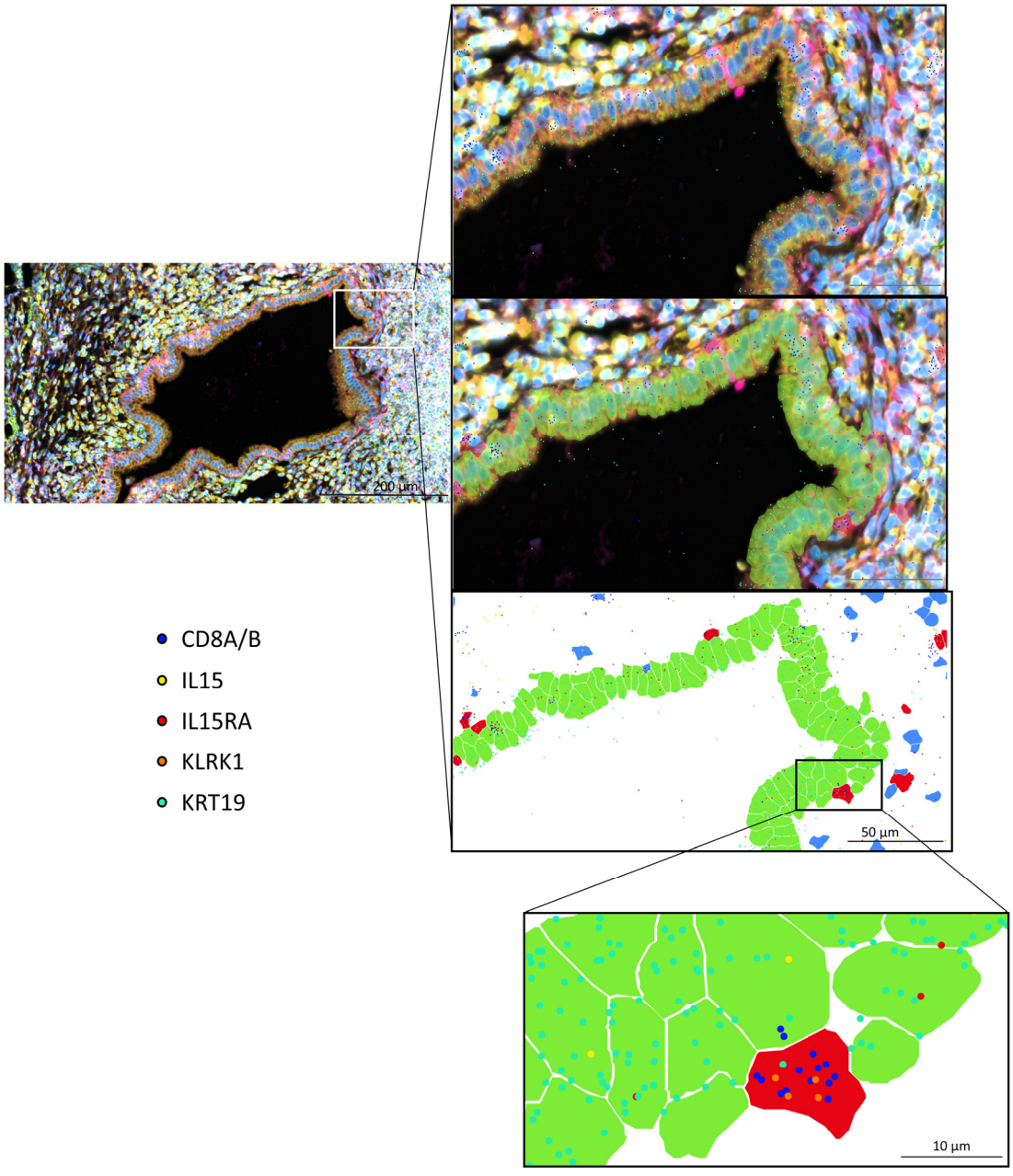

Figure 13: **Spatial gene expression in cholangiocytes and CD8⁺ T cells interacting in late stagePSC.**

High-magnification view of an inflamed bile duct from a late stagePSC liver biopsy. Images show cell segmentation staining (upper left), cell type annotation (bottom), and an overlay of both (upper right). Selected cell populations are highlighted as follows: cholangiocytes (BECs, green), CD8⁺ T cells (red), and other T cells and innate lymphoid cells (ILCs, blue). Spatial gene expression of *CD8A/B* (blue), *IL15* (yellow), *IL15RA* (red), *KLRK1* (orange), and *KRT19* (green) is shown.

sections. Cell segmentation was achieved using a combination of intracellular RNA staining (18S rRNA) and protein markers (α-smooth muscle actin and vimentin), complemented by surface markers (ATPase Na^+/K^+ transporting subunit alpha 1, E-cadherin, and CD45) to facilitate accurate cell-type identification.

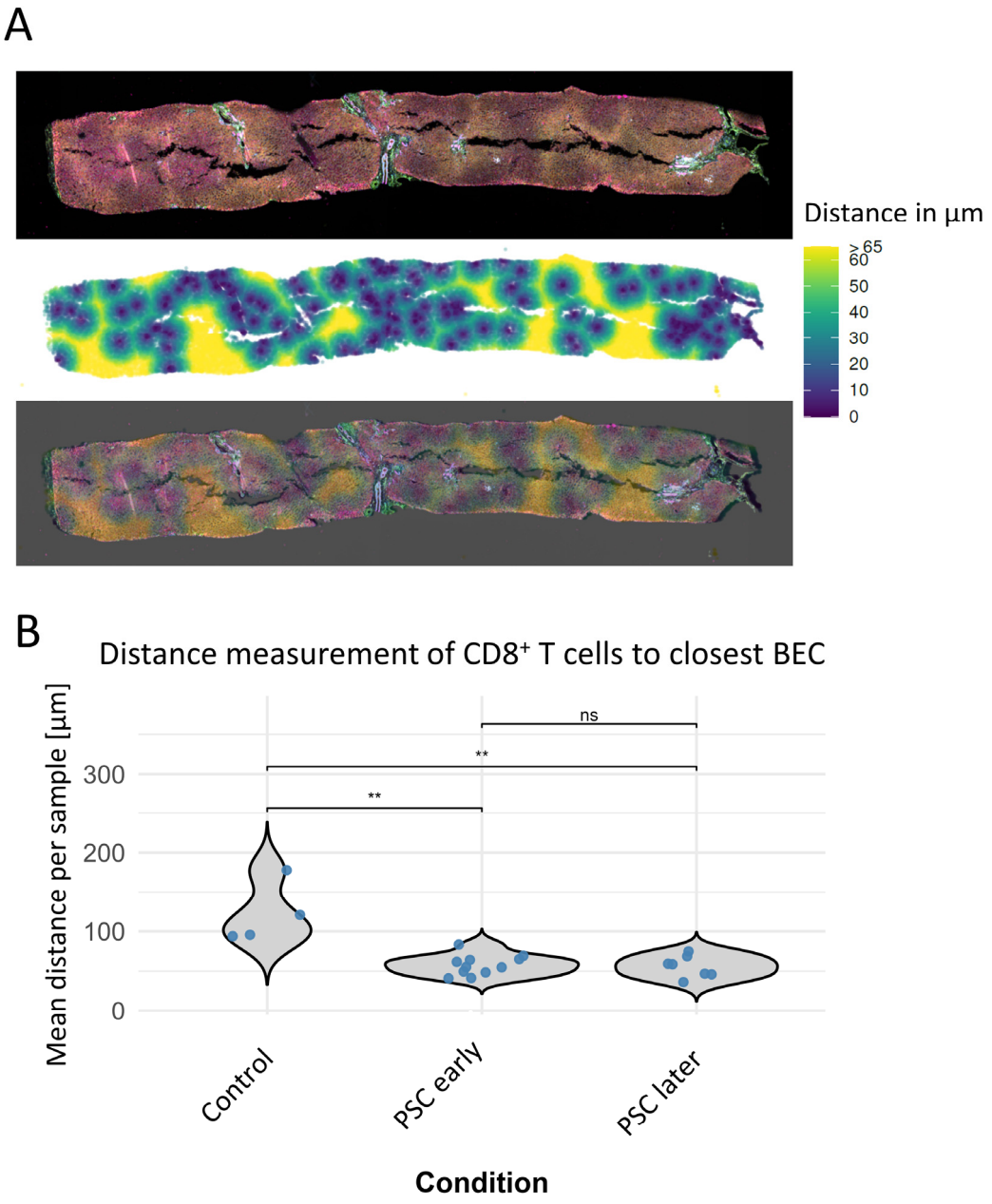

Figure 14: **Spatial proximity between $CD8^+$ T cells and cholangiocytes in PSC liver tissue.**

(A) Distance map illustrating the spatial relationship between $CD8^+$ T cells and cholangiocytes, with close proximity indicated in dark blue and increasing distances shown in yellow. For each $CD8^+$ T cell, the nearest cholangiocyte was identified using a k-d tree-based nearest-neighbor algorithm. Euclidean distances were calculated in pixel units and converted to micrometers (µm) using the Xenium image-specific scaling factor. **(B)** Violin plot showing the average minimal distance between $CD8^+$ T cells and biliary epithelial cells (BECs) per sample, stratified by condition. Each dot represents one individual sample. Statistical significance was assessed using the Wilcoxon test (**$p \leq 0.01$).

Figure 11 shows representative biopsy sections from control, early stage PSC, and late-stage PSC samples. Disease progression was marked by pronounced bile duct proliferation (magenta) and expansion of fibrotic areas (green) surrounding bile ducts.

To investigate immune-epithelial interactions, the spatial relationship between CD8⁺ T cells and cholangiocytes was analyzed. Figure 12 presents a magnified view of an inflamed bile duct in late-stage PSC, surrounded by fibrotic tissue. Cholangiocytes (bright green), CD8⁺ T cells (red), and other T cells and ILCs (blue) are visualized. In this representative image, five CD8⁺ T cells are in direct contact with cholangiocytes, indicating close spatial association within inflamed bile ducts.

Notably, CD8⁺ T cells in direct contact with cholangiocytes expressed KLRK1 (NKG2D), a receptor associated with IL-15-driven auto-aggression, while neighboring cholangiocytes expressed *IL15* and *IL15RA* (Figure 13).

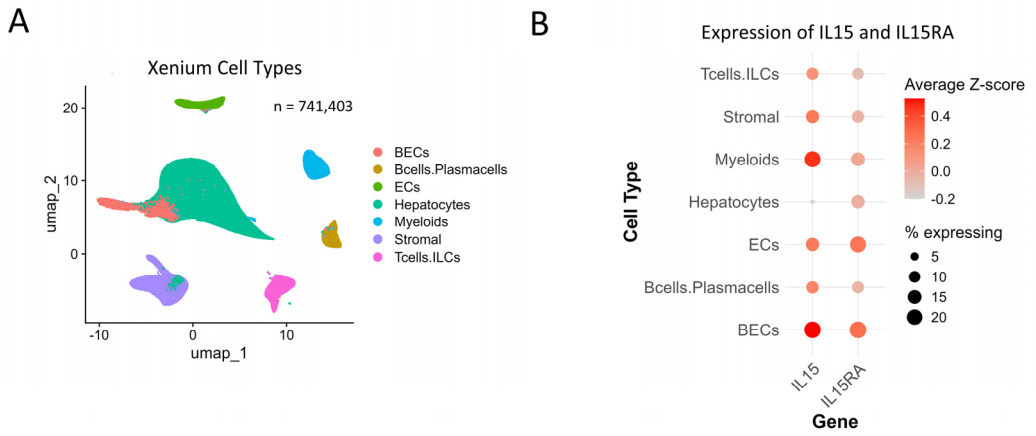

Figure 15: **UMAP projection and cell type–specific *IL15* and *IL15RA* expression in the Xenium spatial transcriptomics dataset.**

(A) UMAP projection of the spatial transcriptomics dataset generated from 22 liver biopsies using the Xenium in situ platform. **(B)** Z-score-scaled expression of *IL15* and *IL15RA* across annotated cell types in the spatial transcriptomics dataset.

To quantitatively assess spatial interactions, the distance between each CD8⁺ T cell and the nearest cholangiocyte was calculated. For quantitative analysis, pairwise distances were computed using a nearest-neighbor approach. For each cell, the closest CD8⁺ T cell was identified using a k-dimensional tree algorithm, enabling efficient spatial indexing. The Euclidean distance between each cell and its nearest CD8⁺ T cell was calculated in pixel units and subsequently converted to micrometers (µm) using image-specific scaling factors provided by the Xenium platform. This allowed precise quantification of CD8⁺ T cell proximity across tissue regions and experimental conditions.

Figure 14A shows a representative heatmap from an early stage PSC biopsy, with distances ranging from dark blue (close proximity) to yellow (greater distance). Fibrotic regions were predominantly dark blue, indicating a close spatial relationship between $CD8^+$ T cells and BECs, consistent with portal infiltration of $CD8^+$ T cells in PSC.

Furthermore, the minimal distance between cholangiocytes and $CD8^+$ T cells was summarized per sample. $CD8^+$ T cells were found to be in significantly closer proximity to cholangiocytes in PSC samples compared to controls (Figure 14B). Importantly, this spatial relationship was independent of fibrosis stage, indicating that close $CD8^+$ T cell–cholangiocyte interactions are a consistent feature throughout PSC disease progression.

3.7 Portal niches exhibit high *IL15* and *IL15RA* expression and are enriched for bystander-activated $CD8^+$ T cells

Beyond analyzing the spatial distance between BECs and $CD8^+$ T cells, a computational framework was applied to characterize cellular phenotypes within the portal inflammatory niche, the central site of PSC pathogenesis.

To ensure high data quality and robust spatial assignment, several preprocessing steps were performed. Due to the nature of spatial transcriptomic platforms, transcript contamination from neighboring cells can occur more frequently than in single-cell approaches. To address this, the FastReseg method was applied to the Xenium dataset prior to downstream analysis[136]. FastReseg refines cell segmentation by re-evaluating cell boundaries based on nuclear features and local transcript distributions, thereby improving spatial accuracy. After refining the segmentation, cell states were annotated through a combination of label transfer from the corresponding sNucSeq dataset and manual review.

UMAP projection of the cleaned dataset revealed 741,403 cells, distributed across the same seven major cell states previously identified in the sNucSeq dataset (Figure 15A). Analysis of cytokine expression demonstrated that *IL15* and *IL15RA* expression was highest in BECs (Figure 15B).

Given the highly zonated architecture of the liver (Figure 10A) and the portal and periportal predominance of inflammation in PSC, spatial transcriptomics enables targeted analysis of cell phenotypes within defined anatomical compartments. To

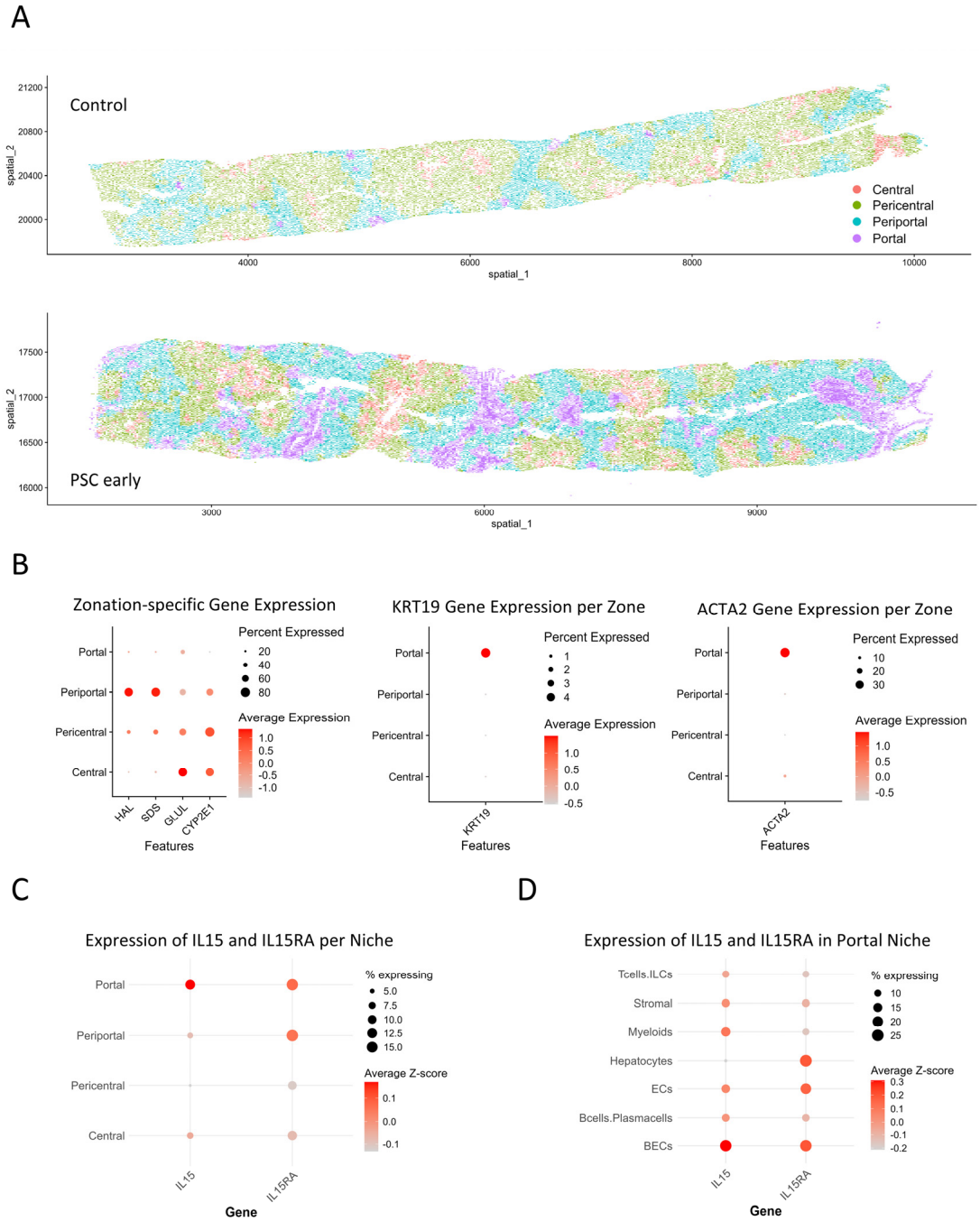

Figure 16: **Spatial niche analysis of PSC and control liver samples.**

(A) Representative spatial niche maps of a histologically normal control biopsy (top) and an early stage PSC biopsy (bottom), showing portal, periportal, pericentral, and central regions. **(B)** Dot plots of zonation marker genes (*HAL*, *SDS*, *GLUL*, and *CYP2E1*), the cholangiocyte marker *KRT19*, and the fibroblast marker *ACTA2* across the defined spatial niches. **(C)** Niche-specific expression of *IL15* and *IL15RA* across spatial regions. **(D)** Cell type-specific expression of *IL15* and *IL15RA* within the portal niche.

facilitate such analysis, a spatial niche segmentation approach was applied following the framework described by Farah et al. (2024)[137]. In this approach, cells are assigned to distinct microanatomical niches based on tissue architecture and local gene expression patterns. Each cell was classified into one of four niches: portal, periportal, pericentral, or central, enabling niche-specific comparisons of cellular composition and transcriptional states.

Figure 16A shows representative spatial maps from a control biopsy (top) and an early stage PSC biopsy (bottom). In PSC, a marked expansion of the portal and periportal niches was evident, reflecting fibrotic remodeling surrounding bile ducts. To validate niche identity, selected marker genes are shown in Figure 16B. Hepatic zonation was confirmed using hepatocyte-specific markers, with *HAL* and *SDS* enriched in portal regions and *GLUL* and *CYP2E1* predominantly expressed in pericentral zones[138]. The portal niche was further defined by high expression of *KRT19* and *ACTA2*, indicating bile duct enrichment and fibrotic remodeling. The combination of low hepatocyte marker expression and elevated *ACTA2* confirms extensive structural remodeling within portal regions in PSC.

Mapping of *IL15* and *IL15RA* expression across spatial niches revealed the highest expression of both genes within the portal niche (Figure 16C) Cell-type–specific analysis further demonstrated that BECs were the dominant source of *IL15* and *IL15RA* within this niche (Figure 16D) supporting a key role for cholangiocytes in shaping the inflammatory microenvironment of PSC.

While IL-15 can contribute to $CD8^+$ T cell recruitment, its strongest biological effect is mediated through trans-presentation via IL-15Rα, which requires direct cell–cell contact. In contrast, chemokines act in a concentration-dependent manner to recruit immune cells over longer distances. The chemokines CXCL9, CXCL10, and CXCL11, which bind to CXCR3, and CXCL16, which recruits $CXCR6^+$ cells, are known to attract activated and cytotoxic $CD8^+$ T cells. All four chemokines can be induced by interferon gamma and were detected in cholangiocytes within the spatial transcriptomic dataset (Figure 17A). Correspondingly, *CXCR3* and *CXCR6* expression was primarily observed in memory $CD8^+$ T cell subsets (Figure 17B).

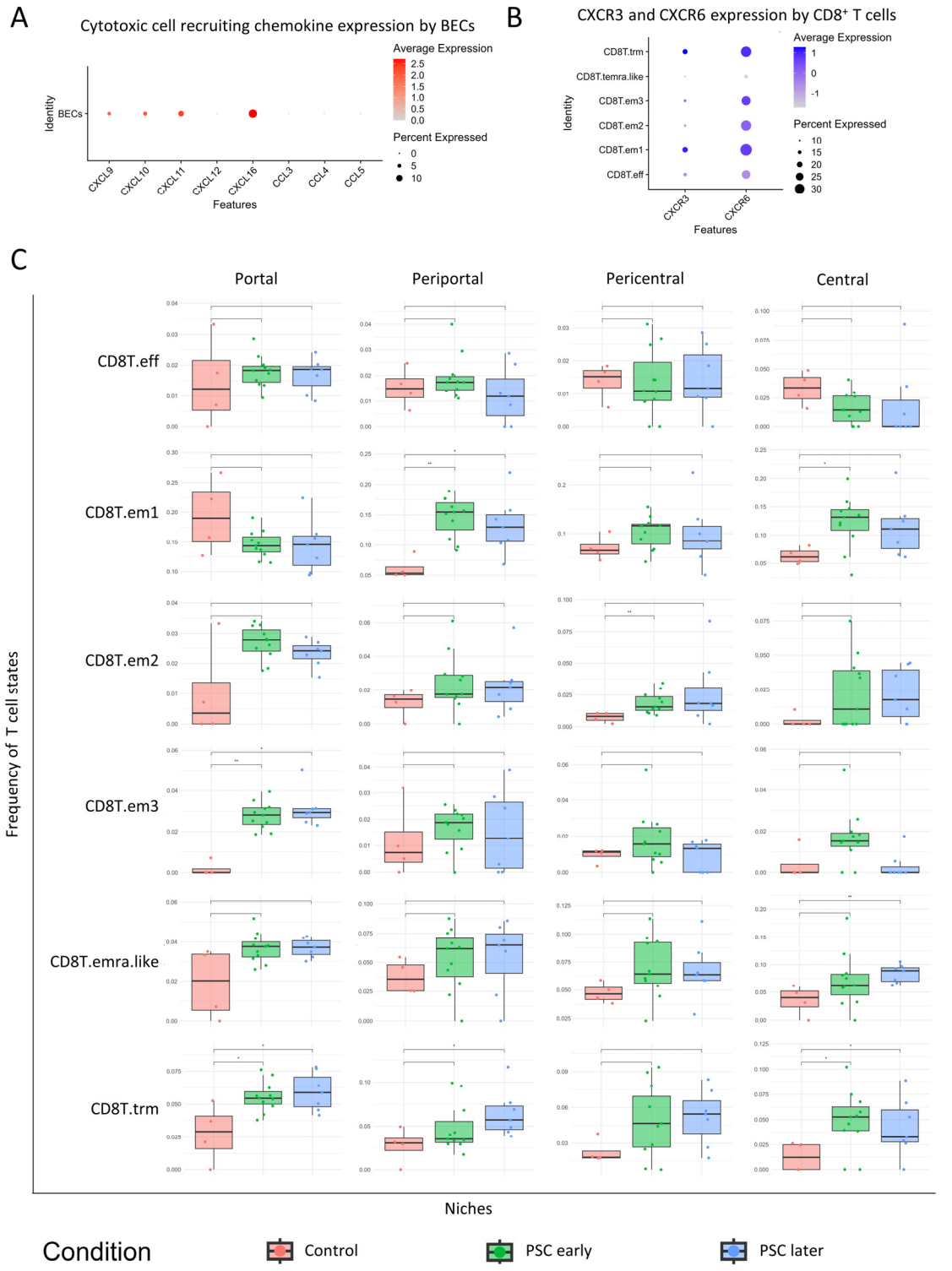

Figure 17: **Cholangiocyte-derived chemokine expression and spatial enrichment of CD8⁺ T cells across liver niches**

(A) Expression of chemokines involved in recruitment of cytotoxic lymphocytes (*CXCL9*, *CXCL10*, *CXCL11*, and *CXCL16*) by cholangiocytes (BECs) in the spatial transcriptomics dataset. **(B)** Expression of the corresponding chemokine receptors *CXCR3* and *CXCR6* in CD8⁺ T cells across spatial niches. **(C)** Relative abundance of CD8⁺ T cell subsets among total T cells and innate lymphoid cells (ILCs) within the portal, periportal, pericentral, and central niches. Statistical significance was assessed using the Wilcoxon test (*$p \leq 0.05$, **$p \leq 0.01$).

Analysis of $CD8^+$ T cell subset distribution across spatial niches (as frequency of total T cells) revealed that clusters with high *CXCR3* and *CXCR6* expression, including CD8T.trm, CD8T.em1, CD8T.em2, and CD8T.em3, were enriched in the portal and periportal niches of PSC samples (Figure 17C). Notably, CD8T.em1 cells were predominantly enriched in the periportal niche, whereas their abundance was reduced within the portal niche itself. In contrast, CD8T.em2 and CD8T.em3 subsets were enriched within the portal niche. Given their transcriptional similarity and increased expression of exhaustion-associated markers in CD8T.em2, these findings suggest a potential differentiation trajectory from CD8T.em1 toward more exhausted states within the inflammatory portal microenvironment. This could be an interesting addition to the RNA velocity data (Figure 5B), were a smaller subset: HLA-DR^{low} $GZMK^+$ (similar expression profile to CD8T.em2) originated from an HLA-DR^{high} $GZMK^+$ cluster (similar to CD8T.em1).

In summary, spatial transcriptomics confirmed the close spatial association between $CD8^+$ T cells and cholangiocytes in PSC. Portal and periportal niches were enriched for effector memory $CD8^+$ T cells exhibiting an IL-15-associated, bystander-activated phenotype, characterized by high CXCR6 expression. Furthermore, cholangiocytes emerged as the principal source of *IL15* and *IL15RA*, alongside expression of *CXCL9*, *CXCL10, CXCL11,* and *CXCL16*, within inflamed portal regions. Together, these data identify cholangiocytes as central orchestrators of $CD8^+$ T cell recruitment, activation, and dysfunction in PSC, providing mechanistic insight into their role in disease pathogenesis.

3.8 Mouse model of acute cholangitis showed increased frequencies of intrahepatic bystander-activated $CD8^+$ T cells

To investigate the impact of IL-15 on liver inflammation *in vivo*, the K14-OVAp mouse model was employed. This well-established transgenic model allows the study of antigen-specific $CD8^+$ T cell–mediated acute cholangitis. In K14-OVAp mice, the ovalbumin-derived peptide sequence SIINFEKL ($OVA_{257-264}$), a defined MHC class I epitope, is expressed under the control of the human keratin 14 (K14) promoter, resulting in antigen presentation predominantly by biliary epithelial cells. Following adoptive transfer of antigen-specific ovalbumin transgenic OT-1 $CD8^+$ T cells, which specifically recognize SIINFEKL presented on H-$2K^b$, a targeted cytotoxic immune response is initiated[139].

After adoptive OT-1 T cell transfer, liver inflammation peaked approximately four days post-transfer, characterized by pronounced immune cell infiltration in portal areas (Figure 18A) and a significant increase in serum transaminases (AST and ALT) (Figure 18B). Over time, an increasing number of congenic OT-1 CD8$^+$ T cells infiltrated the liver, with the majority of infiltration occurring between day 3 and day 4 after transfer (Figure 18C).

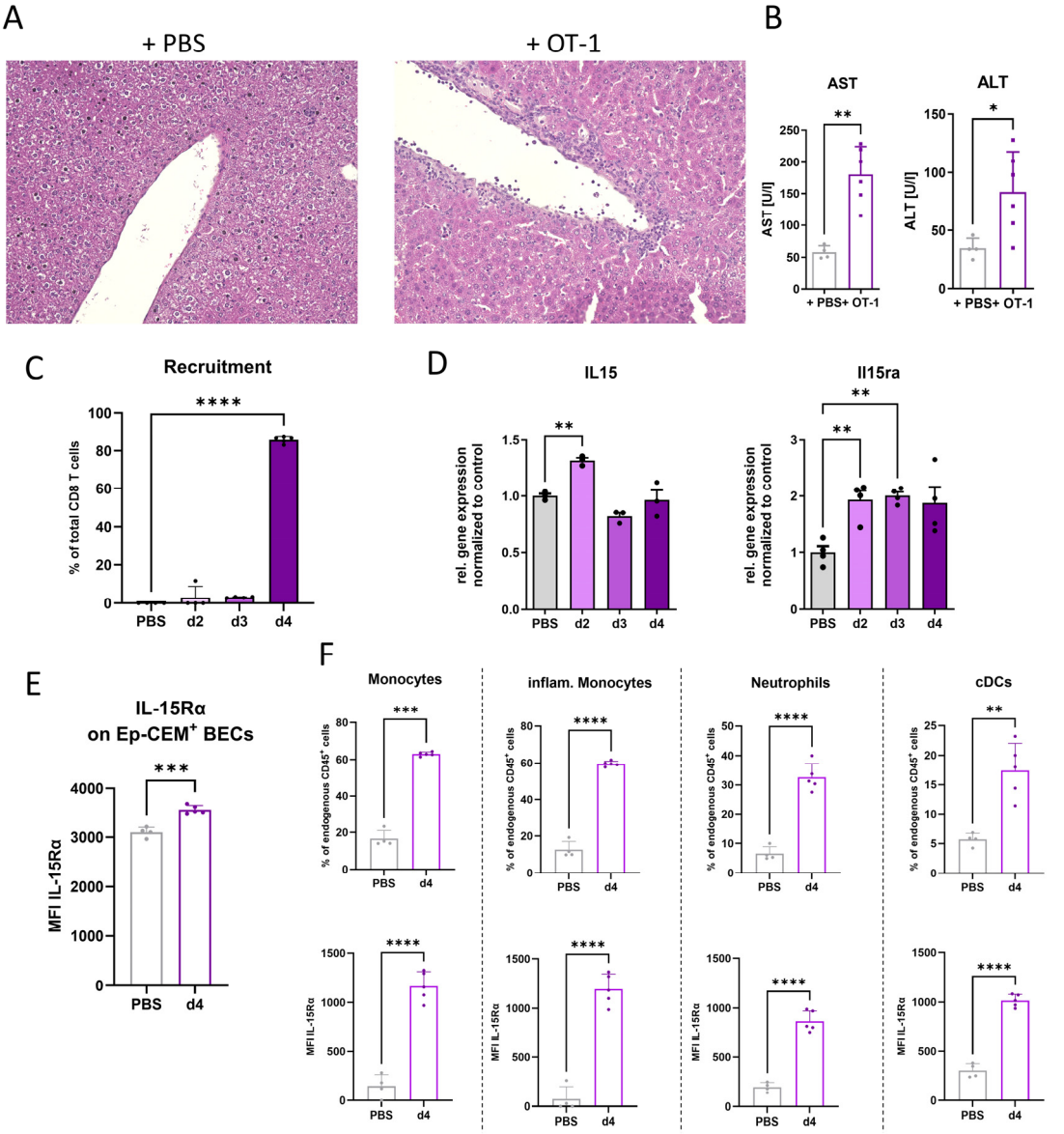

Figure 18: **IL-15 and IL-15Rα expression in a mouse model of acute experimental cholangitis.**

(A) Representative hematoxylin and eosin (H&E)–stained sections of portal fields from K14-OVAp mice 4 days after adoptive transfer of OT-1 CD8$^+$ T cells (right) or PBS control (left). **(B)** Serum aspartate aminotransferase (AST) and alanine aminotransferase (ALT) levels in K14-OVAp mice 4 days after OT-1 T cell transfer compared with PBS-treated controls. **(C)** Time course of OT-1 CD8$^+$ T cell recruitment to the liver following adoptive transfer. **(D)** Fold change in *Il15* and *Il15ra* mRNA expression in whole liver tissue from day 2 to day 4 after OT-1 transfer. **(E)** Flow cytometric analysis of IL-15Rα surface expression on cholangiocytes 4 days after OT-1 transfer compared with PBS controls. **(F)** Abundance (top) and IL-15Rα mean fluorescence intensity (MFI; bottom) of monocytes, inflammatory monocytes, neutrophils, and classical dendritic cells (cDCs) 4 days after OT-1 transfer and in PBS-treated controls. Pairwise comparisons were performed using Welch's *t* test, and multiple group comparisons were analyzed using one-way ANOVA (*$p \leq 0.05$, **$p \leq 0.01$, ***$p \leq 0.001$, ****$p \leq 0.0001$).

Notably, transcriptional changes within the liver parenchyma were detectable at earlier time points. Two days post-transfer, whole-liver gene expression analysis revealed increased levels of *Il15* and *Il15ra*. While *Il15* expression normalized by day 3, *Il15ra* expression remained approximately two-fold elevated throughout the observation period (Figure 18D).

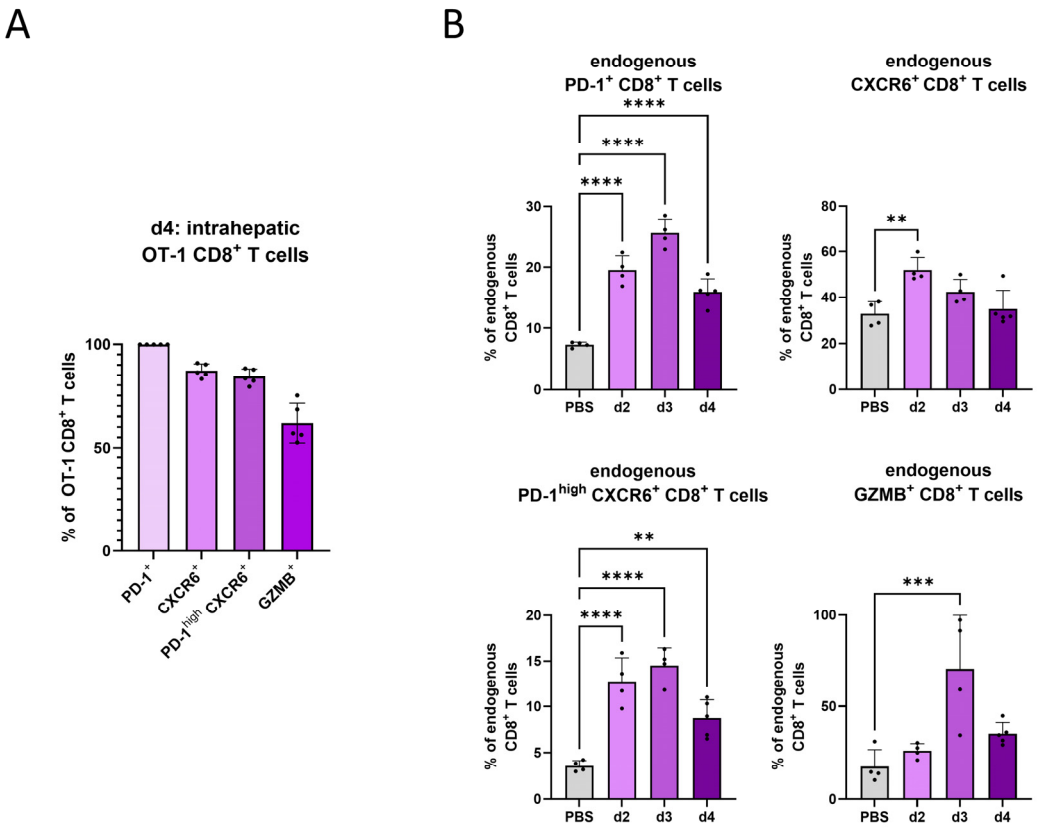

Figure 19: **Time course of bystander-activated phenotypes in transferred and endogenous CD8⁺ T cells.**

(A) Frequencies of PD-1⁺, CXCR6⁺, PD-1^{high}CXCR6⁺, and GZMB⁺ OT-1 CD8⁺ T cells isolated from the liver of K14-OVAp mice 4 days after adoptive transfer. **(B)** Temporal development of endogenous CD8⁺ T cell phenotypes following OT-1 transfer, showing frequencies of PD-1⁺ (top left), CXCR6⁺ (top right), PD-1^{high}CXCR6⁺ (bottom left), and GZMB⁺ (bottom right) cells from day 2 to day 4 post-transfer. Statistical analysis was performed using one-way ANOVA (**p ≤ 0.01, ***p ≤ 0.001, ****p ≤ 0.0001).

Flow cytometric analysis confirmed upregulation of IL-15Rα on primary EpCAM⁺ cholangiocytes at day 4 following OT-1 transfer (Figure 18E). In parallel, endogenous immune cell populations, including monocytes, inflammatory monocytes, neutrophils, and conventional dendritic cells, were increased at day 4. Importantly, these cell types also exhibited enhanced IL-15Rα surface expression, indicating a broader increase in IL-15 trans-presentation capacity within the inflamed liver (Figure 18F).

Transferred OT-1 CD8⁺ T cells isolated from the liver were further analyzed by flow cytometry. All OT-1 cells expressed PD-1, likely reflecting strong antigen exposure in

early stages of T cell activation[140]. In mice, CXCR6 expression, particularly in combination with high PD-1 levels, has been described as a marker of IL-15–induced bystander-activated $CD8^+$ T cells[99]. The majority of intrahepatic OT-1 $CD8^+$ T cells displayed CXCR6 expression, and a substantial fraction exhibited $CXCR6^+PD\text{-}1^{high}$ co-expression, consistent with IL-15 exposure. At the same time, these cells showed a highly cytotoxic phenotype, with more than 60 % expressing granzyme B (Figure 19A). This phenotype is not generated by IL-15 alone. However, IL-15 expression by antigen-presenting cells may amplify cytotoxic differentiation during antigen-specific $CD8^+$ T cell responses.

Interestingly, endogenous $CD8^+$ T cells, which are unable to recognize the SIINFEKL antigen, also displayed signs of activation. Expression of the co-inhibitory receptor PD-1 was increased between day 2 and day 4 following OT-1 transfer. Although the total number of $CXCR6^+$ endogenous $CD8^+$ T cells was only transiently increased at day 2 and normalized at later time points, the frequency of $PD\text{-}1^{high}$ $CXCR6^+$ endogenous $CD8^+$ T cells remained elevated from day 2 to day 4. Expression of the effector molecule Granzyme B showed an increasing trend, reaching statistical significance at day 3 (Figure 19B).

In summary, the K14-OVAp model of acute cholangitis demonstrates enhanced IL-15 trans-presentation by cholangiocytes and intrahepatic immune cells, as evidenced by increased IL-15Rα surface expression. Antigen-specific OT-1 $CD8^+$ T cells exhibited a pronounced IL-15-associated phenotype, while endogenous $CD8^+$ T cells displayed features of bystander-activation, consistent with IL-15 exposure. These findings support a role for IL-15 as a key mediator of $CD8^+$ T cell activation and could link it to dysfunction in inflammatory cholangitis.

4 Discussion

PSC is a chronic, progressive cholestatic liver disease characterized by inflammation and fibrosis of the intra- and extrahepatic bile ducts, ultimately leading to biliary cirrhosis and liver failure[123]. Despite clear evidence for immune involvement and a strong association with inflammatory bowel disease, disease-modifying therapies are lacking, and the mechanisms driving biliary injury remain poorly understood. While lymphocytic infiltration of portal tracts and bile ducts is a hallmark of PSC, the functional contribution of specific immune cell subsets to disease pathogenesis has not been fully elucidated[49].

Accumulating evidence points to a central role of $CD8^+$ T cells in PSC. Histological analyses have shown that $CD8^+$ T cells are frequently present within inflamed portal tracts and in close spatial proximity to cholangiocytes[74]. Their enrichment within portal fields suggests selective recruitment or retention within the biliary microenvironment. Despite this prominent localization, $CD8^+$ T cells have remained comparatively understudied in PSC, and their activation state, effector phenotype, and contribution to biliary injury have not been clearly defined.

Recently, a new IL-15 mediated antigen-independent activation of $CD8^+$ T cells with cytotoxic and pro-inflammatory properties in several chronic liver disease has been described[99,100]. IL-15 is a pleiotropic cytokine with a central role in the activation, survival, and tissue retention of cytotoxic lymphocytes, particularly memory and tissue-resident $CD8^+$ T cells and NK cells. IL-15 signaling is tightly regulated and typically occurs via trans-presentation by IL-15Rα-expressing cells, enabling potent local effects within tissue microenvironments. However, whether IL-15 contributes to immune dysregulation in PSC, its cellular sources within the PSC liver, and its impact on $CD8^+$ T cell behavior have not been addressed to date.

This study aimed to fill this knowledge gap by investigating the role of IL-15 in shaping $CD8^+$ T cell phenotypes and their interaction with cholangiocytes in PSC. By integrating high-dimensional immune profiling of peripheral blood and liver tissue with single-cell, single-nucleus, and spatial transcriptomic approaches, *in vitro* cholangiocyte models, and a translational mouse model of cholangitis, strong evidence is provided for an IL-15-associated, bystander-activated $CD8^+$ T cell phenotype in PSC, which may contribute to disease pathogenesis.

Across systemic and intrahepatic compartments, $CD8^+$ T cells in PSC display a phenotype consistent with IL-15–associated bystander activation. Peripheral blood $CD8^+$

T cells already in early disease stages show increased PD-1 and HLA-DR expression and altered granzyme profiles. In the liver, single-cell and single-nucleus transcriptomic analyses identify effector memory $CD8^+$ T cell populations enriched for IFNγ, exhaustion markers, NK-associated receptors, and IL-15–related signaling pathways, with one subset expanding with disease progression. Biliary epithelial cells emerge as a prominent source of *IL15* and *IL15RA*, with expression detectable in early PSC and increasing with disease severity, and inducible by IFNγ *in vitro*. Spatial transcriptomics further demonstrates close proximity of *IL15*–expressing cholangiocytes and activated $CD8^+$ T cells within inflamed portal niches. Finally, a mouse model of acute cholangitis confirms induction of IL-15 signaling and bystander activation of endogenous $CD8^+$ T cells *in vivo*.

In summary, bystander-activated $CD8^+$ T cells are increased in both the liver and peripheral blood of individuals with PSC and are enriched in close spatial proximity to inflamed bile ducts. Moreover, biliary epithelial cells emerge as a prominent source of IL-15 and IL-15Rα, capable of locally shaping $CD8^+$ T cell activation states within the portal niche.

The present study identifies an expanded population of IL-15-associated, bystander-activated $CD8^+$ T cells in both the liver and peripheral blood of individuals with PSC. Bystander-activated $CD8^+$ T cells are characterized by cytokine-driven activation independent of cognate TCR engagement and have been shown to acquire cytotoxic and pro-inflammatory effector functions in response to local tissue-derived signals. While these cells were not functionally tested for direct cytotoxicity toward cholangiocytes in PSC tissue, insights from other chronic inflammatory liver diseases provide important context for their potential pathogenic relevance.

In this context, Dudek et al. (2021) demonstrated that IL-15-primed $CD8^+$ T cells in murine metabolic liver disease respond to metabolic stimuli such as cyclic AMP, which licenses cytotoxic activity in a TCR-independent manner[99]. This finding provides a mechanistic framework by which IL-15-activated $CD8^+$ T cells may mediate tissue injury without antigen recognition. Emerging, unpublished data from the same group further suggest that human bystander-activated $CD8^+$ T cells can respond to extracellular histones via innate-like receptors. Given the extensive epithelial damage, cell death, and tissue remodeling characteristic of inflamed bile ducts in PSC, histones are likely abundant within the biliary microenvironment and may therefore represent a plausible trigger for TCR-independent $CD8^+$ T cell activation and epithelial injury.

Besides direct cytotoxicity, bystander-activated CD8⁺ T cells may contribute to disease progression through effects on fibrotic remodeling. A prominent feature of the CD8⁺ T cell populations identified in this study is the high expression of granzyme K. GZMK⁺ CD8⁺ T cells are enriched in inflamed tissues and have recently been shown to promote fibroblast activation through cleavage of protease-activated receptor-1 (PAR-1), thereby driving fibrogenic responses[127,129]. In PSC, where progressive fibrosis is a defining pathological hallmark, sustained GZMK release may link immune activation directly to structural bile duct remodeling.

At the same time, GZMK has been described as a mediator of complement activation[141]. Complement activation enhances bacterial defense by opsonizing pathogens, recruiting immune cells through anaphylatoxins, and directly lysing bacteria via the membrane attack complex (MAC)[142]. Given the microbial background of PSC and its close association with intestinal inflammation, this function may initially be protective. However, chronic or dysregulated GZMK expression could shift this balance toward persistent inflammation and fibrosis, thereby exacerbating disease progression.

IL-15 itself is known to exert context-dependent effects on CD8⁺ T cells, promoting cytotoxic effector functions during acute immune responses while inducing cellular dysfunction, exhaustion, or senescence upon prolonged exposure. Persistent IL-15 signaling within the biliary microenvironment may therefore sustain epithelial injury while simultaneously driving maladaptive immune activation[107]. Over time, this combination of chronic inflammation, epithelial stress, and fibrotic remodeling could contribute to the increased risk of cholangiocarcinoma observed in PSC.

The possibility that bystander-activation originates outside the liver further highlights the relevance of the gut–liver axis in PSC. IL-15-driven TCR-independent activation of CD8⁺ T cells was first described by Meresse et al. (2004) in celiac disease, where epithelial IL-15 expression primed cytotoxic lymphocytes independently of antigen specificity[122]. Because PSC is closely linked to inflammatory bowel disease, a comparable priming process may also take place in the intestinal mucosa. Indeed, intestinal inflammation in PSC is often persistent even in the absence of overt gastrointestinal symptoms[143]. IL-15–primed, CXCR3⁺ and CXCR6⁺ CD8⁺ T cells generated in the gut may subsequently be recruited to the liver via cholangiocyte-derived chemokines, where their phenotype could further evolve within the inflamed biliary niche.

The present data support a model in which cholangiocyte-derived IL-15 and CD8⁺ T cell-derived IFNγ form a self-amplifying feedback loop (Figure 20). IFNγ potently induces IL-15 and IL-15Rα expression in cholangiocytes and simultaneously promotes the production of chemokines such as CXCL9, CXCL10, CXCL11, and CXCL16, facilitating further recruitment of activated CD8⁺ T cells. IL-15 signaling in turn enhances CD8⁺ T cell activation and has been shown to prime NK cells towards increased IFNγ production by increasing Tbet expression[133,144]. Furthermore, this expression can be counteracted by IL-15-mediated FOXO1 signaling, which appeared to be downregulated in bystander-activated CD8⁺ T cells in a MASH mouse model. Importantly, IFNγ also induces PD-L1

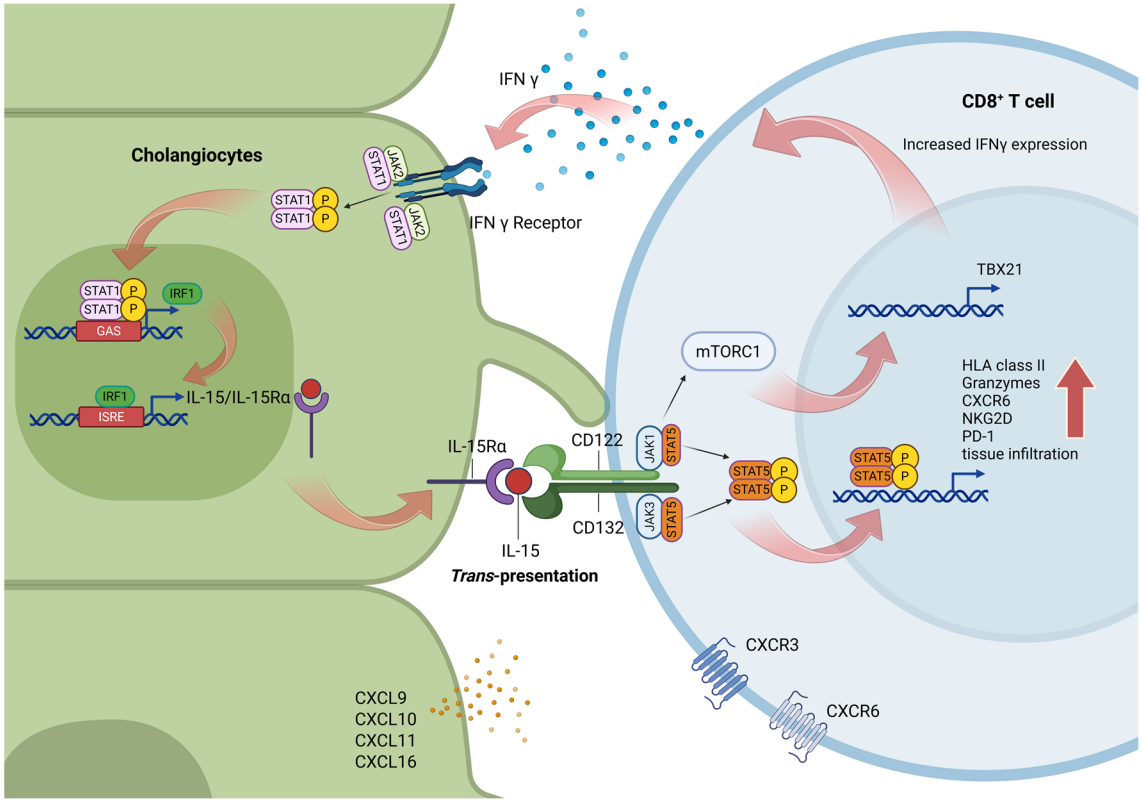

Figure 20: **Proposed model of IL-15-dependent crosstalk between cholangiocytes and CD8⁺ T cells in PSC forming a potential positive feedback loop**

This schematic summarizes a putative positive feedback loop between cholangiocytes and CD8⁺ T cells that may contribute to biliary inflammation in PSC. Interferon-γ (IFNγ), predominantly produced by activated CD8⁺ T cells, induces IL-15 and IL-15Rα expression in cholangiocytes through STAT1 phosphorylation, nuclear translocation, and binding to gamma-activated sequences (GAS), leading to induction of interferon regulatory factor 1 (IRF1). IRF1 subsequently binds to interferon-stimulated response elements (ISRE) within the promoter regions of *IL15* and *IL15RA*. Following translation, IL-15 forms a complex with IL-15Rα, which is transported to the cell surface and presented in trans to neighboring CD8⁺ T cells. Engagement of this complex by the IL-15 receptor β/γ heterodimer (CD122/CD132) on CD8⁺ T cells activates JAK1 and JAK3, resulting in STAT5 phosphorylation, dimerization, and nuclear translocation. Sustained IL-15 signaling is associated with increased expression of HLA class II molecules, granzymes, NK cell receptors such as NKG2D or CXCR6 and the inhibitory receptor PD-1, as well as enhanced tissue infiltration capacity of CD8⁺ T cells. In parallel, IL-15 signaling may promote mTORC1-dependent upregulation of *TBX21* (encoding T-bet), a key transcription factor driving effector CD8⁺ T cell differentiation and IFNγ production. Together, these processes may establish a self-amplifying inflammatory loop between cholangiocytes and CD8⁺ T cells that sustains biliary inflammation and tissue remodeling in PSC. Created with Biorender.com.

expression on cholangiocytes, which may serve as a counter-regulatory mechanism by limiting STAT5 signaling downstream of IL-15. Dysregulation of this balance, either through excessive IL-15 signaling or impaired inhibitory feedback, could result in sustained bystander-activation of $CD8^+$ T cells. Once established, this loop may perpetuate bile duct injury, promote fibrotic remodeling, and contribute to long-term malignant transformation.

Genetic susceptibility may further lower the threshold for IL-15–driven immune dysregulation in PSC. Multiple PSC-associated SNPs are linked to pathways involved in IL-2 signaling[23], which shares key signaling components with IL-15, including CD122, CD132, and downstream JAK-STAT pathways. Notably, variants in SH2B3, a negative regulator of cytokine signaling, have been associated with PSC development[145]. In murine models, SH2B3 deficiency results in heightened sensitivity of $CD8^+$ T cells to common γ-chain cytokines, including IL-2, IL-7, and IL-15, accompanied by increased expression of cytotoxic markers such as CXCR3[146]. Such genetic alterations may predispose $CD8^+$ T cells in PSC to exaggerated bystander-activation in response to IL-15.

From a therapeutic perspective, IL-15-induced STAT5 activation in $CD8^+$ T cells depends on JAK signaling, suggesting potential relevance of JAK inhibition. JAK inhibitors such as tofacitinib are already approved for the treatment of inflammatory bowel disease, and clinical observations suggest a trend toward reduced liver transaminases in people with PSC receiving tofacitinib for concomitant IBD[147]. While this effect may reflect improved intestinal inflammation, inhibition of IL-15–mediated bystander-activation of $CD8^+$ T cells represents an alternative and mechanistically plausible explanation. Future studies analyzing $CD8^+$ T cell phenotypes in people with PSC undergoing JAK inhibitor therapy will be essential to clarify this possibility.

In addition, preliminary data from Dudek et al. (2021) identified C-type lectin receptors as mediators of histone-driven activation of bystander-activated $CD8^+$ T cells, with downstream signaling dependent on spleen tyrosine kinase (SYK). Their data suggest that SYK inhibition may attenuate bystander-activated killing, highlighting another potential therapeutic avenue. However, validation of this approach in preclinical models is required before clinical translation.

Several limitations of this study should be acknowledged. While close spatial proximity between activated $CD8^+$ T cells and cholangiocytes was demonstrated, direct cytotoxic effects on cholangiocytes were not assessed. Notably, prior studies in primary biliary

cholangitis have described close interactions between $CD8^+$ T cells and biliary epithelial cells, including epithelial invasion, without overt cytotoxicity. Whether IL-15-associated bystander-activated $CD8^+$ T cells exert direct cytotoxic effects on cholangiocytes in PSC therefore remains to be determined. Furthermore, bystander-activation may occur prior to direct interaction with cholangiocytes, as multiple hepatic and extrahepatic cell types can express IL-15. Our sNucSeq data suggest also a potential contribution of the myeloid or hepatocyte compartment. Conditional deletion of IL-15 in cholangiocytes in murine models will be required to definitively establish the contribution of cholangiocyte-derived IL-15 to PSC pathogenesis.

5 Conclusion and outlook

In summary, these data present a comprehensive characterization of $CD8^+$ T cells in PSC across peripheral blood and liver tissue and across different disease stages. Using high-dimensional immune profiling approaches, a distinct population of $CD8^+$ T cells with a bystander-activated phenotype was identified. These cells are characterized by the expression of NK cell-associated markers, MHC class II molecules, interferon-γ, and cytotoxic effector molecules, a constellation of features that has been previously linked to cytokine-driven activation rather than antigen-specific T cell receptor engagement. The consistent presence of this phenotype in both the circulation and the inflamed liver suggests that bystander-activated $CD8^+$ T cells represent a relevant immunological component of PSC.

Beyond defining the $CD8^+$ T cell compartment, this work identifies biliary epithelial cells as a prominent source of IL-15 and IL-15Rα within the PSC liver. By combining single-nucleus and spatial transcriptomic analyses in combination with *in vitro* cholangiocyte experiments and a translational mouse model, a previously unrecognized mechanism of antigen-independent $CD8^+$ T cell activation by cholangiocytes is proposed. These findings extend the role of biliary epithelial cells beyond passive targets of immune-mediated injury and position them as active regulators of the local immune microenvironment in PSC.

Together, the identification of IL-15–associated, bystander-activated $CD8^+$ T cells and their potential induction by cholangiocyte-derived IL-15 provides new mechanistic insight into PSC pathogenesis. This cytokine-driven interaction between cholangiocytes and $CD8^+$ T cells offers a plausible link between chronic biliary inflammation, fibrotic remodeling, and progressive tissue damage in PSC. Importantly, it also highlights the IL-15 axis as a potential therapeutic target. Future studies should aim to directly assess the functional consequences of bystander-activated $CD8^+$ T cells on cholangiocyte integrity, to define the relative contribution of cholangiocyte-derived IL-15 *in vivo*, and to explore pharmacological strategies targeting IL-15-associated signaling pathways. Ultimately, a better understanding of this immune-epithelial crosstalk may contribute to the development of novel, mechanism-based treatment approaches for PSC, a disease for which curative therapies beyond liver transplantation are still lacking.

6 Methods

6.1 Patient selection and acquisition of blood and tissue samples

Peripheral blood was collected from people with autoimmune liver diseases (AILD) at early disease stages, including PSC (n = 21) and primary biliary cholangitis (PBC, n = 13), who attended the outpatient service of the I. Department of Medicine, University Medical Centre Hamburg-Eppendorf (UKE; Hamburg, Germany), as well as from age- and sex-matched healthy donors (HD, n = 18 [m: 12, f:6, age: 43.4±11.7 years]). These samples were used for immunophenotyping and functional assays.

In addition, liver tissue samples were obtained from people undergoing liver biopsy (PSC: n = 17, no histological findings: n = 4) or transplantation at the University Medical Center Hamburg-Eppendorf (UKE, Hamburg, Germany). Included were people with PSC (n = 4) and alcoholic liver disease (ALD, n = 3). Tissue collection was performed at the time of surgery. Clinical parameters were recorded immediately prior to surgery. These samples were used to generate cholangiocytes organoid cultures.

All patients and healthy donors gave written informed consent in line with the ethical standards approved by the Institutional Review Board of the Medical Faculty at the University of Hamburg (approval number PV4081). Diagnoses and treatment decisions were made according to the current guidelines of the European Association for the Study of the Liver (EASL).[32]

Tabelle 1: Clinical data for blood cohorts of people with PSC and PBC.

	Age [years]	Sex	Colitis yes/no	Immunosuppression yes/no	Fibroscan [kPa]	UDCA yes/no	Total bilirubin [mg/dl]
PSC	44.5 ± 11.4	m: 15 f: 7	y: 14 n: 8	y: 1 n: 21	6.9 ± 2,6	y:22 n:0	0.9 ± 0.3
PBC	52.0 ± 11.3	m: 4 f: 9	y: 0 n: 13	y: 0 n: 13	5.5 ± 1.8	y:12 n:1	0.67 ± 0.3
	AST [U/l]	**ALT [U/l]**	**GGT [U/l]**	**AP [U/l]**	**AMA-M2 yes/no**	**anti-Sp100 yes/no**	**anti-gp210 yes/no**
PSC	41,8 ± 27,7	54.3 ± 32.7	154.3 ± 183.9	184.2 ± 158.1	-	-	-
PBC	32.1 ± 14.0	44.4 ± 41.2	86.8 ± 93.8	149.8 ± 72.0	y: 13 n: 0	y: 8 n: 5	y: 3 n: 10

Tabelle 2: Clinical data of persons undergoing liver transplantation. Smaples were used for organoid cultures.

	Age [years]	Sex	Colitis yes/no	Immunosuppression yes/no	UDCA yes/no	Cirrhosis yes/no
PSC	42.5 ± 12.2	m: 2 f: 2	y: 2 n: 2	y: 0 n: 4	y: 2 n: 2	y: 4 n: 0
ALD	57.3 ± 2.6	m: 2 f: 1	y: 0 n: 3	y: 1 n: 0	y: 0 n: 3	y: 3 n: 0
	Fibroscan [kPa]	**Total bilirubin [mg/dl]**	**AST [U/l]**	**ALT [U/l]**	**GGT [U/l]**	**AP [U/l]**
PSC	49.5 ± 12.0	9.2 ± 6.8	945.5 ± 1115.4	315.8 ± 339.6	152.5 ± 116.6	471.7 ± 262.9
ALD	-	14.7 ± 2.0	426.0 ± 472.9	217.7 ± 249.2	36 ± 17.2	172.0 ± 61.0

Tabelle 3: Clinical data of people with PSC and controls for spatial transcriptomic analysis.

	Age [years]	Sex	Colitis yes/no	Immunosuppression yes/no	UDCA yes/no	Cirrhosis yes/no	Fibrosis
Control	45 ± 8.9	m: 2 f: 2	y: 0 n: 4	y: 0 n: 4	y: 0 n: 4	y: 0 n: 4	0
PSC early	33.2 ± 8.4	m: 10 f: 1	y: 10 n: 1	y: 5 n: 6	y: 10 n: 1	y: 0 n: 11	1.4 ± 0.7
PSC later	48 ± 18.3	m: 5 f: 2	y: 4 n: 3	y: 2 n: 5	y: 6 n: 1	y: 3 n: 4	3.3 ± 0.7
	mHAI	**Total bilirubin [mg/dl]**	**AST [U/l]**	**ALT [U/l]**	**GGT [U/l]**	**AP [U/l]**	
Control	0	0.7 ± 0.1	34.7 ± 13.8	62.3 ± 27.1	184 ± 67.1	215 ± 125.1	
PSC early	2.0 ± 1.3	2.0 ± 1.7	138.6 ± 137.8	285.3 ± 441.4	438.4 ± 387.2	364.0 ± 248.1	
PSC later	2.7 ± 0.9	2.4 ± 2.2	182.6 ± 271.9	82.7 ± 30.0	281.1 ± 116.5	326.2 ± 190.9	

6.2 Human cell isolations from liver tissue and peripheral blood

6.2.1 Isolation of mononuclear cells from peripheral blood for spectral flow cytometry

Mononuclear cells form whole blood have been isolated using Ficoll Paque density centrifugation. EDTA pre-treated whole blood has been diluted 2/3 with PBS and layered over Ficoll Paque. After centrifugation (20 min, 600 x *g*, reduced acceleration and no break) the layer containing mononuclear cells was collected and cells were washed twice with PBS. Cells have been frozen in defined cell numbers in FCS containing 10 % DMSO or directly used for further experiments.

6.2.1.1 Flow cytometry of PBMCs

Staining was initiated immediately after thawing the PBMCs. Cells were resuspended in PBS containing a live/dead stain and incubated for 15 min at 4 °C, then washed and labeled with surface antibodies for 30 min at 4 °C. After an additional wash with PBS, the samples were resuspended in Fix/Perm solution and incubated for 30 min at 4 °C. Cells were washed with Perm-Wash Buffer and resuspended in wash buffer containing antibodies for intracellular staining and incubated 1 h at RT or at 4°C over night. Cells were washed and resuspended in PBS before acquired with the Cytek® Aurora 5 laser system. Flow cytometry data were analyzed by manual gating in the FlowJo™ 10 software.

6.2.2 Magnetic-activated cell sorting of $CD8^+$ T cells

$CD8^+$ T cells of cryopreserved or freshly isolated mononuclear cells has been enriched according to the user's manual of the human $CD8^+$ T cell isolation Kit (Miltenyi, Germany).

6.3 Culturing and stimulation of H69 biliary epithelial cells

H69 human biliary epithelial cells were cultured in H69 BECs medium (Table 12) under standard conditions. For passaging, cells were washed with DPBS, detached using TrypLE (3 mL for T25 or 7 mL for T75 flasks), and incubated for 5 min at 37 °C. TrypLE was neutralized with complete medium, and cells were collected, centrifuged (400 x *g*, 5 min, RT), resuspended, and counted. Cells were seeded at appropriate density in 24-well plates and allowed to adhere and recover for 24 hours. Stimulation experiments were conducted 24 hours post-seeding.

6.4 Generation and stimulation of human intrahepatic cholangiocytes organoids

Cholangiocyte organoids with intrahepatic origin were generated from explant liver tissue. Tissue cut liver tissue from liver transplantation has been automatically homogenized in the gentlaMACS™ Octo Dissociator in digestion solution (EBSS, Collagenase D and DNAse) at 37 °C with rotation for to 36 min. Afterwards cell suspension gets processed through a tissue strainer (100 μm mesh size). Cells were washed with basal media (Advanced DMEM + 1 % P/S + 1 % L-Glutamine) and centrifuged for 5 min at 500 x *g* and 4 °C. The cell pellet was resuspended in 3 ml cold PBS and layered over a two times 3.5 mL of 77 and 33 % of Percoll mixed with PBS. Gradient centrifugation was performed at 500 x *g* for 30 min at 4 °C (acceleration: 1; break: 0). Biliary progenitor cells containing layer of the gradient was collected and washed with basal media. Isolated cells were seeded into Matrigel (BME) and cultured for 72 h in differentiation media (Table 1). Afterwards, media is changed to expansion medium (Table 12). Organoids are passaged every 7-10 days by disrupting formed organoids and seeding them into new Matrigel. Afterwards cholangiocytes organoids are cultured for 72 h in differentiation medium. All organoids experiments has been performed between passage 4 and 8.

Stimulation of cholangiocyte organoids has been performed for 24 h with: IFNγ (100 ng/mL), IL-17A (50 ng/mL) and IL1β (1 ng/mL). Cholangiocyte oragnoids have been at least 24 h in expansion media before stimulation.

6.5 Flow cytometry of H69 BECs

Medium was removed from H69 BECs and washed with PBS. Supernatant was removed and cells were incubated in tripleE at 37 °C for 5 min. Single cells were washed using magnetic-activated cell sorting (MACS) buffer and centrifuged at 400 x *g*. Cells were stained with propidium iodide stain in MACS buffer for 15 min at 4 °C, washed and stained with surface master mix. Cells were washed and resuspended in MACS buffer before acquired with the Cytek® Aurora 5 laser system. Flow cytometry data were analyzed by manual gating in the FlowJo™ 10 software.

The same protocol has been performed for H69 BECs. Adherent cells were washed with DPBS and incubated for 5 min with Triple E. Washed afterwards with culture media stained as described above.

6.6 pSTAT5 quantification after $CD8^+$ T cell and H69 BEC co-culture

H69 BECs were seeded under standard culture conditions in 96-well flat-bottom plates at a density of 15,000 cells per well. After 24 h, cells were stimulated with 50 ng/mL IFNγ for 24 hours. Following stimulation, cells were washed with culture medium to remove residual cytokine. $CD8^+$ T cells were magnetically enriched from PBMCs. Isolated $CD8^+$ T cells were then cultured for 24 hours in cytokine-free RPMI medium supplemented with 10 % FCS, 1 % L-glutamine, and 1 % P/S. After IFNγ stimulation and washing, H69 BECs were co-cultured with $CD8^+$ T cells for 1 hour in a 1:1 mixture of H69 medium and RPMI medium. Anti-human IL-15 antibodies were added 30 min prior to co-culture and maintained throughout the co-culture period. pSTAT5 levels were quantified using the BD™ Phosflow staining protocol according to the manufacturer's instructions.

6.7 Gene expression assays

Total RNA was isolated using the NucleoSpin RNA Mini Kit (MACHEREY-NAGEL, #740955) according to the manufacturer's instructions. RNA was reverse transcribed into cDNA using the High-Capacity cDNA Reverse Transcription Kit (Applied Biosystems, #4368814). Gene expression was assessed using TaqMan assays, with hypoxanthine-guanine phosphoribosyltransferase (HPRT) as the endogenous control. Relative gene expression was quantified using the ΔΔCt method. List of TaqMan probes in Table 9.

6.8 Mice

All animal experiments were conducted in accordance with the ARRIVE guidelines[148] and approved by the ethics committee of the State of Hamburg, Germany (G36/16 and ORG846). K14-OVAp (kindly provided by Kirsten Hoquist; Mineapolis, USA) and OT-1 mice, both on a C57BL/6 background, were used in this study. Mice were bred in-house at the animal facility of the University Medical Center Hamburg-Eppendorf. Genotypes were confirmed regularly by PCR. Animals were housed under specific pathogen-free conditions with a 12 hour light/dark cycle and had unrestricted access to standard chow (Altromin, Germany) and water. All experiments including mice were performed in cooperation with Sabrina Pilz (I. Department of Medicine University Medical Center Hamburg-Eppendorf).

6.8.1 Induction of acute cholangitis in mice

For the induction of acute experimental cholangitis, only female K14-OVAp mice aged 7-10 weeks were used. This decision was based on prior findings by Schwinge et al. (2015), which demonstrated a stronger disease phenotype in female mice within this model[149]. $CD8^+$ T cells were isolated from the spleens of female OT-1 donor mice using FITC-conjugated anti-CD8 antibodies and MACS (Miltenyi Biotec, Germany), following the manufacturer's protocol. To trigger cholangitis, freshly isolated OT-1 $CD8^+$ T cells were administered intravenously into K14-OVAp recipient mice at a dose of 5×10^5 T cells per 200 µL per animal. The onset of cholangitis symptoms typically occurred within 4 days after adoptive transfer.

6.8.2 Isolation of lymphocytes from liver and spleen

Lymphocytes from spleen were isolated by mechanically dissociating the tissue through 100 µm strainers in PBS, followed by centrifugation for 5 min at 400 x *g*. To eliminate erythrocytes from spleen cell suspensions, red blood cells were lysed using 1× Ammonium-Chloride-Potassium (ACK) lysis buffer.

For liver non-parenchymal cell isolation, livers were first perfused with PBS and then mechanically disrupted. Hepatocytes and cellular debris were removed by two sequential centrifugation steps at 40 x *g*. The remaining non-parenchymal cells were enriched by

density gradient centrifugation using a 35 % Optiprep solution at 400 g. ACK buffer was again used to lyse residual erythrocytes in the liver cell preparations.

6.9 Data analysis of single-cell CITE sequencing dataset

All subsequent steps involving the processing and analysis of single-cell sequencing data were carried out in collaboration with Christian Casar from the Bioinformatics Core Facility at the University Medical Center Hamburg-Eppendorf (Hamburg, Germany).

6.9.1 Data processing:

Publicly available CITE-sequencing data generated by Poch et al. (2021) were used for this study[69]. The dataset was derived from sorted $CD3^+$ T cells from liver tissue of individuals with end stage PSC and ALD. Initial processing steps, including: demultiplexing, alignment to the GRCh38 reference genome (release 93), and summarization, were performed using the Cell Ranger pipeline (v3.0.2, 10x Genomics). Subsequent data analysis was carried out in R (v3.6.2) using the Seurat package (v3.1)[150].

Cell hashing had been applied to a subset of samples (frozen PSC and ALD) using anti-CD45 antibody-derived tags (CD45-BC32 and CD45-MK33). These samples were demultiplexed using the HTODemux function from Seurat following centered log-ratio transformation. Cells were classified based on tag expression profiles using K-medoids clustering and a fitted negative binomial distribution. Doublets were excluded from downstream analysis.

For quality control, cells with low UMI counts, abnormally high or low gene expression, or elevated mitochondrial transcript levels were filtered out based on thresholds defined in the original study. Data normalization and identification of highly variable genes were performed using Seurat's SCTransform function, applying a regularized negative binomial regression model to stabilize variance across genes. No correction for cell cycle effects was applied, as no bias was evident upon principal component analysis of cell cycle genes.

For the present study, analysis was restricted to $CD8^+$ T cells from PSC-derived samples. These were identified based on co-expression of CD8A and CD8B transcripts, along with

positive ADT signal for CD8. Cells expressing CD4 mRNA or showing a positive ADT signal for CD4 were excluded to ensure purity of the $CD8^+$ population.

Batch effects across donors and sample types were corrected using Seurat's anchor-based integration method, applying a common set of highly variable genes (n = 2,000) shared across samples. ADT normalization was performed using centered log-ratio transformation with Seurat's NormalizeData function, followed by rescaling to a range of -4 to 4.

6.9.2 Dimension reduction, clustering and expression analysis:

Batch-corrected expression values from the integration anchors were used for dimensionality reduction via UMAP and for clustering based on a shared nearest neighbor graph. Up to 20 principal components were included in these analyses. Clustering resolution was incrementally increased until no further biologically interpretable clusters with distinct marker gene expression could be identified. Cluster markers were identified by conducting differential gene expression analysis for each cluster against all other cells, applying logistic regression to the sample-normalized RNA expression data. Donor identity was included as a covariate in the model, and statistical significance was assessed using a likelihood ratio test against a null model.

Cluster identities were assigned by integrating multiple layers of information, including differentially expressed genes, ADT expression patterns, and UMAP projection of manually gated cell populations based on ADT profiles.

6.9.3 Gene set expression scoring and pathway enrichment analysis

To assess functional gene expression programs, per-cell expression scores were calculated for selected gene sets. Normalized expression values were extracted from the SingleCellExperiment object, and scores were computed as the mean expression across all genes within each set. These scores were added to the cell metadata for downstream comparative analysis.

In addition, ORA was performed separately for each Seurat-defined cluster. Differentially expressed genes per cluster were identified, and enrichment testing was carried out against the human MSigDB Collections database using standard hypergeometric testing.

This allowed identification of pathways and biological processes significantly enriched within specific T cell subsets.

6.10 Data analysis of single-nuclei sequencing dataset

All subsequent steps involving the lab work, processing and analysis of single-nuclei sequencing data were carried out in collaboration with Laura Anne Liebig from the Max Delbrück Center (Berlin, Germany).

The snSeq. dataset includes samples from individuals undergoing liver transplantation or biopsy for PSC (n = 25), ALD (n = 10), MASLD (n = 5) or gastric bypass surgery for obesity (n = 12). For the analysis presented in this thesis, AIH samples were excluded. Nuclei were isolated and processed using the 10x Genomics Chromium Single Cell 3' v3.1 platform and sequenced on an Illumina HiSeq 4000 (targeting 30,000–50,000 reads per nucleus). Data preprocessing included Cell Ranger alignment, ambient RNA removal with CellBender, and quality control filtering. Normalization, batch correction (harmonypy), dimensionality reduction (UMAP), and clustering (Leiden algorithm) were performed in Scanpy.

6.11 Spatial transcriptomics of human liver biopsies

Formalin-fixed, paraffin-embedded (FFPE) liver biopsies originally collected for routine diagnostic purposes at the outpatient service of the I.Department of Medicine, University Medical CentreHamburg-Eppendorf (UKE; Hamburg, Germany), were used for spatial transcriptomic analysis. The cohort included samples from 4 histologically normal controls, 11 individuals with early stage primary sclerosing cholangitis (PSC; fibrosis stage 1–2), and 7 individuals with late-stage PSC (fibrosis stage 3-4).

Spatial transcriptomic profiling was performed using the Xenium platform (10x Genomics). Tissue processing was conducted in collaboration with the group of Ulf Panzer (UKE Hamburg), and Xenium runs were carried out by the UKE Single Cell Core Facility. The 10x Genomics Immuno-Oncology gene panel was used, supplemented with 100 custom add-on genes (listed in Table 10).

All downstream processing and analysis of spatial transcriptomics data were performed in collaboration with Christian Casar from the Bioinformatics Core Facility at the

University Medical Center Hamburg-Eppendorf and Laura Anne Liebig (Max Delbrück Center, Berlin). Integration of Xenium datasets was carried out using the Harmony package in R. Niche analysis have been performed according to Farah *et al.* (2024) with a 40 µm radius around the cells[137].

To assess spatial relationships between cell types, the nearest $CD8^+$ T cell was identified for each cell using a k-dimensional tree algorithm. The Euclidean distance in pixels was then calculated and converted to µm using a predefined scaling factor.

6.12 Statistical analysis

Statistical analyses were performed using GraphPad Prism (version 10.6.1, GraphPad Software, San Diego, USA). Outliers were identified and excluded using the ROUT method (Q = 0.1 %). After outlier removal, normality of data distribution was assessed using the Shapiro-Wilk test.

For normally distributed data, comparisons between two groups were made using Welch's t-test. When more than two groups were compared, one-way ANOVA was applied, followed by appropriate post hoc testing. For non-normally distributed data, the Mann–Whitney U test was used for two-group comparisons, and the Kruskal-Wallis test for comparisons involving more than two groups.

Statistical significance was defined as follows: $p < 0.05$ (*), $p < 0.01$ (**), $p < 0.001$ (***), $p < 0.0001$ (****).

Unless specified otherwise, all statistical tests were two-sided, and a p-value below 0.05 was regarded as statistically significant.

7 Materials

The following tables include all used materials, chemicals, media, buffers, kits, antibodies, devices and software used for this study.

Table 1: List of Consumables

Consumables	Catalogue Number	Manufacturer	Country
96-Well Plates	83.3925.500	Sarstedt AG	Germany
Cryotubes 1.6 ml	72.380.002	Sarstedt AG	Germany
Culture plates, 24-well	83.3922.300	Sarstedt AG	Germany
ELISA plate, High bind	1023421	Sarstedt AG	Germany
FACS Tubes	551579	Sarstedt AG	Germany
gentleMACS(TM) C Tubes	130096334	Miltenyi Biotech	Germany
LS Cloumns	130-042-401	Mitenyi Biotec	Germany
Microscope slides Supeforst®	1879.1	Carl Roth	Germany
Petri Dishes 92 x 16 mm	82.1473.001	Sarstedt AG	Germany
Pipette tips 0.01 ml	1130100	Sarstedt AG	Germany
Pipette tips 0.2 ml	760012	Sarstedt AG	Germany
Pipette tips 1 ml	762	Sarstedt AG	Germany
Pipettes 10 ml	1688010	Sarstedt AG	Germany
Pipettes 25 ml	1685020	Sarstedt AG	Germany
Pipettes 5 ml	1687010	Sarstedt AG	Germany
Prazisa, Standard Disposable Scalpel	11.000.00.710	DAHLHAUSEN CZ, spol. s r.o.	Czech republic
S-Monovette® 9ml K3E	21.066.001	Sarstedt AG	Germany
TC Flask T25	83.3910.002	Sarstedt AG	Germany
TC Flask T75	83.3911.002	Sarstedt AG	Germany
Tissue strainer 100 um	833.945.100	Sarstedt AG	Germany
Tubes 1.5 ml	72.690.001	Sarstedt AG	Germany
Tubes 13 ml	62.515.006	Sarstedt AG	Germany
Tubes 15 ml	188271	Greiner Bio-One	Germany
Tubes 2 ml	72.691	Sarstedt AG	Germany
Tubes 5 ml	72.701	Sarstedt AG	Germany
Tubes 5 ml, for FACS	551579	Sarstedt AG	Germany
Tubes 50 ml	227261	Greiner Bio-One	Germany

Table 2: List of Comercial avaliable Solutions

Solution	Catalogue Number	Manufacturer	Country
Ficoll® Paque Plus	17-1440-03	Merck KGaA	Germany
Anti-FITC MicroBeads	130-048-701	Mitenyi Biotec	Germany
B27	12587-010	Thermofisher Scientific	USA
CD8 + T Cell Isolation Kit human	130-096-495	Miltenyi Biotec	Germany
N2	17502-048	Thermofisher Scientific	USA
Optiprep	07820	Stemcell Technologies	Canada
Percoll	P4937-500ML	Sigma-Aldrich	USA
Trypan Blue Stain (0.4 %)	15250-061	Gibco	USA
TrypLE™ Express Enzym (1 x), Phenolrot	12605010	Gibco	USA

Table 3: List of cell lines

Cell line	Catalog Number	Company	Country
H69 BECs	Provided by Ulrich Beuers, UMC Amsterdam		Netherlands
Rspo1 Producing Cells	Provided by Calvin J Kuo, Stanford University		USA
Wnt Producing Cells	ATCC-CRL-2647	ATCC	USA

Table 4: List of proteins and enzymes

Protein/Enzyme	Catalogue Number	Manufacturer	Country
Collagenase D	11088882001	Roche Diagnostics	Switzerland
HGF	100-39	Peprotech	USA
Albumin Fraktion V	0163.4	Carl Roth	Germany
DNAse	11284932001	Roche	Switzerland
FGF10	AF 100-26	Peprotech	USA
Forskolin	1099	Tocris Bioscience	USA
GASTRIN	G9145	Sigma-Aldrich	USA
Human EGF	AF-100-15-1MG	Preprotech	USA
human IFNg	300-02-20UG	Thermofisher Scientific	USA
human IL-15	200-15-10UG	Thermofisher Scientific	USA
human IL-17A	AF-200-17-100UG	Thermofisher Scientific	USA
human IL1b	130-093-563	Milteniy Biotech	Germany

Table 5: List of chemicals and solvents

Chemical/Solvent	Catalogue Number	Manufacturer	Country
Distilled water	0082479E	Braun	Germany
0.5 M EDTA, pH 8.0	15575-038	Invitrogen	USA
A83-01	2939	Tocris Bioscience	USA
DMSO	20385.01	SERVA Electrophoresis	Germany
KCl	1.049.361.000	Merck	Germany
KH_2PO_4	1.048.771.000	Merck	Germany
$KHCO_3$	1166397	Merck	Germany
Na_2HPO_4	4984.1	Carl Roth	Germany
N-acetylcysteine amide	A0737	Sigma-Aldrich	USA
NaCl	13.675.000	Th. Geyer GmbH & Co. KG	Germany
NH_4Cl	A779545	Merck	Germany
Nicotinamide	N0636	Sigma-Aldrich	USA

Table 6: List of media, cell culture supplements and buffers

Medium/Supplement/Buffer	Catalogue Number	Manufacturer	Country
EBSS	24010-043	Gibco	USA
Adenine	A2786	Sigma-Aldrich	USA
Advanced DMEM/F12	12634010	Thermofisher Scientific	USA
Cultrex Reduced Growth Factor Basement Membrane Extract, Type 2, Pathclear	3533-010-02	R&D Systems, Inc.	USA
DMEM / HAM-F12	11320-033	Gibco	USA
DMEM, high glucose	11965092	Thermofisher Scientific	USA
DPBS	14040-091	Gibco	USA
eBioscience™ Foxp3 / Transcription Factor Staining Buffer Set	00-5523-00	Thermofisher Scientific	USA
Epinephrine	E4250	Sigma-Aldrich	USA
FCS	P40-37500	PAN - Biotech	Germany
Hydrocortisone	H0135	Sigma-Aldrich	USA
Insulin-Transferrin-Selenium-X 100x	15710-064	Gibco	USA
L-Glutamine	51500-056	Thermofisher Scientific	USA
Penicillin-Streptomycin (10’000 U/ml)	15140122	Thermofisher Scientific	USA
Recovery™ Cell Culture Freezing Medium	12648010	Thermofisher Scientific	USA
Rspo1-containing culture supernatent	self produced		
Triiodothyronine	T5516	Sigma-Aldrich	USA
Wnt-containing culture supernatent	self produced		
Zeocin	P/N 46-0509	Invitrogen	USA

Table 7: List of anti-human antibodies

Antigen	Fluorochrome	Clone	Catalogue Number	Company
CCR7	BUV395	3D12	740267	BD Bioscience
CD103	PE	Ber-ACT8	350205	Biolegend
CD107a	BB700	H4A3	566558	Biolegend
CD161	BUV563	HP-3G10	749223	BD Bioscience
CD215	PE	JM7A4	330208	Biolegend
CD274	PE-Cy7	29E.2A3	329717	Biolegend
CD3	PE-Cy7	Okt 03	317334	Biolegend
CD324 (E-Cadherin)	BV480	67A4	752951	BD Bioscience
CD326 (Ep-CAM)	AF488	MH99	53-8326-42	Invitrogen
CD4	BUV 496	SK3	612936	BD Bioscience
CD45RA	BUV737	5H9	741871	BD Bioscience
CD69	PE/Dazzle	FN50	310942	Biolegend
CD8	BV510	RPA-T8	301048	Biolegend
CD8a	BV421	RPA-T8	301036	Biolegend
CXCR6	BV421	K041E5	356013	Biolegend
GZMA	AF488	CB9	507212	Biolegend
GZMB	AF700	GB11	560213	BD Bioscience
GZMK	AF647	GM26E7	370504	Biolegend
HLA-DR	BV785	L243	307642	Biolegend
IFNg	BV650	4S.B3	502538	Biolegend
IL15	AF647	34559	IC2471R	R&D
IL-17A	BV605	BL168	512326	Biolegend
PD-1	BUV615	EH12.1	612991	BD Bioscience
Perforin	BV711	DG9	308130	Biolegend
TCRα/β	Pacific Blue	IP26	306716	Biolegend
TCRVa7.2	BUV805	OF-5A12	749485	BD Bioscience
TNF	PerCP	MAb11	502924	Biolegend
TOX	Vio B515	REA773	130-129-259	Miltenyi

Table 8: List of anti-mouse Antibodies

Antigen	Fluorochrome	Clone	Catalogue Number	Company
CD45.2	AF532	104	58-0454-82	eBioscience
BZMB	PerCP-Fire 780	QA16A02	372230	Biolegend
CD11b	BV395	M1/70	563553	BD Bioscience
CD11c	BUV737	HL3	612796	BD Bioscience
CD146	PE/Cy7	ME-9F1	134713/4	Biolegend
CD215	APC	6B4C88	153505	Biolegend
CD25	BV650	PC61	102037	Biolegend
CD3	BV510	17A2	100234	Biolegend
CD326 (Ep-CAM)	BV711	G8.8	118233	Biolegend

CD4	PerCP	RM4-5	553052	BD Bioscience
CD45.1	Pacific Blue	A20	110722	Biolegend
CD8	BV785	53-6.7	100749	Biolegend
CXCR6	BV711	SA051D1	151111	Biolegend
GZMA	PE	QA16A02	149704	Biolegend
Ly-6C	AF700	AF700	128024	Biolegend
Ly-6G	BV421	1A8	127627	Biolegend
PD-1	PE-Dazzle 594	29F.1A12	135228	Biolegend
PD-L1	BUV615	MIH5	752339	BD Bioscience

Table 9: List of TaqMan Probes.

Target Gene	**Full Name of Gene Product**	**Catalog Number**
HPRT1	Hypoxanthine Phosphoribosyltransferase 1	Hs028006595_m1
IL15	Interleukin 15	Hs01003716_m1
IL15RA	Interleukin 15 Receptor Subunit Alpha	Hs00542602_g1
Hprt1	Hypoxanthine Phosphoribosyltransferase 1	Mm01545399_m1
Il15	Interleukin 15	Mm00434210_m1
Il15ra	Interleukin 15 Receptor Subunit Alpha	Mm04336046_m1

Table 10: Geneset for spatial transcriptomics anaylsis.

Geneset/Gene	**Ensembl ID**	**Probe-sets**	**Gene**	**Ensembl ID**	**Probe-sets**
Human Immuno-Oncology Panel	1000654	-	*TGFB2*	ENSG00000092969	8
Candida-albicans	NR-125332.1	7	*HAL*	ENSG00000084110	8
Enterococcus-faecium	NR-042054.1	6	*SDS*	ENSG00000135094	3
Klebsiella-pneumoniae	NR-117686.1	4	*CYP2E1*	ENSG00000130649	5
Streptococcus-mitis-oralis-infantis	NR-028664.1	7	*GLUL*	ENSG00000135821	3
Epstein-Barr-Virus	GU563886.1	4	*KRT23*	ENSG00000108244	8
gyrB	NZ-KB944666.1	8	*ASGR1*	ENSG00000141505	8
16S	NZ-KB944666.1	5	*TLR1*	ENSG00000174125	8
gyrB	NZ-CP038996.1	7	*TLR2*	ENSG00000137462	4
gyrB-Klebsiellapneumoniae	NC-016845.1	5	*TLR4*	ENSG00000136869	8
KRT19	ENSG00000171345	8	*TLR5*	ENSG00000187554	8
KRT7	ENSG00000135480	8	*OCLN*	ENSG00000197822	8
MUC1	ENSG00000185499	8	*TRAF6*	ENSG00000175104	8

MUC5B	ENSG00000117983	8
SCTR	ENSG00000080293	8
TRAC	ENSG00000277734	8
ICOS	ENSG00000163600	8
RUNX2	ENSG00000124813	8
PIK3R1	ENSG00000145675	6
PRDM1	ENSG00000057654	7
ITGAL	ENSG00000005844	8
LEF1	ENSG00000138795	8
BACH2	ENSG00000112182	8
CD69	ENSG00000110844	8
S100A4	ENSG00000196153	4
SLC4A10	ENSG00000144290	8
IL18R1	ENSG00000115604	8
TRAV7	ENSG00000211781	5
MR1	ENSG00000153029	8
HLA-DRA	ENSG00000204287	3
HLA-DRB1	ENSG00000196126	3
HLA-DPA1	ENSG00000231389	3
CLEC2B	ENSG00000110852	3
CLEC2D	ENSG00000069493	8
HLA-DQA1	ENSG00000196735	3
F2R	ENSG00000181104	8
KLRG1	ENSG00000139187	8
TNFSF10	ENSG00000121858	5
TRDC	ENSG00000211829	8
IFNA1	ENSG00000197919	8
IFNG	ENSG00000111537	8
IRAK4	ENSG00000198001	8
CDH1	ENSG00000039068	8
CLDN1	ENSG00000163347	8
CLDN2	ENSG00000165376	8
CLDN3	ENSG00000165215	6
TJP1	ENSG00000104067	8
GPBAR1	ENSG00000179921	8
HNF1A	ENSG00000135100	8
WNT2	ENSG00000105989	8
VCAM1	ENSG00000162692	3
COL4A1	ENSG00000187498	8
CLDN6	ENSG00000184697	8
ITGB6	ENSG00000115221	8
TNFSF11	ENSG00000120659	8
NEGR1	ENSG00000172260	8
FGFR1	ENSG00000077782	8
FGF1	ENSG00000113578	8
CLEC4M	ENSG00000104938	8
STAB2	ENSG00000136011	8
FGF23	ENSG00000118972	8
VWF	ENSG00000110799	8
ANO2	ENSG00000047617	8
PECAM1	ENSG00000261371	8
IL21R	ENSG00000103522	8
CPE	ENSG00000109472	8
ACKR1	ENSG00000213088	8
SEMA3A	ENSG00000075213	8
MMRN1	ENSG00000138722	8

IL17A	ENSG00000112115	8	*COL25A1*	ENSG00000188517	8
IL17F	ENSG00000112116	8	*ADAMTSL1*	ENSG00000178031	8
IL22	ENSG00000127318	8	*FBLN5*	ENSG00000140092	8
IL12A	ENSG00000168811	8	*DCLK1*	ENSG00000133083	8
CXCL8	ENSG00000169429	3	*GEM*	ENSG00000164949	3
TGFBR1	ENSG00000106799	8	*CASP3*	ENSG00000164305	8
IL17RA	ENSG00000177663	8	*MYH11*	ENSG00000133392	8
IL6R	ENSG00000160712	8	*RGS6*	ENSG00000182732	8
NFKB1	ENSG00000109320	3	*CNN1*	ENSG00000130176	8
IL17RC	ENSG00000163702	8			

Table 11: List of Devices.

Device	Catalog Number	Manufacturer	Country
CO2 Incubator	Modell: CB-S 170	Binder	Germany
Eppendorf 5427R	5409000010	Eppendorf	Germany
Eppendorf 5810R	5810000010	Eppendorf	Germany
Eppendorf 5920R	5948000010	Eppendorf	Germany
Gentle MACS Octo Dissociator	130-096-427	Miltenyi Biotec	Germany
NanoDrop 2000		Thermo Fisher Scientific	USA
Pipetboy Acu 2	155000	Integra Biosciences	Germany
QuantStudio 3	A28567	Applied Bioscience	USA
Thermo shaker	5355	Eppendorf	Germany
Vortex-Genie 2	SI-0236	Scientific industries	USA
Water bath	PURA 4	Julabo	Germany

Table 12: Composition of self-assambied Buffers and Media

Medium/Buffer	Concentration	Component
ACK Buffer		
		Distilled water
	100 mM	EDTA
	10 mM	$KHCO_3$
	150 mM	NH_4Cl
Basal medium		
		Advanced DMEM/F12
	1 %	L-Glut
	1 %	P/S
differentiation media		

		Advanced DMEM-F12
	10 %	Rspo1
	30 %	Wnt
	1 %	P/S
	1 %	L-GluT
	2 %	B27
	1 %	N2
	1 mM	N-acetylcysteine
	10 mM	Nicotinamide
	10 nM	GASTRIN
Expansion media		
		Advanced DMEM-F12
	10 %	Rspo1
	1 %	P/S
		L-GluT
	2 %	B27
	1 %	N2
	1 mM	N-acetylcysteine
	10 mM	Nicotinamide
	10 nM	GASTRIN
MACS buffer		
		PBS
	5 g/L	Albumin Fraktion V, biotinfrei,
	5%	0.5 M EDTA, pH 8.0
PBS, pH 7,4		
		Distilled water
	1,5 mM	KH2PO4
	6,5 mM	Na2HPO4
	2,7 mM	KCl
	137 mM	NaCl
WNT /R-Spondin1 Medium Conditioning Medium		
		DMEM (high Glucose)
	10 %	FBS
	1 %	P/S
	0.3 %	Zeocin

Table 13: List of Softwares

Software	**Version**	**Developer**	**Country**
FlowJo	V10.10.0	BD Bioscience	USA
GraphPad Prism	V10.6.1	GraphPad Software	USA
ImageJ/FIJI	V1.52	Wayne Rasband	USA
NanoDrop 2000/2000c Software	V1.6.198	Thermo Fisher Scientific	USA
QuatnStudio Software	V1.6.1	Applied Biosystems	USA

R	R-4.5.1	University of Auckland	New Zealand
R Studio	V37.2.6	Posit, PBC	USA
Xenium Explorer	4	10X Genomics	USA

8 References

1 Cancado, G. G. L. & Hirschfield, G. M. Management of primary sclerosing cholangitis: Current state-of-the-art. *Hepatol Commun* **8** (2024). https://doi.org/10.1097/HC9.0000000000000590

2 Mehta, T. I. *et al.* Global incidence, prevalence and features of primary sclerosing cholangitis: A systematic review and meta-analysis. *Liver Int* **41**, 2418-2426 (2021). https://doi.org/10.1111/liv.15007

3 Nardelli, M. J. *et al.* Clinical Features and Outcomes of Primary Sclerosing Cholangitis in the Highly Admixed Brazilian Population. *Can J Gastroenterol Hepatol* **2021**, 7746401 (2021). https://doi.org/10.1155/2021/7746401

4 Lundberg Bave, A., von Seth, E., Ingre, M., Nordenvall, C. & Bergquist, A. Autoimmune diseases in primary sclerosing cholangitis and their first-degree relatives. *Hepatology* **80**, 527-535 (2024). https://doi.org/10.1097/HEP.0000000000000823

5 Chalasani, N. *et al.* Cholangiocarcinoma in patients with primary sclerosing cholangitis: a multicenter case-control study. *Hepatology* **31**, 7-11 (2000). https://doi.org/10.1002/hep.510310103

6 Bergquist, A. *et al.* Hepatic and extrahepatic malignancies in primary sclerosing cholangitis. *J Hepatol* **36**, 321-327 (2002). https://doi.org/10.1016/s0168-8278(01)00288-4

7 Trivedi, P. J., Bowlus, C. L., Yimam, K. K., Razavi, H. & Estes, C. Epidemiology, Natural History, and Outcomes of Primary Sclerosing Cholangitis: A Systematic Review of Population-based Studies. *Clin Gastroenterol Hepatol* **20**, 1687-1700 e1684 (2022). https://doi.org/10.1016/j.cgh.2021.08.039

8 Steenstraten, I. C. *et al.* Systematic review with meta-analysis: risk factors for recurrent primary sclerosing cholangitis after liver transplantation. *Aliment Pharmacol Ther* **49**, 636-643 (2019). https://doi.org/10.1111/apt.15148

9 Goldberg, D. S. *et al.* Risk of waitlist mortality in patients with primary sclerosing cholangitis and bacterial cholangitis. *Liver Transpl* **19**, 250-258 (2013). https://doi.org/10.1002/lt.23587

10 Kummen, M. *et al.* The gut microbial profile in patients with primary sclerosing cholangitis is distinct from patients with ulcerative colitis without biliary disease and healthy controls. *Gut* **66**, 611-619 (2017). https://doi.org/10.1136/gutjnl-2015-310500

11 Zigmond, E. *et al.* Bile Duct Colonization With Enterococcus sp. Associates With Disease Progression in Primary Sclerosing Cholangitis. *Clin Gastroenterol Hepatol* **21**, 1223-1232 e1223 (2023). https://doi.org/10.1016/j.cgh.2022.09.006

12 Liao, L. *et al.* Intestinal dysbiosis augments liver disease progression via NLRP3 in a murine model of primary sclerosing cholangitis. *Gut* **68**, 1477-1492 (2019). https://doi.org/10.1136/gutjnl-2018-316670

13 Awoniyi, M. *et al.* Protective and aggressive bacterial subsets and metabolites modify hepatobiliary inflammation and fibrosis in a murine model of PSC. *Gut* **72**, 671-685 (2023). https://doi.org/10.1136/gutjnl-2021-326500

14 Alvaro, D., Gigliozzi, A. & Attili, A. F. Regulation and deregulation of cholangiocyte proliferation. *J Hepatol* **33**, 333-340 (2000). https://doi.org/10.1016/s0168-8278(00)80377-3

15 Carpino, G. *et al.* Activation of biliary tree stem cells within peribiliary glands in primary sclerosing cholangitis. *J Hepatol* **63**, 1220-1228 (2015). https://doi.org/10.1016/j.jhep.2015.06.018

16 Cardinale, V. *et al.* Multipotent stem/progenitor cells in human biliary tree give rise to hepatocytes, cholangiocytes, and pancreatic islets. *Hepatology* **54**, 2159-2172 (2011). https://doi.org/10.1002/hep.24590

17 Lemoinne, S. *et al.* Portal myofibroblasts promote vascular remodeling underlying cirrhosis formation through the release of microparticles. *Hepatology* **61**, 1041-1055 (2015). https://doi.org/10.1002/hep.27318

18 Kobayashi, S., Werneburg, N. W., Bronk, S. F., Kaufmann, S. H. & Gores, G. J. Interleukin-6 contributes to Mcl-1 up-regulation and TRAIL resistance via an Akt-signaling pathway in cholangiocarcinoma cells. *Gastroenterology* **128**, 2054-2065 (2005). https://doi.org/10.1053/j.gastro.2005.03.010

19 Komichi, D., Tazuma, S., Nishioka, T., Hyogo, H. & Chayama, K. Glycochenodeoxycholate plays a carcinogenic role in immortalized mouse cholangiocytes via oxidative DNA damage. *Free Radic Biol Med* **39**, 1418-1427 (2005). https://doi.org/10.1016/j.freeradbiomed.2005.07.005

20 Keitel, V. *et al.* The G-protein coupled bile salt receptor TGR5 is expressed in liver sinusoidal endothelial cells. *Hepatology* **45**, 695-704 (2007). https://doi.org/10.1002/hep.21458

21 Hohenester, S. *et al.* A biliary HCO3- umbrella constitutes a protective mechanism against bile acid-induced injury in human cholangiocytes. *Hepatology* **55**, 173-183 (2012). https://doi.org/10.1002/hep.24691

22 Bergquist, A. *et al.* Increased risk of primary sclerosing cholangitis and ulcerative colitis in first-degree relatives of patients with primary sclerosing cholangitis. *Clin Gastroenterol Hepatol* **6**, 939-943 (2008). https://doi.org/10.1016/j.cgh.2008.03.016

23 Karlsen, T. H. *et al.* Genome-wide association analysis in primary sclerosing cholangitis. *Gastroenterology* **138**, 1102-1111 (2010). https://doi.org/10.1053/j.gastro.2009.11.046

24 Ji, S. G. *et al.* Genome-wide association study of primary sclerosing cholangitis identifies new risk loci and quantifies the genetic relationship with inflammatory bowel disease. *Nat Genet* **49**, 269-273 (2017). https://doi.org/10.1038/ng.3745

25 Farh, K. K. *et al.* Genetic and epigenetic fine mapping of causal autoimmune disease variants. *Nature* **518**, 337-343 (2015). https://doi.org/10.1038/nature13835

26 Bowlus, C. L. *et al.* AASLD practice guidance on primary sclerosing cholangitis and cholangiocarcinoma. *Hepatology* **77**, 659-702 (2023). https://doi.org/10.1002/hep.32771

27 Paumgartner, G. & Beuers, U. Mechanisms of action and therapeutic efficacy of ursodeoxycholic acid in cholestatic liver disease. *Clin Liver Dis* **8**, 67-81, vi (2004). https://doi.org/10.1016/S1089-3261(03)00135-1

28 Karlsen, T. H., Vesterhus, M. & Boberg, K. M. Review article: controversies in the management of primary biliary cirrhosis and primary sclerosing cholangitis. *Aliment Pharmacol Ther* **39**, 282-301 (2014). https://doi.org/10.1111/apt.12581

29 Olsson, R. *et al.* High-dose ursodeoxycholic acid in primary sclerosing cholangitis: a 5-year multicenter, randomized, controlled study. *Gastroenterology* **129**, 1464-1472 (2005). https://doi.org/10.1053/j.gastro.2005.08.017

30 Lindstrom, L., Hultcrantz, R., Boberg, K. M., Friis-Liby, I. & Bergquist, A. Association between reduced levels of alkaline phosphatase and survival times of patients with primary sclerosing cholangitis. *Clin Gastroenterol Hepatol* **11**, 841-846 (2013). https://doi.org/10.1016/j.cgh.2012.12.032

31 Lindor, K. D. *et al.* High-dose ursodeoxycholic acid for the treatment of primary sclerosing cholangitis. *Hepatology* **50**, 808-814 (2009). https://doi.org/10.1002/hep.23082

32 European Association for the Study of the, L. EASL Clinical Practice Guidelines on sclerosing cholangitis. *J Hepatol* **77**, 761-806 (2022). https://doi.org/10.1016/j.jhep.2022.05.011

33 Fickert, P. *et al.* 24-norUrsodeoxycholic acid is superior to ursodeoxycholic acid in the treatment of sclerosing cholangitis in Mdr2 (Abcb4) knockout mice. *Gastroenterology* **130**, 465-481 (2006). https://doi.org/10.1053/j.gastro.2005.10.018

34 Fickert, P. *et al.* norUrsodeoxycholic acid improves cholestasis in primary sclerosing cholangitis. *J Hepatol* **67**, 549-558 (2017). https://doi.org/10.1016/j.jhep.2017.05.009

35 Michael Trauner, P. J. T., Gerald Denk, Martti Färkkilä, Peter Schirmacher, Stefan G. Hübscher, Michael Dill, Gerda Elisabeth Villadsen8, Christoph P. Berg, Kristin K. Jørgensen, Marcel Vetter, Münevver Demir, Andreas E. Kremer, Christoph Schramm, Christian Strassburg, Heike Bantel, Tobias Böttler, Ulrich Beuers, Alexandre Louvet, Emina Halilbasic, Michael Stiess, Markus Proels, Ralph Müller, Peter Fickert, Michael P. Manns. in *EASL Conference 2025* (Journal of Hepatology, Amsterdam, 2025).

36 Schnabl, B. PPAR Agonists in Primary Biliary Cholangitis. *N Engl J Med* **390**, 855-858 (2024). https://doi.org/10.1056/NEJMe2313802

37 Farkkila, M. *et al.* Metronidazole and ursodeoxycholic acid for primary sclerosing cholangitis: a randomized placebo-controlled trial. *Hepatology* **40**, 1379-1386 (2004). https://doi.org/10.1002/hep.20457

38 Tabibian, J. H. *et al.* Randomised clinical trial: vancomycin or metronidazole in patients with primary sclerosing cholangitis - a pilot study. *Aliment Pharmacol Ther* **37**, 604-612 (2013). https://doi.org/10.1111/apt.12232

39 Knox, T. A. & Kaplan, M. M. A double-blind controlled trial of oral-pulse methotrexate therapy in the treatment of primary sclerosing cholangitis. *Gastroenterology* **106**, 494-499 (1994). https://doi.org/10.1016/0016-5085(94)90610-6

40 Wagner, A. Azathioprine treatment in primary sclerosing cholangitis. *Lancet* **2**, 663-664 (1971). https://doi.org/10.1016/s0140-6736(71)80107-1

41 Lynch, K. D. *et al.* Effects of Vedolizumab in Patients With Primary Sclerosing Cholangitis and Inflammatory Bowel Diseases. *Clin Gastroenterol Hepatol* **18**, 179-187 e176 (2020). https://doi.org/10.1016/j.cgh.2019.05.013

42 Hedin, C. R. H. *et al.* Effects of Tumor Necrosis Factor Antagonists in Patients With Primary Sclerosing Cholangitis. *Clin Gastroenterol Hepatol* **18**, 2295-2304 e2292 (2020). https://doi.org/10.1016/j.cgh.2020.02.014

43 Shah, A. *et al.* Efficacy and safety of biologics in primary sclerosing cholangitis with inflammatory bowel disease: A systematic review and meta-analysis. *Hepatol Commun* **8** (2024). https://doi.org/10.1097/HC9.0000000000000347

44 Robinson, M. W., Harmon, C. & O'Farrelly, C. Liver immunology and its role in inflammation and homeostasis. *Cell Mol Immunol* **13**, 267-276 (2016). https://doi.org/10.1038/cmi.2016.3

45 Xia, X. *et al.* Structural diversity and concentration dependence of pyrazine formation: Exogenous amino substrates and reaction parameters during thermal processing of l-alanyl-l-glutamine Amadori compound. *Food Chem* **390**, 133144 (2022). https://doi.org/10.1016/j.foodchem.2022.133144

46 Vujasinovic, M. *et al.* The Role of Immunoglobulin G4 in Outcomes of Primary Sclerosing Cholangitis. *J Clin Med* **13** (2023). https://doi.org/10.3390/jcm13010079

47 Bjorkstrom, N. K., Ljunggren, H. G. & Michaelsson, J. Emerging insights into natural killer cells in human peripheral tissues. *Nat Rev Immunol* **16**, 310-320 (2016). https://doi.org/10.1038/nri.2016.34

48 Cameron, R. G., Blendis, L. M. & Neuman, M. G. Accumulation of macrophages in primary sclerosing cholangitis. *Clin Biochem* **34**, 195-201 (2001). https://doi.org/10.1016/s0009-9120(01)00215-6

49 Zimmer, C. L. *et al.* A biliary immune landscape map of primary sclerosing cholangitis reveals a dominant network of neutrophils and tissue-resident T cells. *Sci Transl Med* **13** (2021). https://doi.org/10.1126/scitranslmed.abb3107

50 Herrero-Cervera, A., Soehnlein, O. & Kenne, E. Neutrophils in chronic inflammatory diseases. *Cell Mol Immunol* **19**, 177-191 (2022). https://doi.org/10.1038/s41423-021-00832-3

51 Zweers, S. J. *et al.* Elevated interleukin-8 in bile of patients with primary sclerosing cholangitis. *Liver Int* **36**, 1370-1377 (2016). https://doi.org/10.1111/liv.13092

52 Greenman, R. *et al.* The Role of CCL24 in Primary Sclerosing Cholangitis: Bridging Patient Serum Proteomics to Preclinical Data. *Cells* **13** (2024). https://doi.org/10.3390/cells13030209

53 Cabeza-Cabrerizo, M., Cardoso, A., Minutti, C. M., Pereira da Costa, M. & Reis e Sousa, C. Dendritic Cells Revisited. *Annu Rev Immunol* **39**, 131-166 (2021). https://doi.org/10.1146/annurev-immunol-061020-053707

54 Cormican, S. & Griffin, M. D. Human Monocyte Subset Distinctions and Function: Insights From Gene Expression Analysis. *Front Immunol* **11**, 1070 (2020). https://doi.org/10.3389/fimmu.2020.01070

55 Kunzmann, L. K. *et al.* Monocytes as Potential Mediators of Pathogen-Induced T-Helper 17 Differentiation in Patients With Primary Sclerosing Cholangitis (PSC). *Hepatology* **72**, 1310-1326 (2020). https://doi.org/10.1002/hep.31140

56 Chung, B. K., Ogaard, J., Reims, H. M., Karlsen, T. H. & Melum, E. Spatial transcriptomics identifies enriched gene expression and cell types in human liver fibrosis. *Hepatol Commun* **6**, 2538-2550 (2022). https://doi.org/10.1002/hep4.2001

57 Stankey, C. T. *et al.* A disease-associated gene desert directs macrophage inflammation through ETS2. *Nature* **630**, 447-456 (2024). https://doi.org/10.1038/s41586-024-07501-1

58 Muller, A. L. *et al.* Inflammatory type 2 conventional dendritic cells contribute to murine and human cholangitis. *J Hepatol* **77**, 1532-1544 (2022). https://doi.org/10.1016/j.jhep.2022.06.025

59 Cornillet, M., Geanon, D., Bergquist, A. & Bjorkstrom, N. K. Immunobiology of primary sclerosing cholangitis. *Hepatology* **82**, 911-926 (2025). https://doi.org/10.1097/HEP.0000000000001080

60 Zecher, B. F. *et al.* HLA-DPA1*02:01~B1*01:01 is a risk haplotype for primary sclerosing cholangitis mediating activation of NKp44+ NK cells. *Gut* **73**, 325-337 (2024). https://doi.org/10.1136/gutjnl-2023-329524

61 Deshpande, A. *et al.* Evaluation of a commercial real-time polymerase chain reaction assay for detection of environmental contamination with Clostridium difficile. *J Hosp Infect* **85**, 76-78 (2013). https://doi.org/10.1016/j.jhin.2013.06.011

62 von Seth, E. *et al.* Primary sclerosing cholangitis leads to dysfunction and loss of MAIT cells. *Eur J Immunol* **48**, 1997-2004 (2018). https://doi.org/10.1002/eji.201847608

63 Ito, E. *et al.* Sulfated bile acid is a host-derived ligand for MAIT cells. *Sci Immunol* **9**, eade6924 (2024). https://doi.org/10.1126/sciimmunol.ade6924

64 Hu, Y. *et al.* gammadelta T cells: origin and fate, subsets, diseases and immunotherapy. *Signal Transduct Target Ther* **8**, 434 (2023). https://doi.org/10.1038/s41392-023-01653-8

65 Tedesco, D. *et al.* Alterations in Intestinal Microbiota Lead to Production of Interleukin 17 by Intrahepatic gammadelta T-Cell Receptor-Positive Cells and Pathogenesis of Cholestatic Liver Disease. *Gastroenterology* **154**, 2178-2193 (2018). https://doi.org/10.1053/j.gastro.2018.02.019

66 Jiang, X. & Karlsen, T. H. Genetics of primary sclerosing cholangitis and pathophysiological implications. *Nat Rev Gastroenterol Hepatol* **14**, 279-295 (2017). https://doi.org/10.1038/nrgastro.2016.154

67 Jiang, X. *et al.* Cholangiocytes Modulate CD100 Expression in the Liver and Facilitate Pathogenic T-Helper 17 Cell Differentiation. *Gastroenterology* **166**, 667-679 (2024). https://doi.org/10.1053/j.gastro.2023.11.283

68 Katt, J. *et al.* Increased T helper type 17 response to pathogen stimulation in patients with primary sclerosing cholangitis. *Hepatology* **58**, 1084-1093 (2013). https://doi.org/10.1002/hep.26447

69 Poch, T. *et al.* Single-cell atlas of hepatic T cells reveals expansion of liver-resident naive-like CD4(+) T cells in primary sclerosing cholangitis. *J Hepatol* **75**, 414-423 (2021). https://doi.org/10.1016/j.jhep.2021.03.016

70 Poch, T. *et al.* Intergenic risk variant rs56258221 skews the fate of naive CD4(+) T cells via miR4464-BACH2 interplay in primary sclerosing cholangitis. *Cell Rep Med* **5**, 101620 (2024). https://doi.org/10.1016/j.xcrm.2024.101620

71 Kamihira, T. *et al.* Biliary epithelial cells regulate autoreactive T cells: implications for biliary-specific diseases. *Hepatology* **41**, 151-159 (2005). https://doi.org/10.1002/hep.20494

72 Oo, Y. H. *et al.* CXCR3-dependent recruitment and CCR6-mediated positioning of Th-17 cells in the inflamed liver. *J Hepatol* **57**, 1044-1051 (2012). https://doi.org/10.1016/j.jhep.2012.07.008

73 Andrews, T. S. *et al.* Single-cell, single-nucleus, and spatial transcriptomics characterization of the immunological landscape in the healthy and PSC human liver. *J Hepatol* **80**, 730-743 (2024). https://doi.org/10.1016/j.jhep.2023.12.023

74 Stein, S. *et al.* IL-17A/F enable cholangiocytes to restrict T cell-driven experimental cholangitis by upregulating PD-L1 expression. *J Hepatol* **74**, 919-930 (2021). https://doi.org/10.1016/j.jhep.2020.10.035

75 Schrumpf, E. *et al.* The biliary epithelium presents antigens to and activates natural killer T cells. *Hepatology* **62**, 1249-1259 (2015). https://doi.org/10.1002/hep.27840

76 Grakoui, A. & Crispe, I. N. Presentation of hepatocellular antigens. *Cell Mol Immunol* **13**, 293-300 (2016). https://doi.org/10.1038/cmi.2015.109

77 Mortezaee, K. & Majidpoor, J. CD8(+) T Cells in SARS-CoV-2 Induced Disease and Cancer-Clinical Perspectives. *Front Immunol* **13**, 864298 (2022). https://doi.org/10.3389/fimmu.2022.864298

78 Lee, S. W., Lee, G. W., Kim, H. O. & Cho, J. H. Shaping Heterogeneity of Naive CD8(+) T Cell Pools. *Immune Netw* **23**, e2 (2023). https://doi.org/10.4110/in.2023.23.e2

79 Yewdell, J. W., Bennink, J. R., Smith, G. L. & Moss, B. Influenza A virus nucleoprotein is a major target antigen for cross-reactive anti-influenza A virus cytotoxic T lymphocytes. *Proc Natl Acad Sci U S A* **82**, 1785-1789 (1985). https://doi.org/10.1073/pnas.82.6.1785

80 Koh, C. H., Lee, S., Kwak, M., Kim, B. S. & Chung, Y. CD8 T-cell subsets: heterogeneity, functions, and therapeutic potential. *Exp Mol Med* **55**, 2287-2299 (2023). https://doi.org/10.1038/s12276-023-01105-x

81 Shah, K., Al-Haidari, A., Sun, J. & Kazi, J. U. T cell receptor (TCR) signaling in health and disease. *Signal Transduct Target Ther* **6**, 412 (2021). https://doi.org/10.1038/s41392-021-00823-w

82 Voskoboinik, I., Whisstock, J. C. & Trapani, J. A. Perforin and granzymes: function, dysfunction and human pathology. *Nat Rev Immunol* **15**, 388-400 (2015). https://doi.org/10.1038/nri3839

83 Xie, A. *et al.* TCR stimulation without co-stimulatory signals induces expression of "tolerogenic" genes in memory CD4 T cells but does not compromise cell

proliferation. *Mol Immunol* **63**, 406-411 (2015). https://doi.org/10.1016/j.molimm.2014.09.013

84 Arias, I. M. *et al.* The Liver Biology and Pathobiology Preface. *Liver: Biology and Pathobiology, 6th Edition, 6 Edition*, Xx-Xx (2020).

85 Sironi, L. *et al.* In vivo flow mapping in complex vessel networks by single image correlation. *Sci Rep* **4**, 7341 (2014). https://doi.org/10.1038/srep07341

86 Warren, A. *et al.* T lymphocytes interact with hepatocytes through fenestrations in murine liver sinusoidal endothelial cells. *Hepatology* **44**, 1182-1190 (2006). https://doi.org/10.1002/hep.21378

87 Ficht, X. & Iannacone, M. Immune surveillance of the liver by T cells. *Sci Immunol* **5** (2020). https://doi.org/10.1126/sciimmunol.aba2351

88 Pham, B. N. *et al.* Flow cytometry CD4+/CD8+ ratio of liver-derived lymphocytes correlates with viral replication in chronic hepatitis B. *Clin Exp Immunol* **97**, 403-410 (1994). https://doi.org/10.1111/j.1365-2249.1994.tb06102.x

89 Bertolino, P., Bowen, D. G., McCaughan, G. W. & Fazekas de St Groth, B. Antigen-specific primary activation of CD8+ T cells within the liver. *J Immunol* **166**, 5430-5438 (2001). https://doi.org/10.4049/jimmunol.166.9.5430

90 Limmer, A. *et al.* Efficient presentation of exogenous antigen by liver endothelial cells to CD8+ T cells results in antigen-specific T-cell tolerance. *Nat Med* **6**, 1348-1354 (2000). https://doi.org/10.1038/82161

91 De Creus, A. *et al.* Low TLR4 expression by liver dendritic cells correlates with reduced capacity to activate allogeneic T cells in response to endotoxin. *J Immunol* **174**, 2037-2045 (2005). https://doi.org/10.4049/jimmunol.174.4.2037

92 Guidotti, L. G. *et al.* Immunosurveillance of the liver by intravascular effector CD8(+) T cells. *Cell* **161**, 486-500 (2015). https://doi.org/10.1016/j.cell.2015.03.005

93 Sheng, H. *et al.* Distinct PLZF(+)CD8alphaalpha(+) Unconventional T Cells Enriched in Liver Use a Cytotoxic Mechanism to Limit Autoimmunity. *J Immunol* **203**, 2150-2162 (2019). https://doi.org/10.4049/jimmunol.1900832

94 Rosato, P. C., Wijeyesinghe, S., Stolley, J. M. & Masopust, D. Integrating resident memory into T cell differentiation models. *Curr Opin Immunol* **63**, 35-42 (2020). https://doi.org/10.1016/j.coi.2020.01.001

95 Pallett, L. J. *et al.* IL-2(high) tissue-resident T cells in the human liver: Sentinels for hepatotropic infection. *J Exp Med* **214**, 1567-1580 (2017). https://doi.org/10.1084/jem.20162115

96 Huang, L. R. *et al.* Intrahepatic myeloid-cell aggregates enable local proliferation of CD8(+) T cells and successful immunotherapy against chronic viral liver infection. *Nat Immunol* **14**, 574-583 (2013). https://doi.org/10.1038/ni.2573

97 Kim, J. *et al.* Innate-like Cytotoxic Function of Bystander-Activated CD8(+) T Cells Is Associated with Liver Injury in Acute Hepatitis A. *Immunity* **48**, 161-173 e165 (2018). https://doi.org/10.1016/j.immuni.2017.11.025

98 Holz, L. E. *et al.* CD8(+) T Cell Activation Leads to Constitutive Formation of Liver Tissue-Resident Memory T Cells that Seed a Large and Flexible Niche in the Liver. *Cell Rep* **25**, 68-79 e64 (2018). https://doi.org/10.1016/j.celrep.2018.08.094

99 Dudek, M. *et al.* Auto-aggressive CXCR6(+) CD8 T cells cause liver immune pathology in NASH. *Nature* **592**, 444-449 (2021). https://doi.org/10.1038/s41586-021-03233-8

100 Fan, J. *et al.* IL-15-induced CD38(+)HLA-DR(+)CD8(+) T cells correlate with liver injury via NKG2D in chronic hepatitis B cirrhosis. *Clin Transl Immunology* **13**, e70007 (2024). https://doi.org/10.1002/cti2.70007

101 Grabstein, K. H. *et al.* Cloning of a T cell growth factor that interacts with the beta chain of the interleukin-2 receptor. *Science* **264**, 965-968 (1994). https://doi.org/10.1126/science.8178155

102 Giri, J. G. *et al.* Utilization of the beta and gamma chains of the IL-2 receptor by the novel cytokine IL-15. *EMBO J* **13**, 2822-2830 (1994). https://doi.org/10.1002/j.1460-2075.1994.tb06576.x

103 Leonard, W. J., Lin, J. X. & O'Shea, J. J. The gamma(c) Family of Cytokines: Basic Biology to Therapeutic Ramifications. *Immunity* **50**, 832-850 (2019). https://doi.org/10.1016/j.immuni.2019.03.028

104 Huntington, N. D. *et al.* Interleukin 15-mediated survival of natural killer cells is determined by interactions among Bim, Noxa and Mcl-1. *Nat Immunol* **8**, 856-863 (2007). https://doi.org/10.1038/ni1487

105 Intlekofer, A. M. *et al.* Effector and memory CD8+ T cell fate coupled by T-bet and eomesodermin. *Nat Immunol* **6**, 1236-1244 (2005). https://doi.org/10.1038/ni1268

106 Wang, Y. *et al.* The IL-15-AKT-XBP1s signaling pathway contributes to effector functions and survival in human NK cells. *Nat Immunol* **20**, 10-17 (2019). https://doi.org/10.1038/s41590-018-0265-1

107 Lee, H., Park, S. H. & Shin, E. C. IL-15 in T-Cell Responses and Immunopathogenesis. *Immune Netw* **24**, e11 (2024). https://doi.org/10.4110/in.2024.24.e11

108 Mortier, E., Woo, T., Advincula, R., Gozalo, S. & Ma, A. IL-15Ralpha chaperones IL-15 to stable dendritic cell membrane complexes that activate NK cells via trans presentation. *J Exp Med* **205**, 1213-1225 (2008). https://doi.org/10.1084/jem.20071913

109 Ota, N., Takase, M., Uchiyama, H., Olsen, S. K. & Kanagawa, O. No requirement of trans presentations of IL-15 for human CD8 T cell proliferation. *J Immunol* **185**, 6041-6048 (2010). https://doi.org/10.4049/jimmunol.0901834

110 Bergamaschi, C. *et al.* Circulating IL-15 exists as heterodimeric complex with soluble IL-15Ralpha in human and mouse serum. *Blood* **120**, e1-8 (2012). https://doi.org/10.1182/blood-2011-10-384362

111 Jabri, B. & Abadie, V. IL-15 functions as a danger signal to regulate tissue-resident T cells and tissue destruction. *Nat Rev Immunol* **15**, 771-783 (2015). https://doi.org/10.1038/nri3919

112 Colpitts, S. L. *et al.* Cutting edge: the role of IFN-alpha receptor and MyD88 signaling in induction of IL-15 expression in vivo. *J Immunol* **188**, 2483-2487 (2012). https://doi.org/10.4049/jimmunol.1103609

113 Dominguez-Andres, J. *et al.* Inflammatory Ly6C(high) Monocytes Protect against Candidiasis through IL-15-Driven NK Cell/Neutrophil Activation. *Immunity* **46**, 1059-1072 e1054 (2017). https://doi.org/10.1016/j.immuni.2017.05.009

114 Mattei, F., Schiavoni, G., Belardelli, F. & Tough, D. F. IL-15 is expressed by dendritic cells in response to type I IFN, double-stranded RNA, or lipopolysaccharide and promotes dendritic cell activation. *J Immunol* **167**, 1179-1187 (2001). https://doi.org/10.4049/jimmunol.167.3.1179

115 Lucas, M., Schachterle, W., Oberle, K., Aichele, P. & Diefenbach, A. Dendritic cells prime natural killer cells by trans-presenting interleukin 15. *Immunity* **26**, 503-517 (2007). https://doi.org/10.1016/j.immuni.2007.03.006

116 Kim, T. S., Rha, M. S. & Shin, E. C. IFN-gamma Induces IL-15 Trans-Presentation by Epithelial Cells via IRF1. *J Immunol* **208**, 338-346 (2022). https://doi.org/10.4049/jimmunol.2100057

117 Dubois, S., Mariner, J., Waldmann, T. A. & Tagaya, Y. IL-15Ralpha recycles and presents IL-15 In trans to neighboring cells. *Immunity* **17**, 537-547 (2002). https://doi.org/10.1016/s1074-7613(02)00429-6

118 Becker, T. C. *et al.* Interleukin 15 is required for proliferative renewal of virus-specific memory CD8 T cells. *J Exp Med* **195**, 1541-1548 (2002). https://doi.org/10.1084/jem.20020369

119 Mueller, Y. M. *et al.* IL-15 enhances survival and function of HIV-specific CD8+ T cells. *Blood* **101**, 1024-1029 (2003). https://doi.org/10.1182/blood-2002-07-1957

120 Deshpande, P. *et al.* IL-7- and IL-15-mediated TCR sensitization enables T cell responses to self-antigens. *J Immunol* **190**, 1416-1423 (2013). https://doi.org/10.4049/jimmunol.1201620

121 Kennedy, M. K. *et al.* Reversible defects in natural killer and memory CD8 T cell lineages in interleukin 15-deficient mice. *J Exp Med* **191**, 771-780 (2000). https://doi.org/10.1084/jem.191.5.771

122 Meresse, B. *et al.* Coordinated induction by IL15 of a TCR-independent NKG2D signaling pathway converts CTL into lymphokine-activated killer cells in celiac disease. *Immunity* **21**, 357-366 (2004). https://doi.org/10.1016/j.immuni.2004.06.020

123 Karlsen, T. H., Folseraas, T., Thorburn, D. & Vesterhus, M. Primary sclerosing cholangitis - a comprehensive review. *J Hepatol* **67**, 1298-1323 (2017). https://doi.org/10.1016/j.jhep.2017.07.022

124 Rea, I. M., McNerlan, S. E. & Alexander, H. D. CD69, CD25, and HLA-DR activation antigen expression on CD3+ lymphocytes and relationship to serum TNF-alpha, IFN-gamma, and sIL-2R levels in aging. *Exp Gerontol* **34**, 79-93 (1999). https://doi.org/10.1016/s0531-5565(98)00058-8

125 Ahn, E. *et al.* Role of PD-1 during effector CD8 T cell differentiation. *Proc Natl Acad Sci U S A* **115**, 4749-4754 (2018). https://doi.org/10.1073/pnas.1718217115

126 Wherry, E. J. *et al.* Molecular signature of CD8+ T cell exhaustion during chronic viral infection. *Immunity* **27**, 670-684 (2007). https://doi.org/10.1016/j.immuni.2007.09.006

127 Cigalotto, L. & Martinvalet, D. Granzymes in health and diseases: the good, the bad and the ugly. *Front Immunol* **15**, 1371743 (2024). https://doi.org/10.3389/fimmu.2024.1371743

128 Russ, B. E. *et al.* Defining the molecular blueprint that drives CD8(+) T cell differentiation in response to infection. *Front Immunol* **3**, 371 (2012). https://doi.org/10.3389/fimmu.2012.00371

129 Jonsson, A. H. *et al.* Granzyme K(+) CD8 T cells form a core population in inflamed human tissue. *Sci Transl Med* **14**, eabo0686 (2022). https://doi.org/10.1126/scitranslmed.abo0686

130 Schall, T. J., Bacon, K., Toy, K. J. & Goeddel, D. V. Selective attraction of monocytes and T lymphocytes of the memory phenotype by cytokine RANTES. *Nature* **347**, 669-671 (1990). https://doi.org/10.1038/347669a0

131 Xie, C. B., Zhou, J., Mackay, S. & Pober, J. S. Complement-activated human endothelial cells stimulate increased polyfunctionality in alloreactive T cells. *Am J Transplant* **21**, 1902-1909 (2021). https://doi.org/10.1111/ajt.16485

132 Liberzon, A. *et al.* The Molecular Signatures Database (MSigDB) hallmark gene set collection. *Cell Syst* **1**, 417-425 (2015). https://doi.org/10.1016/j.cels.2015.12.004

133 Cimpean, M. *et al.* IL-15 Priming Alters IFN-gamma Regulation in Murine NK Cells. *J Immunol* **211**, 1481-1493 (2023). https://doi.org/10.4049/jimmunol.2300283

134 Berndt, N. *et al.* Functional Consequences of Metabolic Zonation in Murine Livers: Insights for an Old Story. *Hepatology* **73**, 795-810 (2021). https://doi.org/10.1002/hep.31274

135 European Association for the Study of the, L. EASL Clinical Practice Guidelines on nutrition in chronic liver disease. *J Hepatol* **70**, 172-193 (2019). https://doi.org/10.1016/j.jhep.2018.06.024

136 Wu, L., Beechem, J. M. & Danaher, P. Using transcripts to refine image based cell segmentation with FastReseg. *Sci Rep* **15**, 30508 (2025). https://doi.org/10.1038/s41598-025-08733-5

137 Farah, E. N. *et al.* Spatially organized cellular communities form the developing human heart. *Nature* **627**, 854-864 (2024). https://doi.org/10.1038/s41586-024-07171-z

138 Halpern, K. B. *et al.* Single-cell spatial reconstruction reveals global division of labour in the mammalian liver. *Nature* **542**, 352-356 (2017). https://doi.org/10.1038/nature21065

139 Bursch, L. S., Rich, B. E. & Hogquist, K. A. Langerhans cells are not required for the CD8 T cell response to epidermal self-antigens. *J Immunol* **182**, 4657-4664 (2009). https://doi.org/10.4049/jimmunol.0803656

140 Chen, R. Y. *et al.* The role of PD-1 signaling in health and immune-related diseases. *Front Immunol* **14**, 1163633 (2023). https://doi.org/10.3389/fimmu.2023.1163633

141 Donado, C. A. *et al.* Granzyme K activates the entire complement cascade. *Nature* **641**, 211-221 (2025). https://doi.org/10.1038/s41586-025-08713-9

142 Ricklin, D., Hajishengallis, G., Yang, K. & Lambris, J. D. Complement: a key system for immune surveillance and homeostasis. *Nat Immunol* **11**, 785-797 (2010). https://doi.org/10.1038/ni.1923

143 Wittek, A. *et al.* A Gradient of Intestinal Inflammation in Primary Sclerosing Cholangitis. *Inflamm Bowel Dis* **30**, 900-910 (2024). https://doi.org/10.1093/ibd/izad137

144 Huang, C. & Bi, J. Expression Regulation and Function of T-Bet in NK Cells. *Front Immunol* **12**, 761920 (2021). https://doi.org/10.3389/fimmu.2021.761920

145 Goode, E. C. *et al.* Fine-mapping and molecular characterisation of primary sclerosing cholangitis genetic risk loci. *Nat Commun* **15**, 9594 (2024). https://doi.org/10.1038/s41467-024-53602-w

146 Watson, T. K. *et al.* Reduced Function of the Adaptor SH2B3 Promotes T1D via Altered Cytokine-Regulated, T-Cell-Intrinsic Immune Tolerance. *Diabetes* **74**, 943-955 (2025). https://doi.org/10.2337/db24-0655

147 Schregel, I. *et al.* Evaluation of Tofacitinib in Primary Sclerosing Cholangitis and Associated Colitis: A Multicenter, Retrospective Study. *Clin Gastroenterol Hepatol* **21**, 3448-3450 e3443 (2023). https://doi.org/10.1016/j.cgh.2023.01.014

148 Kilkenny, C., Browne, W. J., Cuthill, I. C., Emerson, M. & Altman, D. G. Improving bioscience research reporting: the ARRIVE guidelines for reporting animal research. *PLoS Biol* **8**, e1000412 (2010). https://doi.org/10.1371/journal.pbio.1000412

149 Schwinge, D. *et al.* Testosterone suppresses hepatic inflammation by the downregulation of IL-17, CXCL-9, and CXCL-10 in a mouse model of experimental acute cholangitis. *J Immunol* **194**, 2522-2530 (2015). https://doi.org/10.4049/jimmunol.1400076

150 Stuart, T. *et al.* Comprehensive Integration of Single-Cell Data. *Cell* **177**, 1888-1902 e1821 (2019). https://doi.org/10.1016/j.cell.2019.05.031

9 Use of artificial intelligence tools

Artificial intelligence-based tools (ChatGPT, OpenAI) were used solely for language editing and improvement of clarity. All scientific content, data analysis, interpretation, and conclusions were independently developed by the author.

10 Danksagung

Zunächst möchte ich mich herzlich bei Prof. Dr. Christoph Schramm und Dr. Dorothee Schwinge für die hervorragende Betreuung bedanken. Ihre stetige Unterstützung, ihre konstruktive Kritik und ihr Vertrauen haben diese Arbeit maßgeblich geprägt. Ich hätte mir keinen besseren Ort für meine Doktorarbeit wünschen können.

Ebenso danke ich Prof. Dr. Johannes Herkel und Dr. Antonella Carambia für das angenehme Miteinander, ihr Interesse an meiner Arbeit und ihr wertvolles Feedback.

Mein besonderer Dank gilt Angelika Schmidt, Marko Hilken, Melanie Stahlbuhk und Sabrina Kress für die ausgezeichnete technische Unterstützung. Danke für die unzähligen Male, in denen ihr mich bei meinen Experimenten unterstützt habt. Ohne euch wäre diese Arbeit nicht möglich gewesen.

Für die bioinformatische Unterstützung und den regen fachlichen Austausch danke ich Christian Casar und Laura Liebig. Sabrina Pilz danke ich für die Mitgestaltung der Mausversuche. Silja Steinmann gilt mein Dank für den nahezu täglichen Austausch von Ideen, der diese Arbeit in vielerlei Hinsicht bereichert hat.

Dem gesamten Liver Lab Team möchte ich für das großartige Gruppenklima danken. Selbst wenn Experimente schief gingen, wusste ich immer, dass ich mich auf die Menschen neben mir verlassen kann und sie mich auffangen.

Zum Schluss möchte ich den wichtigsten Personen in meinem Leben danken. Danke, Evy, dass du mich in dieser intensiven Zeit begleitet, unterstützt und manchmal auch einfach ausgehalten hast. Meinen Eltern und Großeltern danke ich von Herzen dafür, dass sie mir mein Studium überhaupt ermöglicht haben und mich zu der Person gemacht haben, die ich heute bin.